Function of Elongation Factor P in Translation

Dissertation

for the award of the degree

”Doctor rerum naturalium“
of the Georg-August-Universität Göttingen

within the doctoral program *Biomolecules: Structure–Function–Dynamics*
of the Georg-August University School of Science (GAUSS)

submitted by

Lili Klara Dörfel

from Berlin

Göttingen, 2015

Members of the Examination board / Thesis Committee

Prof. Dr. Marina Rodnina, Department of Physical Biochemistry, Max Planck Institute for Biophysical Chemistry, Göttingen (1st Reviewer)

Prof. Dr. Heinz Neumann, Research Group of Applied Synthetic Biology, Institute for Microbiology and Genetics, Georg August University, Göttingen (2nd Reviewer)

Prof. Dr. Holger Stark, Research Group of 3D Electron Cryo-Microscopy, Max Planck Institute for Biophysical Chemistry, Göttingen

Further members of the Examination board

Prof. Dr. Ralf Ficner, Department of Molecular Structural Biology, Institute for Microbiology and Genetics, Georg August University, Göttingen

Dr. Manfred Konrad, Research Group Enzyme Biochemistry, Max Planck Institute for Biophysical Chemistry, Göttingen

Prof. Dr. Markus T. Bohnsack, Department of Molecular Biology, Institute for Molecular Biology, University Medical Center, Göttingen

Date of the oral examination: 16.11.2015

Affidavit

The thesis has been written independently and with no other sources and aids than quoted. Sections 2.1.2, 2.2.1.1 and parts of section 2.2.1.4 are published in (Doerfel et al, 2013); the translation gel of EspfU is published in (Doerfel & Rodnina, 2013) and section 2.2.3 is published in (Doerfel et al, 2015) (see list of publications).

Lili Klara Dörfel

November 2015

List of publications

EF-P is Essential for Rapid Synthesis of Proteins Containing Consecutive Proline Residues
Doerfel LK[†], Wohlgemuth I[†], Kothe C, Peske F, Urlaub H, Rodnina MV*. *Science* (2013); 339(6115):85-8.

Elongation Factor P: Function and Effects on Bacterial Fitness
Doerfel LK, Rodnina MV*. *Biopolymers* (2013); 99(11):837-45.

Entropic contribution of elongation factor P to proline positioning at the catalytic center of the ribosome
Doerfel LK[†], Wohlgemuth I[†], Kubyshkin V, Starosta AL, Wilson DN*, Budisa N*, Rodnina MV*. *Journal of the American Chemical Society* (2015); 137(40)**:** 12997-13006

** Corresponding author*
† Equal contribution

Content

ABSTRACT 1
1 INTRODUCTION 2
1.1 Translation 2
1.1.1 General overview 2
1.1.2 Peptide bond formation 4
1.2 Elongation factor P 6
1.3 Proline 10
1.4 Aims of the thesis 12
2 RESULTS 13
2.1 The catalytic function of EF-P 13
2.1.1 Initiation 13
2.1.2 Elongation 14
2.1.2.1 The P-site substrate 14
2.1.2.2 The A-site substrate 15
2.1.2.3 Sequence context 16
2.1.2.4 Proline induced stalling leads to peptidyl tRNA dissociation 17
2.1.2.5 EF-P alleviates Pro-induced ribosome stalling in longer model peptides 18
2.1.2.6 Ribosomes stall at PP/G and can be rescued by EF-P. 19
2.1.2.7 EF-P enhances synthesis of E. coli proteins containing polyproline motifs 21
2.1.2.8 Stalling is mainly caused by the Pro moiety of Pro-tRNA^{Pro} 23
2.1.3 Release 25
2.2 Investigation of the catalytic mechanism of EF-P 26
2.2.1 The function of the EF-P body and the modification 27
2.2.1.1 EF-P modification increases its catalytic proficiency 27
2.2.1.2 Slow peptide bond formation competes with the translocation process 30
2.2.1.3 Increasing $MgCl_2$ concentrations reduce peptidyl-tRNA dissociation. 32
2.2.1.4 EF-P selectively accelerates peptide bond formation with poor substrates. 33
2.2.1.5 Impact of the EF-P modification on peptidyl transfer 34
2.2.2 Variation of physico-chemical parameters 35
2.2.2.1 pH-dependence of peptide bond formation with a native A-site substrate 35
2.2.2.2 Activation parameters 38
2.2.3 Variation of the substrate 41
2.2.3.1 Substitution on the prolyl ring modulates steric and electronic properties of proline 41
2.2.3.2 Pro derivatives were accepted by the translation machinery 42
2.2.3.3 Substitutions in the prolyl ring strongly modulate rate of peptide bond formation 42

2.2.3.4 The ribosome-catalysed reaction is more sensitive to substituent effects than the in-solution reaction 45

2.2.3.5 The reactivity does not correlate with the electrophilicity of the P-site substrate 47

2.2.3.6 Isomery 48

2.2.3.7 Impact of Pro analogs on activation parameters 50

3 DISCUSSION 52

3.1 The biological role of EF-P 52

3.1.1 EF-P inactivation causes pleiotropic *in-vivo* phenotypes 52

3.1.1.1 Susceptibility to external stimuli 53

3.1.1.2 Motility 53

3.1.1.3 Virulence 54

3.1.2 Potential regulation by the EF-P modification state 54

3.2 What makes proline slow in peptide bond formation? 55

3.2.1 Poor reactivity of proline 55

3.2.2 Proline in proteins and in the cell 56

3.2.3 Sequence context effects of Pro-induced stalling 56

3.3 EF-P binds to the ribosome in a $tRNA^{Pro}$-specific fashion 57

3.4 How does EF-P catalyze peptide bond formation? 58

3.4.1 EF-P body stabilizes and positions the peptidyl-tRNA 58

3.4.2 The modification of EF-P contributes to catalysis 59

3.4.3 EF-P function does not involve general acid or base catalysis 60

3.4.4 A possible catalytic mechanism of EF-P 61

4 MATERIALS AND METHODS 63

4.1 Equipment 63

4.2 Software 63

4.3 Chemicals and consumables 63

4.4 Reaction buffers 64

4.5 Bacterial strains 64

4.6 Cloning 64

4.6.1 Construct for overexpression of EF-P and its modifying enzymes 65

4.6.2 Generation of mRNA constructs 65

4.6.3 Construction of $tRNA^{Pro}$ template 66

4.6.4 Constructs used in this study 66

4.6.5 Primer 66

4.7 RNA 69

4.7.1 Short mRNA constructs 69

4.7.2 Transcription of long mRNAs 70
4.7.3 Preparation of the $tRNA^{Pro}$ transcript 70
4.7.4 Native tRNAs 71
4.7.5 Isolation of peptidyl-tRNA 71
4.7.6 Aminoacylation of tRNA 71
4.7.7 Misaminoacylation of $tRNA^{Phe}$ 72
4.7.8 Analysis of Pro*-$tRNA^{Pro}$ binding to EF-Tu by native PAGE 72
4.7.9 Purification of tRNA/TC by size-exclusion chromatography (SEC) 72
4.8 Proteins 73
4.8.1 EF-P expression and purification 73
4.8.2 Purification of native EF-P 73
4.8.3 Identification of EF-P-containing fractions by dot blot 74
4.8.4 Other Proteins 74
4.9 Ribosomes 75
4.9.1 Initiation complexes (ICs) 75
4.9.2 Ternary complexes (TCs) 75
4.9.3 Post translocation complexes (PTCs) 75
4.9.4 PTCs containing Pro analogs 75
4.10 Gel electrophoresis 76
4.10.1 Soldium dodecyl sulfate polyacrylamide gel electrophoresis (SDS PAGE) 76
4.10.2 Tris-Tricine PAGE 76
4.10.3 Native polyacrylamide gel electrophoresis (native PAGE) 76
4.10.4 Denaturing polyacrylamide gel electrophoresis (UREA PAGE) 76
4.11 Kinetics 77
4.11.1 Di- and tripeptide formation with puromycin 78
4.11.2 Di- and tripeptide formation 78
4.11.3 Tetra- and pentapeptide formation 79
4.11.4 Hydrolysis of peptidyl-tRNA 79
4.11.5 Aminolysis of peptidyl-tRNA 79
4.11.6 Termination experiments 79
4.11.7 *In-vitro* translation 80
4.11.8 Filter binding experiments 81
4.12 Mass spectrometry 81
4.13 Calculation of Activation Energies 82

4.14 Determination of the pK_a 82
5 SUPPLEMENTARY INFORMATION 85
5.1 Determination of the modification status of EF-P 85
5.2 Confirming the functionality of the tRNA transcript 86
5.3 Purification of the ternary complex Pro*-$tRNA^{Pro}$·EF-Tu·GTP 86
5.4 Determination of the optimal nucleophile concentration to monitor aminolysis 87
5.5 Influence of the $MgCl_2$ concentration on fM-P*P*G formation 88
5.6 Supplementary tables 89
6 REFERENCES 94
7 Appendix 110
7.1 List of abbreviations 110
7.2 List of Figures 111
7.3 List of Tables 112
8 Acknowledgements 113
9 Contribution 113

ABSTRACT

The ribosome translates the genetic information encoded in the mRNA into amino acid sequence of a peptide chain. The catalytic site of the ribosome where peptide bonds are made, the peptidyl transferase center, consists of RNA and usually does not accessory proteins for function. By applying systematic sequence permutations in several *in-vitro* translation assays we discovered that the ribosome – while proficient in making peptide bonds between most amino acids – is surprisingly slow when synthesizing polyproline and PPG motifs. The combination of poor A- and P-site substrates led to the inhibition of peptide bond formation after incorporation of the second proline into the nascent chain resulting in robust ribosomal stalling. Linear-free-energy relationships (LFER) of peptidyl transfer using different proline analogs as well as the investigation of sequence-context effects in the nascent peptidyl chain revealed that the poor reactivity of peptidyl-Pro-tRNA^{Pro} in the P site of the ribosome originates from stereo-electronic properties of proline which induce an unfavorable orientation of the peptidyl-tRNA in the peptidyl transferase center. We showed that the functionally uncharacterized elongation factor P (EF-P) is a specialized translation elongation factor which augments the peptidyl transferase activity of the ribosome by alleviating proline-induced stalling. The identified function of EF-P as facilitator of polyproline synthesis explains the pleiotropic phenotypes observed in EF-P knockout strains *in vivo*. EF-P catalyzes peptidyl transfer entropically, presumably by positioning of the peptidyl-tRNA, its CCA end and/or the attached amino acid in a more active conformation. In *Escherichia coli* EF-P is lysylated and hydroxylated at Lys34 a residue that points to the peptidyl transferase center. Kinetically we show that this unique modification is crucial for the catalytic activity of EF-P. Because the modifications are specific for bacteria, these findings may pave the way for the discovery of new antibiotics.

1 INTRODUCTION

1.1 Translation

1.1.1 General overview

Translation is the last step of gene expression, in which the ribosome decodes the genetic information of messenger RNA (mRNA) into an amino acid sequence determining the structure and function of the newly synthesized protein. The ribosome is , a large ribonucleoprotein complex (~ 2.5 MDa), which is composed of roughly 60% RNA and 40% proteins (in bacteria). The prokaryotic 70S ribosome comprises two functional parts (Fig. 1): the small 30S subunit which consists of 22 proteins (designated S1 - S22) and the 16S rRNA (~1500 nts) and the large 50S subunit which consists of two RNA molecules, the 23S, 5S rRNA (~2900 and ~120 nts, respectively) and 36 proteins (designated L1 - L36). The small subunit contains the decoding center which communicates correct base-pairing of the mRNA codon with the anticodon of transfer RNAs (tRNA) to the translation machinery and the large subunit contains the peptidyl transferase center where peptide bond formation is catalyzed exclusively by the 23S rRNA, defining the ribosome as a ribozyme (Ban et al, 2000; Nissen et al, 2000; Noller et al, 1992).

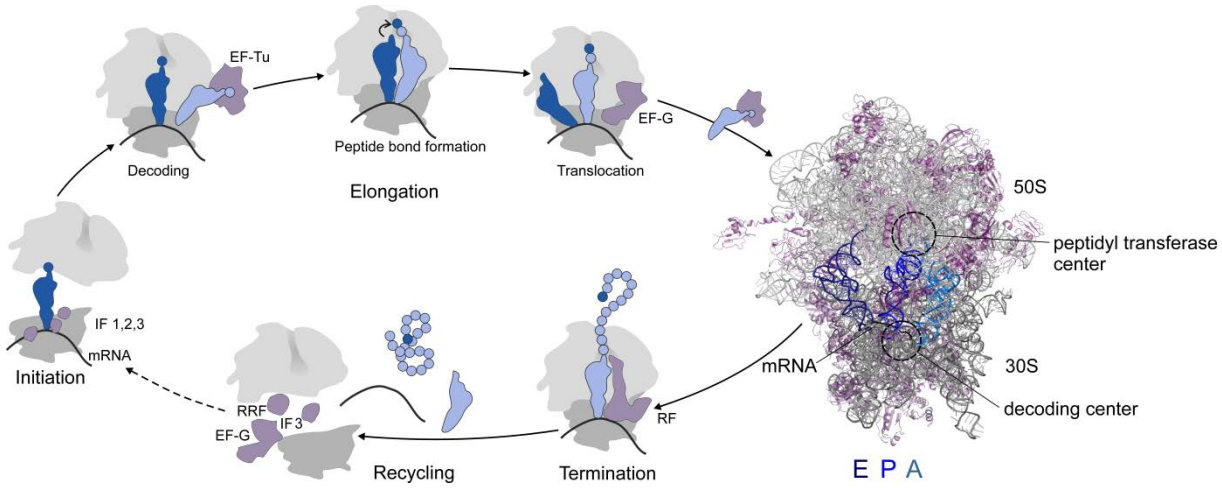

Fig. 1: Overview of the prokaryotic translation cycle

The main phases of translation: Initiation, elongation (which entails decoding, peptide bond formation and translocation), termination and recycling, see description in the text. Ribosomal subunits are depicted in grey, charged initiator tRNA in blue, other tRNAs in light blue (and dark blue in the structure) and proteins are colored violet. The structure was generated in PyMol (https://www.pymol.org) using PDB 4v5d.

tRNAs are short, non-coding RNA molecules which fold in a L-shaped tertiary structure and serve as adaptors which assign mRNA codons to the respective amino acids esterified to their acceptor end. The ribosome provides three tRNA binding sites: the aminoacyl (A) site which accommodates the incoming aminoacyl-tRNA delivered by EF-Tu, the peptidyl (P) site which binds the peptidyl-tRNA and

the exit (E) site from which deacylated tRNA dissociates from the ribosome. The main phases of translation, namely initiation, elongation, termination and ribosome recycling are coordinated by a set of auxiliary protein factors, many of which are GTPases.

In bacteria, protein synthesis begins with the binding of initiation factors (IFs) 1, 2 and 3, charged initiator tRNA (fMet-tRNA^{fMet}) and mRNA to the small ribosomal subunit (Milon & Rodnina, 2012). While interaction of the Shine-Dalgarno sequence of the mRNA with the almost complementary 3' end of the 16S rRNA positions the mRNA (Shine & Dalgarno, 1974; Studer & Joseph, 2006), IF2 recruits and stabilizes the initiator tRNA base paired to the start codon in the P site (Milon et al, 2010). The correct assembly of this so-called 30S initiation complex (30S IC) allows the association of the large subunit catalyzed by IF2 and modulated by IF1 and IF3, which triggers the dissociation of IFs (MacDougall & Gonzalez, 2015; Simonetti et al, 2008). The resulting 70S initiation complexes (IC) with fMet-tRNA^{fMet} bound to the start codon in the P site of the small and large subunit (P/P) is competent to enter the elongation phase of translation.

Translation elongation is an iterative cycle of three steps: It starts with the delivery of aminoacyl-tRNA (aa-tRNA) to the A site in a ternary complex (TC) with elongation factor Tu (EF-Tu) and GTP. Correct base-pairing of the aa-tRNA anticodon with the mRNA codon exposed in the 30S A site leads to conformational changes within the 30S subunit which trigger GTP hydrolysis by EF-Tu. EF-Tu*GDP has a reduced affinity to the tRNA and thus the acceptor end of the aa-tRNA accommodates into the peptidyl transferase center. Accommodation of aa-tRNA starts with a large movement of the tRNA body by more than 70 Å from the so called A/T to the A/A state followed by the relaxation of the CCA end into the peptidyl transferase center. Aa-tRNA is stabilized by interactions with L16 and helices 38 and 69 and locally by interactions of G2553 of the ribosomal A-loop with the CCA end by forming an A-minor interaction with U2506-G2583. tRNA accommodation induces a conformational rearrangement of the peptidyl-tRNA which exposes the labile ester bond in a near-attack conformation (Schmeing et al, 2005b). Subsequently, the peptidyl moiety of the P-site peptidyl-tRNA is transferred to the A site-bound aa-tRNA, resulting in a peptide chain extended by one amino acid bound to the A-site tRNA and a deacylated tRNA bound to the P site. Peptide bond formation shifts the dynamic equilibrium of tRNA movements from the classical (A/A and P/P) towards the hybrid state conformation in which the anticodon stem loop remains in the A (or P) site of the 30S but the acceptor end moves towards the P (or E) site of the 50S (Moazed & Noller, 1989). These hybrid P/E and A/P conformations of tRNAs correlate with a rotation of the small relative to the large ribosomal subunit into a rotated state (Frank & Agrawal, 2000; Julian et al, 2008; Munro et al, 2010) and constitute the transition to elongation factor G (EF-G) induced translocation. Binding of EF-G*GTP strengthens the rotated ribosomal state (Adio et al, 2015; Cornish et al, 2008; Fei et al, 2008) and subsequent GTP hydrolysis drives the translocation of the tRNAs together with the mRNA relative to

the ribosome by one codon (Rodnina et al, 1997). Concomitantly, a backward rotation of the ribosomal subunits results in the formation of the classical, non-rotated conformation of tRNAs and the ribosome (Frank & Agrawal, 2000; Holtkamp et al, 2014). Thus, the peptidyl-tRNA is moved from the A to the P site and the deacylated P-site tRNA is moved to the E site from where it dissociates. As a consequence of translocation, the A site becomes vacant and can accommodate an aa-tRNA corresponding to the next mRNA codon. The stepwise extending peptidyl-chain travels through the ribosomal exit tunnel where it can undergo co-translationally folding restricted by the dimensions of the exit tunnel while finally domain folding occurs post-translationally (Mittelstaet, 2012; Nilsson et al, 2015; Waudby et al, 2013; Wilson & Beckmann, 2011; Ziv et al, 2005).

When the ribosome approaches a stop codon, a release factor (RF) binds to the A site and triggers the hydrolysis of the nascent peptide from its tRNA by positioning a catalytic water molecule (reviewed in (Rodnina, 2013)). Tripeptide sequences in RF1 and RF2 lead to stop codon specificity with RF1 recognizing UAG and UAA and RF2 recognizing UGA and UAA stop codons (Ito et al, 2000). A conserved GGQ motif of which the Gln is post-translationally methylated in both factors (Nakahigashi et al, 2002) is required for optimal coordination of the catalytic water molecule (Dincbas-Renqvist et al, 2000; Shaw & Green, 2007; Weixlbaumer et al, 2008). Subsequent to the peptidyl-chain release, GTP-hydrolysis by RF3 catalyzes the dissociation of RF1/RF2 from the ribosome (Peske et al, 2014). The post-termination complex is disassembled by the concerted action of EF-G, IF3 and the ribosome recycling factor (RRF) into tRNA, mRNA and ribosomal subunits which can participate in a new round of protein synthesis (Hirokawa et al, 2006; Nurenberg & Tampe, 2013).

1.1.2 Peptide bond formation

Upon peptide bond formation the α-amino group of the aa-tRNA in the A site nucleophillically attacks the carbonyl carbon of the peptidyl-tRNA in the P site which results in a tetrahedral adduct. The tetrahedral adduct subsequently dissociates yielding the new peptidyl-tRNA lengthened by one amino acid in the A-site and a deacylated tRNA in the P-site. The uncatalyzed aminolysis reaction in solution is expected to proceed through two tetrahedral intermediates: Attack of the α-NH_2 group results in the zwitterionic intermediate (T±) which involves the formation of an oxyanion. Subsequent deprotonation of the NH_2 group forms a negatively charged intermediate (T-) (Fig. 2) the decomposition of which results in the reaction products (Satterthwait & Jencks, 1974). Biochemical data using small model substrates (Dorner et al, 2003), kinetic analysis with intact P-site substrates (Weinger et al, 2004), molecular dynamics simulations (Trobro & Aqvist, 2006; Wallin & Aqvist, 2010) as well as structural studies (Schmeing et al, 2005a) indicated that the ribosome catalyzed reaction involves a proton-shuttle mechanism in which the proton of the nucleophile is abstracted and

transferred to the leaving group (reviewed in (Rodnina, 2013)). In the proposed mechanism the 2´hydroxyl group of A76 of the P site substrates abstracts the proton from the attacking nucleophile and shuttles it directly or indirectly via additional water molecules to the 3´-hydroxylgroup of the P-site substrate in a step wise or fully concerted manner (reviewed in (Rodnina, 2013)). Investigation of the ribosomal reaction by heavy-atom kinetic isotope effects (KIE) measured on isolated 50S subunits indicated that the formation of the tetrahedral transition state and the proton shuttle take place in a rate-limiting step and are thus concerted (Fig. 2) (Hiller et al, 2011).

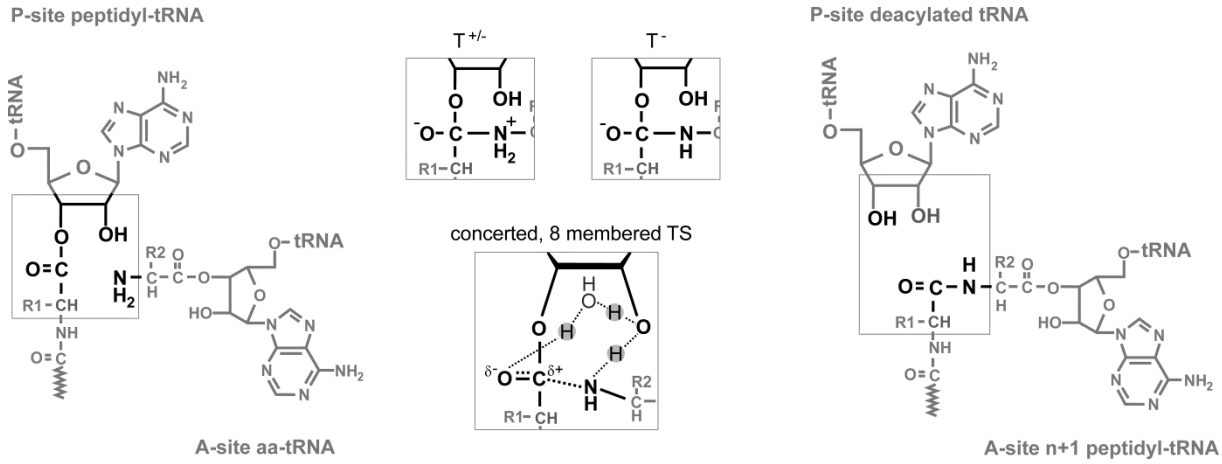

Fig. 2: Reaction scheme of aminolysis in solution and on the ribosome

A- and P-site tRNAs prior to peptidyl transfer are depicted on the left side, deacylated P-site tRNA and A-site peptidyl-tRNA on the right side. The proposed transition states of the in-solution reaction (T± and T-) and ribosome-catalyzed reaction (concerted, 8 membered) are shown in the middle. Adopted from (Rodnina, 2013)

Furthermore, analysis of kinetic solvent isotope effects (KSIE) revealed that three protons are shuttled indicating an 8-membered transition state (Fig. 2) (Kuhlenkoetter et al, 2011). Rapid breakdown of the tetrahedral intermediate in a separate step suggested that in contrast to the in-solution reaction the T± does not accumulate. Consistently, the rate of peptide bond formation does not correlate with the nucleophilicity of the attacking amine, suggesting an uncharged amine in the transition state (Kingery et al, 2008). Recently, the proton wire mechanism as an alternative model to the 6- and 8-membered proton shuttle mechanisms was proposed in which the 5´-phosphate oxygen of A76 (aa-tRNA) and the N-terminal α-amine of ribosomal protein L27 assist in the deprotonation of the nucleophile (Polikanov et al, 2014). Notably, both models are in agreement with the available biochemical and kinetic data. Analysis of the activation parameters revealed that the ribosome catalyzes peptide bond formation by lowering the activation entropy (Sievers et al, 2004) suggesting an important contribution of substrate positioning or desolvation as well as electrostatic shielding to catalysis (Schroeder & Wolfenden, 2007; Sievers et al, 2004; Trobro & Aqvist, 2005). Extensive base substitution studies of rRNA bases in the active site revealed that none of them is essential for peptidyl transfer and that ionizing residues of the ribosomal active site

contribute only little to catalysis which argues against general acid or base catalysis by the ribosome (Beringer et al, 2003; Beringer et al, 2005; Bieling et al, 2006; Youngman et al, 2004) (reviewed in (Beringer, 2008; Beringer & Rodnina, 2007a)). Overall, the ribosome might stabilize the transition state by providing a network of electrostatic interactions and of prearranged hydrogen-bond acceptors/donors which allow fast shuttling of protons (Schmeing et al, 2005a; Sharma et al, 2005; Trobro & Aqvist, 2005; Trobro & Aqvist, 2006). Furthermore, conformational changes within the ribosomal active site modulate peptide bond formation (Beringer et al, 2005; Brunelle et al, 2006; Katunin et al, 2002). Interaction of full-length aa-tRNA with residues of the 23S rRNA induces an active conformation of the ribosomal active site and disruption of this interaction (by small substrate analogs) leads to sensitivity of the reaction towards base substitutions and pH (Beringer & Rodnina, 2007a; Brunelle et al, 2006; Katunin et al, 2002; Youngman et al, 2004), indicating that substrate positioning is a major part of catalysis.

For the most substrate combinations the rate of peptidyl transfer is limited by buffer- dependent accommodation of aminoacyl-tRNA (Johansson et al, 2008; Thomas et al, 1988; Wohlgemuth et al, 2010) which masks the intrinsic reactivity differences of peptide bond formation induced by the A- or P-site substrate (Ledoux & Uhlenbeck, 2008; Wohlgemuth et al, 2008). While peptidyl transfer can be slowed down by protonation at low pH which inactivates the nucleophile, accommodation is pH-independent (Beringer et al, 2005; Bieling et al, 2006). To avoid kinetically obscured reactions, virtually all studies on peptide bond formation rely on the antibiotic puromycin (Pmn) or its derivatives (C-Pmn) as A-site substrate (Beringer & Rodnina, 2007a; Brunelle et al, 2006; Hiller et al, 2011; Katunin et al, 2002; Kingery et al, 2008; Kuhlenkoetter et al, 2011; Sievers et al, 2004; Wohlgemuth et al, 2006; Wohlgemuth et al, 2008). Pmn (3'-deoxy-N,N-dimethyl-3'-[(O-methyl-L-tyrosyl)amino]adenosine) is an analog of aa-A76 of the acceptor arm of aa-tRNA which rapidly diffuses into the peptidyl transferase center without rate-limiting accommodation steps (Sievers et al, 2004). Substrate-dependent reactivity differences (Wohlgemuth et al, 2008), the pH-dependence (Katunin et al, 2002) as well as kinetic isotope effects (Hiller et al, 2011; Kuhlenkoetter et al, 2011) further established that the Pmn reaction kinetically reports the peptidyl-transfer reaction.

1.2 Elongation factor P

Elongation factor P (EF-P) is a small (21 kDa) protein which comprises three mainly β-barrel domains (I, II and III, Fig. 3A). Its domain arrangement and the overall shape resemble that of a tRNA, with the N-terminal domain I representing the acceptor end and the C-terminal domain III resembling the anticodon stem of tRNA (Fig. 3D) (Choi & Choe, 2011; Hanawa-Suetsugu et al, 2004). Furthermore, most of the surface is negatively charged (Hanawa-Suetsugu et al, 2004). Comparison of EF-P structures from different organisms and within different asymmetric units indicates that domain I

can adopt different orientations relative to domain II and III (Choi & Choe, 2011). EF-P is universally conserved in all three domains of life; sequence and structure similarities of EF-P and its archaeal and eukaryotic orthologs called initiation factors 5A (aIF5A and eIF5A, respectively) indicate functional conservation among the bacterial, archaeal and eukaryotic orthologs (Park et al, 2010). Although the archeal and eukaryotic orthologs lack the C-terminal domain III of bacterial EF-P, 42% residues of *Thermus thermophilus* EF-P are conserved or similar in eIF5As and the structures of the remaining domains superimpose very well (Fig. 3D) (Hanawa-Suetsugu et al. 2004). Whether the discrepancy in domain numbers is the result of a deletion event in eukaryotes or a duplication event in bacteria is not known (Hanawa-Suetsugu et al, 2004).

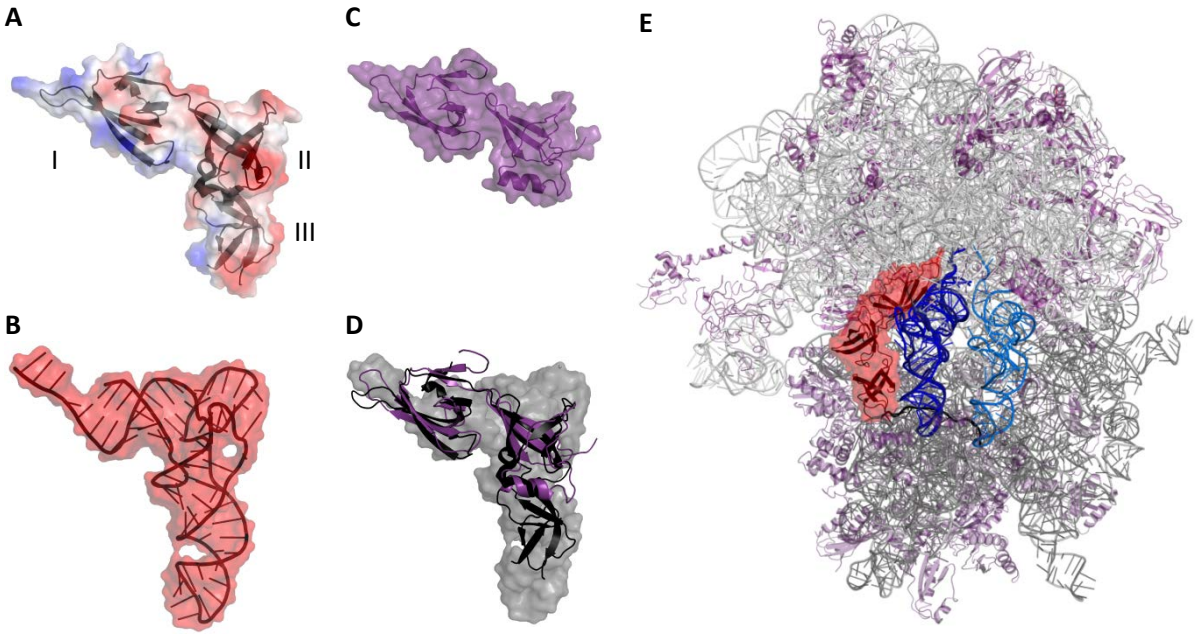

Fig. 3: Structures of EF-P/eIF5A, tRNA and the ribosome

A) EF-P from *E. coli* illustrated as cartoon with electrostatic potential of the surface (PDB: 3A5Z). Domain numbering as indicated. B) $tRNA^{fMet}$ from *T. thermophilus* (PDB: 3HUY). C) eIF5A from *Saccharomyces cerevisiae (*PDB: 3ER0*).* D) Superposition of *E. coli* EF-P (black, PDB: 3A5Z), eIF5A from *S. cerevisiae* (purple, PDB: 3ER0) and initiator tRNA from *T. thermophilus* (grey surface, PDB: 3HUY). E) Ribosome-bound EF-P and initiator tRNA (red and blue, respectively; PDB: 3HUY) aligned onto ribosome-bound A- and P-site tRNAs (light and dark blue, respectively; PDB: 4v5d) from *T. thermophilus.* Figures were generated in PyMOL (https://www.pymol.org).

Deletion strains in *E. coli, Pseudomonas aeruginosa, Agrobacterium tumefaciens* and *Salmonella enterica serovar typhimurium* suggest that EF-P is not essential in bacteria (Baba et al, 2006; Balibar et al, 2013; Peng et al, 2001; Zou et al, 2011). In yeast and higher eukaryotes eIF5A is essential and occurs in different tissue-specific isoforms (reviewed in (Park et al, 2010)). EF-P binds the ribosome in a 1:1 molar ratio (Aoki et al, 2008). A structural investigation showed that it spans both ribosomal subunits and binds between the E and P site (Fig. 3E) (Blaha et al, 2009). Its C-terminal domain III contains a conserved sequence motif (GDT) in a flexible loop (not resolved in the crystal structure) which was proposed to interact with the 30S ribosome or the mRNA (Choi & Choe, 2011). Its N-

terminal domain I - in analogy to the acceptor end of tRNA - points towards the peptidyl transferase center and contacts the CCA end of the P-site tRNA (Blaha et al, 2009). At the very tip of domain I, EF-P and its orthologs are posttranslationally modified at a conserved lysine or arginine residue, notably by different enzymes and with different modifications (Fig. 4). In *E. coli* EF-P is modified at Lys34 with an R-β-lysine and a hydroxyl-group. The first step of the EF-P lysylation pathway (Fig. 4A) involves the conversion of S-α-Lys to R-β-Lys by a homolog of lysine 2,3 aminomutase (LAM) family named EpmB (YjeK) (Bailly & de Crecy-Lagard, 2010; Behshad et al, 2006; Roy et al, 2011). R-β-Lys is then activated by adenylation and the lysyl moiety is transferred to the ε-amino group of Lys34 of EF-P. This step is catalyzed by EpmA (alternative names: YjeA, PoxA or GenX), a homolog of the catalytic domain of class II Lys-tRNA synthetases (Lys-RS2) (Ambrogelly et al, 2010; Bailly & de Crecy-Lagard, 2010; Navarre et al, 2010; Yanagisawa et al, 2010). A third modifying enzyme EpmC (YfcM) hydroxylates the conserved Lys34, presumably at its C5(δ) (Peil et al, 2012). The modification further extends EF-P into the direction of the peptidyl transferase center and a molecular model suggests that it could reach within 2 Å of the C-terminal amino acid of the P site-bound tRNA (Lassak et al, 2015). Lysylation of EF-P is relevant for its catalytic proficiency *in vivo* and *in vitro* (Navarre et al, 2010; Park et al, 2012; Zou et al, 2012).

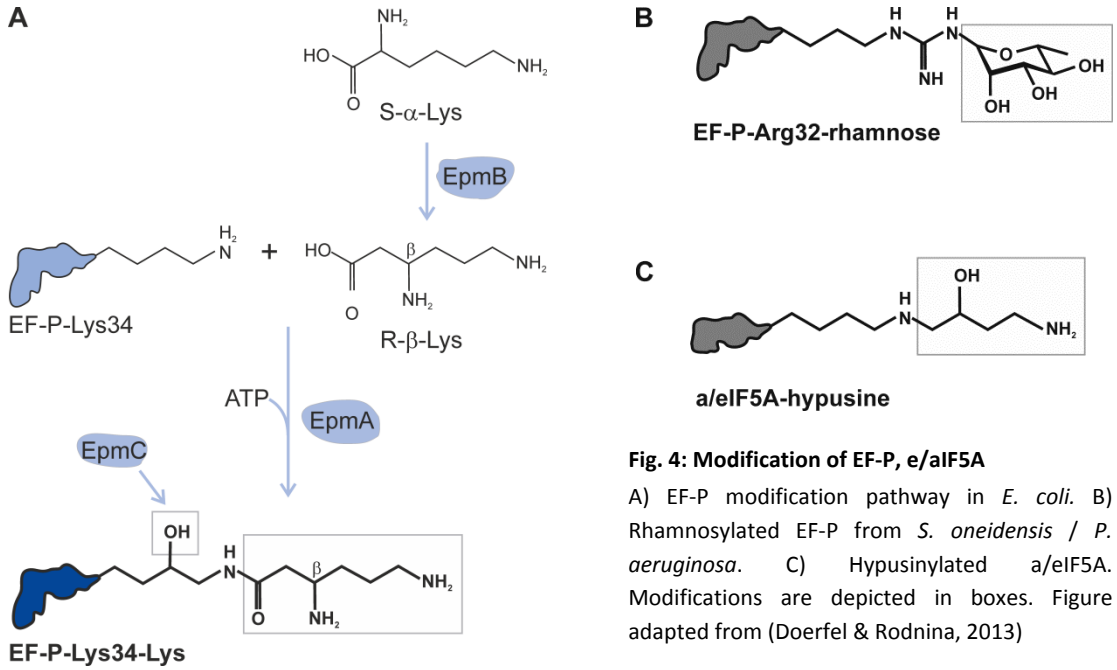

Fig. 4: Modification of EF-P, e/aIF5A

A) EF-P modification pathway in *E. coli.* B) Rhamnosylated EF-P from *S. oneidensis* / *P. aeruginosa*. C) Hypusinylated a/eIF5A. Modifications are depicted in boxes. Figure adapted from (Doerfel & Rodnina, 2013)

Notably, ~70% of bacteria do not encode EpmA or EpmB, suggesting that either EF-P remains unmodified or is modified by different enzymes in these organisms (Bailly & de Crecy-Lagard, 2010). Indeed, recent bioinformatics studies and biochemical data indicate that a wide range of EF-P modifications have evolved among different organisms: For example, *Shewanella oneidensis* and *P. aeruginosa* belong to a subclass of bacteria (~9%) with a strictly conserved Arg and do not encode EpmA, B, C but the glycosyltransferase EarP (Lassak et al, 2015; Rajkovic et al, 2015). In both

organisms EF-P is rhamnosylated by EarP at Arg32/34 (Fig. 4B), a position structurally equivalent to Lys34 of *E. coli* EF-P. Deletion of earP in *S. oneidensis* phenocopys strains where EF-P cannot be modified, indicating that, similar to the lysylation of *E. coli* EF-P, glycolysation is required to activate EF-P in these organisms (Lassak et al, 2015; Rajkovic et al, 2015). Furthermore, several bacterial species encode a gene cognate to deoxyhypusine synthase (DHS) which modifies eIF5A in eukaryotes (Brochier et al, 2004). In eukaryotes eIF5A Lys51 is transformed into hypusine [N^{ε}-(4-aminobutyl-2-hydroxy)-l-lysine] (Fig. 4C) by addition of a spermidine moiety by DHS and subsequent hydroxylation of the deoxyhypusine intermediate by deoxyhypusine hydroxylase (DOHH) (Park, 2006). In archaea aIF5A exists in both hypusinated and deoxyhypusinated forms (Park et al, 2010). While the modification in eIF5A is essential in eukaryotes (Park et al, 2010; Schnier et al, 1991), the deletion of EF-P or of the EF-P-modifying enzymes EpmA or EpmB but not EpmC in bacteria results in pleiotropic phenotypes reducing the general fitness: growth defects (Abratt et al, 1998; Balibar et al, 2013; Charles & Nester, 1993; Iannino et al, 2012; Kaniga et al, 1998; Peng et al, 2001), changed susceptibility to a wide range of external stressors such as antibiotics (Abratt et al, 1998; Balibar et al, 2013; Bearson et al, 2011; Iannino et al, 2012; Navarre et al, 2010; Zou et al, 2012), motility defects (Bearson et al, 2011) and the reduction of the virulence potential (Charles & Nester, 1993; Iannino et al, 2012; Kaniga et al, 1998; Marman et al, 2014; Navarre et al, 2010; Peng et al, 2001) observed in a great range of organisms (*E. coli, P. aeruginosa, S. typhimurium, Bacillus subtilis, A. tumefaciens, Shigella flexneri* and *Brucella abortus*).

EF-P was identified in 1975 as a protein which increases the yield of formylmethionyl-puromycin (fMet-Pmn) (Glick & Ganoza, 1975). In the following, EF-P was shown to stimulate poly-Phe/Lys synthesis and the translation of a natural mRNA (Aoki et al, 1997; Aoki et al, 2008; Ganoza & Aoki, 2000; Ganoza et al, 1985; Glick & Ganoza, 1975; Glick & Ganoza, 1976; Green et al, 1985). However, the identified effects were relatively small (up to 2-fold) and their cellular relevance remained unclear. Based on biochemical and structural investigations, EF-P was proposed to position the $tRNA^{fMet}$ in the P site (Aoki et al, 2008; Blaha et al, 2009) or to promote the first peptide bond (Blaha et al, 2009; Glick & Ganoza, 1975). For a/eIF5A serveral functions have been proposed, e.g. to promote the formation of the first peptide bond, the translation of certain mRNAs, to affect peptide release and to influence cell-cycle progression as well as mRNA decay (reviewed in (Zanelli et al, 2006)). Inactivation of eIF5A leads to accumulation of polysomes and increased ribosome transit times, which indicates that the factor is involved in translation elongation (Gregio et al, 2009; Saini et al, 2009). However, the cellular concentration of EF-P in the cell (1/10 of ribosomes) (An et al, 1980) suggests that its function is not required in general but is restricted to a specific translational event (Saini et al, 2009) which remained unknown.

1.3 Proline

During the course of this thesis the function of EF-P in facilitating translation of polyproline motifs was discovered by us (Doerfel et al, 2013) and others (Ude et al, 2013) and was further validated for EF-P and eIF5A (Bullwinkle et al, 2013; Gutierrez et al, 2013; Peil et al, 2013; Woolstenhulme et al, 2013) (see Discussion). For better understanding why efficient translation of proline runs needs EF-P, it is important to introduce stereo-electronic properties of proline.

Proline is the only proteinogenic imino acid with its five-membered ring spanning the α-carbon (C_α) and the amino group. The cyclic side-chain limits the number of accessible conformations of the prolyl ring by restricting the torsion angle of the N–C_α bond (ϕ = -63 and -75). The prolyl ring can adopt two main conformations with the C_γ puckered away or towards the carboxyl group (*exo* or *endo* conformation, respectively; Fig. 5A) (Ramachandran et al, 1970). Furthermore, proline restricts the backbone conformation of neighboring residues (MacArthur & Thornton, 1991). It influences the torsion angle of the preceding peptide bond by allowing a 180° rotation around the peptide bond resulting in two distinct isomeric states named *cis* and *trans* (Fig. 5B) (Brandts et al, 1975; Grathwohl & Wuthrich, 1976; Pal & Chakrabarti, 1999; Reimer et al, 1998).

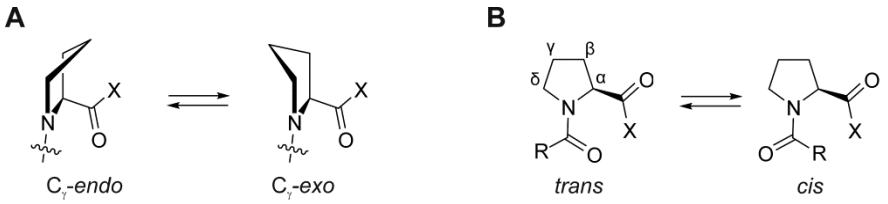

Fig. 5: Steric properties of the prolyl ring

A) *Endo* and *exo* puckered prolyl ring. B) *Cis* and *trans* isomers of proline with R and X representing the N- and C-terminal peptide chain, respectively.

While other proteinogenic amino acids sterically favor the *trans* conformation, *cis* and *trans* isomers of proline are almost isoenergetic (ΔG ~0.7 kcal/mol difference) (Owens et al, 2007). However, isomerization is rather slow and kinetically unfavorable ($\Delta G^{\neq}$ ~20 kcal/mol) (Fischer et al, 1994). Notably, less than 10% of Xaa-Pro bonds in protein structures adopt the *cis* conformation (reviewed in (Dever et al, 2014; Yaron & Naider, 1993)). Due to its steric restrictions and its limited ability to participate in hydrogen bonding proline is rarely found in α-helical structures and not in β-sheets. When proline is not located in the first turn of an α-helix it produces a significant bent (Barlow & Thornton, 1988). Proline is often found in irregular structures such as β-turns, α-helical capping motifs and polyproline helices (Bhattacharyya & Chakrabarti, 2003; Chakrabarti & Pal, 2001; MacArthur & Thornton, 1991) illustrating proline's impact on protein folding and secondary structure (Brandts et al, 1975; Craveur et al, 2013; Raleigh et al, 1992). Moreover, the conformation of the prolyl ring can influence the stability of secondary structures as demonstrated for collagen, which is

the most stable when its Pro-Pro-Gly repeats comprise an *endo*- followed by an *exo*-puckered proline which is strengthened by 4-R-hydroxylation of the middle proline residue (Berg & Prockop, 1973; Vitagliano et al, 2001). On the other hand, proline introduces structural flexibility due to its propensity to *cis-trans* isomerize; this phenomenon can mediate e.g. channel opening, as described for 5-hydroxytryptamine type 3 receptors (Lummis et al, 2005), and can regulate autoinhibition control of the eukaryotic Crk adaptor protein (Sarkar et al, 2007; Xia & Levy, 2014), protein dimerization (Jenko Kokalj et al, 2007; Solbak et al, 2010) and membrane binding (Evans & Nelsestuen, 1996) by providing isomer-dependent binding interfaces (reviewed in (Craveur et al, 2013)).

Despite or perhaps because of these properties defining its functional relevance, proline has a low reactivity in peptide bonds formation as peptidyl acceptor (Johansson et al, 2011; Pavlov et al, 2009) as well as peptidyl donor (Muto & Ito, 2008; Rychlik et al, 1970; Wohlgemuth et al, 2008): while other amino acids have a similar reactivity as P-site substrate (within a ~ 10 fold difference range among them) proline is ~700-fold slower than the fastest measured amino acid (Wohlgemuth et al, 2008). In line with its low reactivity, proline can induce ribosomal stalling at APP or WPP/P sequences during elongation (Tanner et al, 2009; Woolstenhulme et al, 2015; Woolstenhulme et al, 2013). In addition, in mammalian cells PPD and PPE were identified to induce ribosome accumulation (Ingolia et al, 2011). Furthermore, C-terminal prolines in a nascent peptide reduce termination efficiency (Björnsson et al, 1996; Hayes et al, 2002; Sunohara et al, 2002; Tanner et al, 2009) and increase stop codon read-through (Mottagui-Tabar et al, 1994). Consistently, proline is statistically underrepresented at the -1 position of UAA stop codons in *E. coli* (Arkov et al, 1993). Finally, proline is the C-terminal residue of the TnaC leader peptide which induces translational stalling (Cruz-Vera et al, 2006) and unreactive Pro-tRNA^{Pro} in the A site is required for SecM-mediated stalling (Muto et al, 2006). Notably, ribosome stalling upon synthesis of these two leader peptides involves interactions of the nascent chain with the ribosomal exit tunnel in addition to the presence of Pro-tRNA^{Pro} (Cruz-Vera et al, 2006; Muto et al, 2006). Importantly, the amino acid and not the tRNA^{Pro} are essential for stalling (Hayes et al, 2002; Pavlov et al, 2009; Tanner et al, 2009). Possible explanations for proline's poor reactivity in the A site are steric constraints originating from the cyclic prolyl ring and a reduced chemical reactivity of the secondary amine compared to the primary amine in all other proteinogenic amino acids (Pavlov et al, 2009). Because in solution Pro-tRNA^{Pro} has a similar reactivity compared to other aa-tRNAs (Hentzen et al, 1972), its poor reactivity as peptidyl-donor may derive exclusively from steric restrictions inherent to proline (Wohlgemuth et al, 2008) or induced by interactions with the ribosome. Thus, the conformational properties of proline may impose structural constrains on the positioning of proline, the nascent chain and the peptidyl-tRNA, thereby impairing the trajectory for nucleophilic attack (Hayes et al, 2002; Muto et al, 2006; Tanner et al, 2009). Notably, in model

peptides comprising a WPP motif CH···π interactions between the C_α-H of the first proline and the aromatic side chain of tryptophan were reported to stabilize the Trp-*cis*Pro-Pro conformation leading to a back-folded conformation (Ganguly et al, 2012) of this identified stalling motif (Tanner et al, 2009). Alternatively, proline may influence the ribosome conformation leading to slow peptide bond formation (Tanner et al, 2009).

1.4 Aims of the thesis

The primary aim of this study was to identify the function of EF-P in translation. Subsequent aims were to understand the reasons for proline-induced ribosome stalling and the mechanism of EF-P function in alleviating this stalling.

2 RESULTS

2.1 The catalytic function of EF-P

2.1.1 Initiation

To test whether EF-P influences the recruitment of the initiator tRNA (fMet-tRNA^{fMet}) during translation initiation or stabilizes fMet-tRNA^{fMet} on the small ribosomal subunit to support IC formation, 30S initiation complex formation was monitored in the presence and absence of EF-P (Fig. 6A). For this purpose, activated 30S subunits were mixed with mRNA, initiation factors, GTP and different concentrations of f[^{3}H]Met-tRNA^{fMet} and the formation of 30S ICs in the presence or absence of EF-P was quantified by nitrocellulose filtration followed by [^{3}H] scintillation counting (Materials & Methods). These experiments demonstrated that EF-P influences neither the affinity of initiator tRNA ($K_{1/2(\text{without EF-P})}$= 0.081 µM; $K_{1/2(\text{with EF-P})}$= 0.084 µM) nor the efficiency of 30S IC formation (61 and 59% of 30S IC formation in the presence and absence of EF-P, respectively). This indicates that EF-P is not required for 30S IC formation in general. This is corroborated by a chase experiment where 30S ICs containing ^{3}H-labeled fMet-tRNA^{fMet} were mixed with excess of unlabeled fMet-tRNA^{fMet}. The following exchange of bound ^{3}H-labeled initiator tRNA by unlabeled tRNA was virtually identical in the presence and absence of EF-P (Ingo Wohlgemuth, unpublished).

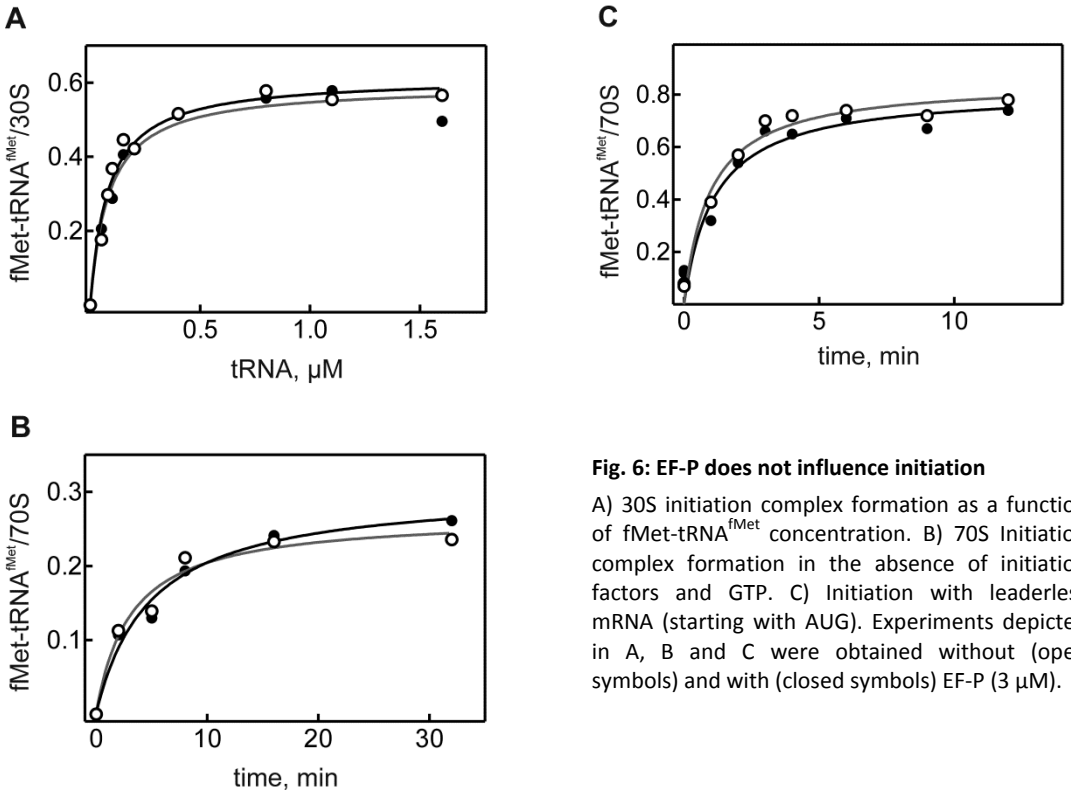

Fig. 6: EF-P does not influence initiation

A) 30S initiation complex formation as a function of fMet-tRNA^{fMet} concentration. B) 70S Initiation complex formation in the absence of initiation factors and GTP. C) Initiation with leaderless mRNA (starting with AUG). Experiments depicted in A, B and C were obtained without (open symbols) and with (closed symbols) EF-P (3 µM).

Finally, EF-P was also not found to have any influence on 70S IC formation in the absence of initiation factors and GTP (Fig. 6B), further supporting the notion that EF-P has no critical function in

translation initiation. To investigate whether EF-P has a function in non-canonical initiation pathways, initiation at an mRNA lacking the 5' Shine-Dalgarno sequence and immediately starting with the AUG codon was monitored. Initiation at this so called leaderless mRNA is regulated by the ratio of IF2 and IF3 with IF2 increasing and IF3 decreasing the efficiency of initiation (reviewed in (Moll et al, 2002)). Initiation at the leaderless mRNA in the presence of IF1, 2 and 3 was not affected by EF-P (Fig. 6C), indicating that EF-P is also not required in this initiation pathway.

2.1.2 Elongation

2.1.2.1 The P-site substrate

To test whether EF-P acts in translation elongation, di-/tri-peptide formation with various P-site substrates and puromycin as A-site substrate in the presence and absence of EF-P was investigated (Fig. 7). If not stated otherwise all experiments were performed with lysylated and hydroxylated EF-P. Puromycin (Pmn; 3'-deoxy-N,N-dimethyl-3'-[(O-methyl-L-tyrosyl)amino]adenosine) is an antibiotic that mimics the acceptor arm of aa-tRNA and does not require mRNA decoding for productive binding to the ribosome (Katunin et al, 2002; Sievers et al, 2004). Accordingly, the chemistry of peptide bond formation can be monitored, as it is not masked by a slower preceding step (e.g. decoding and tRNA accommodation in the A site). To cover a broad range of amino acids with different reactivities (Wohlgemuth et al, 2008), fMet-tRNA^{fMet} or fMet-Xaa-tRNA^{Xaa} with Xaa corresponding to Gly, Pro, Phe, Val, Trp, Lys, Arg, Gln, Glu and Asp were used as P-site substrates. In order to monitor effects on the affinity and reaction catalysis, subsaturating Pmn concentrations were used (Katunin et al, 2002).

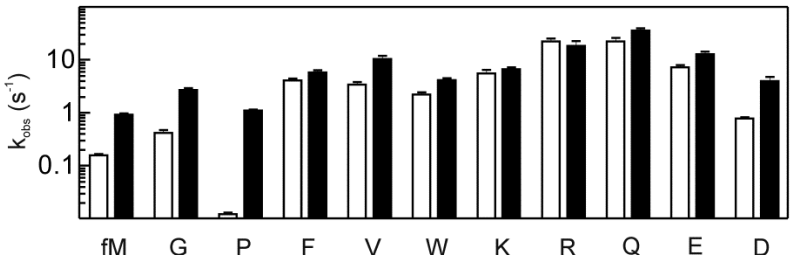

Fig. 7: Influence of EF-P on di- and tripeptide formation with Pmn

Rates of peptide bond formation between fMet-tRNA^{fMet} or fMet-Xaa-tRNA^{Xaa} and subsaturating Pmn, where Xaa stands for different amino acids indicated in single letter code, in the absence (white bars) or presence (black bars) of EF-P. The reaction was performed in buffer A at 37 °C.

Purified initiation or post-translocation complexes (ICs or PTCs) were mixed with Pmn (Katunin et al, 2002). The reaction was stopped after variable incubation times, the tRNA hydrolyzed and educts (fMet-Xaa) and products (fMet-Xaa-Pmn) were separated by reverse phase chromatography followed by their quantification based on ^{3}H or ^{14}C labeled amino acids using scintillation counting (Materials & Methods). The kinetic range of fMet-Xaa-Pmn formation spanned three orders of magnitude with

Xaa = Pro (k_{obs}= 0.012 ± 0.001 s^{-1}) being the slowest and Xaa = Arg/Gln (k_{obs}= 22 ± 4 s^{-1}) being the fastest P-site substrates (Table S1). The reactivity trends of the substrates are the same at saturating and subsaturating Pmn concentration (Wohlgemuth et al, 2008). In agreement with previous results (Glick et al, 1979; Saini et al, 2009), for most P-site substrates the reactions were not or only slightly stimulated by EF-P (up to 6-fold for fMet-Pmn, fMet-Gly-Pmn and fMet-Asp-Pmn formation). In contrast, fMet-Pro-Pmn synthesis was accelerated 85-fold by EF-P (Fig. 7, Table S1). fMet-Pro-tRNA^{Pro} is remarkably slow as peptidyl-donor compared to other P-site substrates (Muto & Ito, 2008; Wohlgemuth et al, 2008). The acceleration by EF-P rendered the rate comparable to that of other substrates and thus compatible with overall translation. This suggests a specific effect of EF-P in accelerating the reaction with an otherwise inefficient P-site substrate.

2.1.2.2 The A-site substrate

To analyze whether the effect of EF-P is observed also with native A-site substrates and whether it is sensitive to the A-site substrate identity, di- and tripeptide formation with different aminoacyl-tRNAs was monitored (Fig. 8, Table S2). Based on the hypothesis that EF-P accelerates peptide bond formation with poor substrates, the poor A-site substrates Pro-tRNA^{Pro} and Gly-tRNA^{Gly} (Johansson et al, 2011; Pavlov et al, 2009) were used. Phe-tRNA^{Phe} was used for comparison. Ribosome complexes containing either fMet-tRNA^{fMet} or fMet-Pro-tRNA^{Pro} in the P site were mixed with saturating ternary complex (TC) EF-Tu·GTP·aa-tRNA concentrations (Materials & Methods). Saturating concentrations were chosen to reflect the potential differences in the rates of peptide bond formation, rather than preceding steps during decoding. Time-resolved di-/tripeptide synthesis was monitored in the presence and absence of EF-P by quench flow technique. Amino acids, di- and tripeptides were separated by reverse phase chromatography and quantified by scintillation counting of ^{3}H- and ^{14}C-labeled amino acids (Materials & Methods).

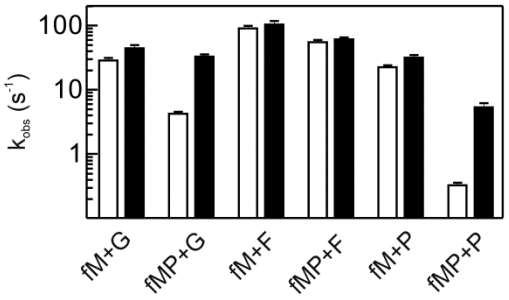

Fig. 8: Influence of EF-P on di- and tripeptide formation with native A-site substrates

Rates of peptide bond formation between fMet-tRNA^{fMet} (fM) or fMet-Pro-tRNA^{Pro} (fMP) in the P site and Gly-tRNA^{Gly}, Phe-tRNA^{Phe}, or Pro-tRNA^{Pro} (G, F, and P, respectively) in the A site in the absence (white bar) and presence (black bar) of EF-P. Reaction was performed in buffer B at 37 °C.

While there was almost no effect (less than two-fold) for most combinations, EF-P enhanced formation of fMet-Pro-Gly (fMP-G) and fMet-Pro-Pro (fMP-P) by 8- and 16-fold, respectively (Fig. 8, Table S2). This indicates that indeed specific amino acid combinations in the P and A sites require EF-P for rapid peptide bond formation. The acceleration by EF-P was particularly strong for the very

slow combinations Pro-Gly and Pro-Pro. Notably, the combination of two consecutive prolines is known to induce ribosome stalling (Tanner et al, 2009). This suggests that the acceleration by EF-P promotes the rapid incorporation of these otherwise unfavorable amino acid combinations.

2.1.2.3 Sequence context

To further investigate the amino acid sequence context which requires EF-P for efficient translation, the sequences fMPF, fMPGF, fMPPF, fMPPPF, fMPPGF and fMPPG were translated in the presence and absence of EF-P (Fig. 9). Based on the previous results, combinations of poor A- and P-site substrates were chosen. By contrast, Phe-tRNA^{Phe} is a good A-site substrate (Johansson et al, 2008; Wohlgemuth et al, 2010) which simplifies chromatographic separation of educts and products due to its hydrophobic character and enables the quantification of full-length peptides such as fMPPF and fMPPPF. In contrast to the previous experimental setup the reaction was started by mixing initiation complexes with EF-G and ternary complexes corresponding to the respective mRNA. Thus, the reaction comprises all steps of multiple consecutive elongation cycles. In contrast to the previous experiment, subsaturating concentrations of TCs were used to reflect more *in-vivo* like conditions.
The translation kinetics varied substantially depending on the peptide sequence (Fig. 9, Table 1).

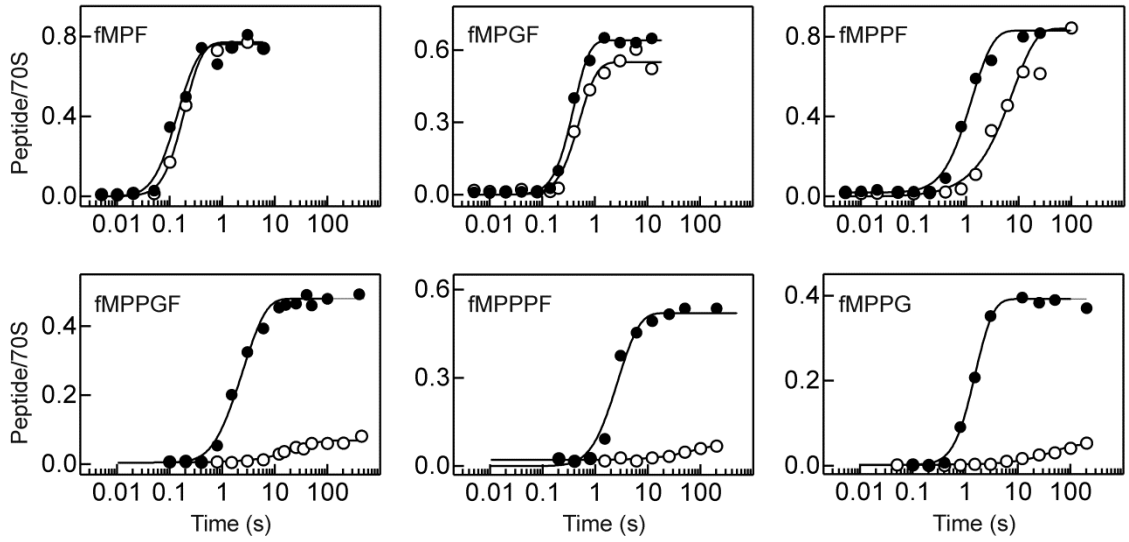

Fig. 9: Oligopeptide formation in the presence and absence of EF-P

Time-resolved formation of model oligopeptides in a reconstituted translation system in the absence (open circles) and presence (closed circles) of EF-P. For rates, see Table 1. Model peptides are indicated in the left corner of each panel and were quantified based on the incorporation of the last amino acid.

In contrast to the previous assay where Pro-Gly formation was stimulated by EF-P (Fig. 8), synthesis of fMPF and fMPGF were not or only marginally influenced by EF-P. This could be explained by an EF-P independent step such as tRNA binding/accommodation and translocation which became rate-limiting under the new conditions. The synthesis of fMPPF was 30-fold slower compared to synthesis of fMPF which might be caused by the combination of poor A- and P-site substrates or indicate that

the reactivity of a Pro can be reduced by a preceding Pro (see also section 2.2.1.4). The reaction was accelerated approximately 5-fold by EF-P which reduced the rate difference between fMPPF and fMPF considerably (from 30- to 9-fold).

In the absence of EF-P only small amounts of fMPPGF, fMPPPF and fMPPG peptides were synthesized at slow rates (Fig. 9, lower panel). Notably, the amount of final product could not be increased by longer incubation times indicating either very strong stalling or the occurrence of side reactions such as drop-off of the tRNA, frameshifting or inactivation of ribosomes/TC (see below). The addition of EF-P accelerated the reaction and increased the amount of final products significantly. These results show that the above identified sequences PPP and PPG are targets for EF-P in a more complex translation system.

Table 1: Oligopeptide formation

	k_{obs}, s^{-1}		acceleration
	no EF-P	**EF-P**	**by EF-P**
fMPF	4.2 ± 0.6	6 ± 1	1.4
fMPGF	1.5 ± 0.3	2.0 ± 0.3	1.3
fMPPF	0.14 ± 0.03	0.7 ± 0.1	5
fMPPG	0.02 ± 0.01	0.56 ± 0.04	28
fMPPGF	0.03 ± 0.01	0.36 ± 0.04	12
fMPPPF	0.015 ± 0.004	0.30 ± 0.06	20

IC (0.2 µM final) vs. TC (2 µM each) in the presence of EF-G (1 µM) ± EF-P (3 µM). The reactions were performed in buffer B at 37 °C.

2.1.2.4 Proline induced stalling leads to peptidyl tRNA dissociation

Short peptidyl-tRNAs tend to dissociate from the ribosome (Heurgue-Hamard et al, 1998; Karimi & Ehrenberg, 1996; Karimi et al, 1998). Because fMPPGF, fMPPPF and fMPPG peptide translation was very slow (Table 1), the low yield of final product could be due to a drop-off of the peptidyl-tRNA from the ribosome prior to incorporation of the last amino acid. To test this possibility, the stability of peptidyl-tRNA binding to the ribosome during the synthesis of fMPPG and fMFFF was monitored over time (section 2.1.2.3) by nitrocellulose filter binding (Materials & Methods).

For fMPPG the ratio of fMPP/ribosome decreased with time in the absence of EF-P (Fig. 10). This indicates a spontaneous dissociation of the fMPP-$tRNA^{Pro}$ from the ribosome which reduces the yield of fMPPG peptide. With EF-P the ratio fMPP/ribosome stayed constant leading to efficient fMPPG synthesis. In the control with fMFFF-$tRNA^{Phe}$, peptidyl-tRNA remained stably bound to the ribosome, even in the absence of EF-P. These data indicate that EF-P can stabilize the peptidyl-$tRNA^{Pro}$ in the P site and thus extends the time window for peptide bond formation between the poor substrates fMetProPro-$tRNA^{Pro}$ and Gly-$tRNA^{Gly}$ (see also sections 2.2.1-2.2.3).

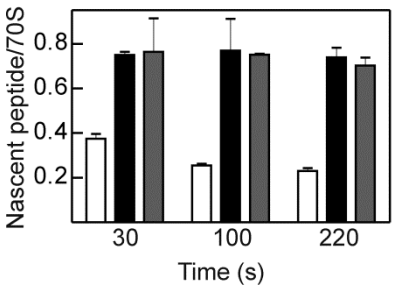

Fig. 10: Drop-off of peptidyl-tRNA from the ribosome

Ribosome-bound fraction of short peptidyl-tRNAs resulting from translation of fMPPGF in the absence (white bars) or presence (black bars) of EF-P (3 µM) or of fMFFF in the absence of EF-P (gray bars). Peptides were labeled with f[^{14}C]Met and [^{14}C]Pro (fMPPG) or f[^{3}H]Met and [^{14}C]Phe (fMFFF). Error bars represent standard deviations (SD) from three replicates.

2.1.2.5 EF-P alleviates Pro-induced ribosome stalling in longer model peptides

To test whether the identified Pro-containing sequences can induce ribosome stalling in a larger sequence context and whether stalling can be alleviated by EF-P, the *in-vitro* translation of the model protein PrmC was investigated (Fig. 11). For this purpose, mRNAs encoding PG, PP, PPG, and PPP sequences at positions 19-22 of a 75 amino acids (aa) long N-terminal fragment of the protein PrmC were engineered. Initiation complexes were prepared using the mRNA of the desired sequence and fluorescence-labeled BodipyFL-Met-tRNA^{fMet} (BOF-Met-tRNA^{fMet}). The reaction was started by mixing ICs with EF-Tu·GTP, total aa-tRNAs and EF-G. The translation products were separated by SDS-PAGE and visualized by BOF fluorescence detection (Materials & Methods). To estimate the length of the predominant peptide products and thus the position of pause sites, PrmC peptide markers of different length were generated and visualized on the same SDS-PAGE.

Wild type prmC, which contains no potential stalling site, was rapidly translated to the full-length product independently of EF-P (Fig. 11). Synthesis of PrmC containing a Gly residue after the native Pro20 was slowed down as visualized by the appearance of a peptide of approx. 20 aa in length. However, this translational pausing was transient and independent of EF-P. Instead, two consecutive Pro residues at position 19 and 20 induced a stronger pausing event which was less pronounced in the presence of EF-P. When PPG or PPP motifs were introduced into the sequence, translation was strongly affected: in the absence of EF-P these sequences led to robust stalling with essentially no full-length product formation. In the presence of EF-P translation proceeded without remarkable pausing events, resulting in the formation of the full-length product.

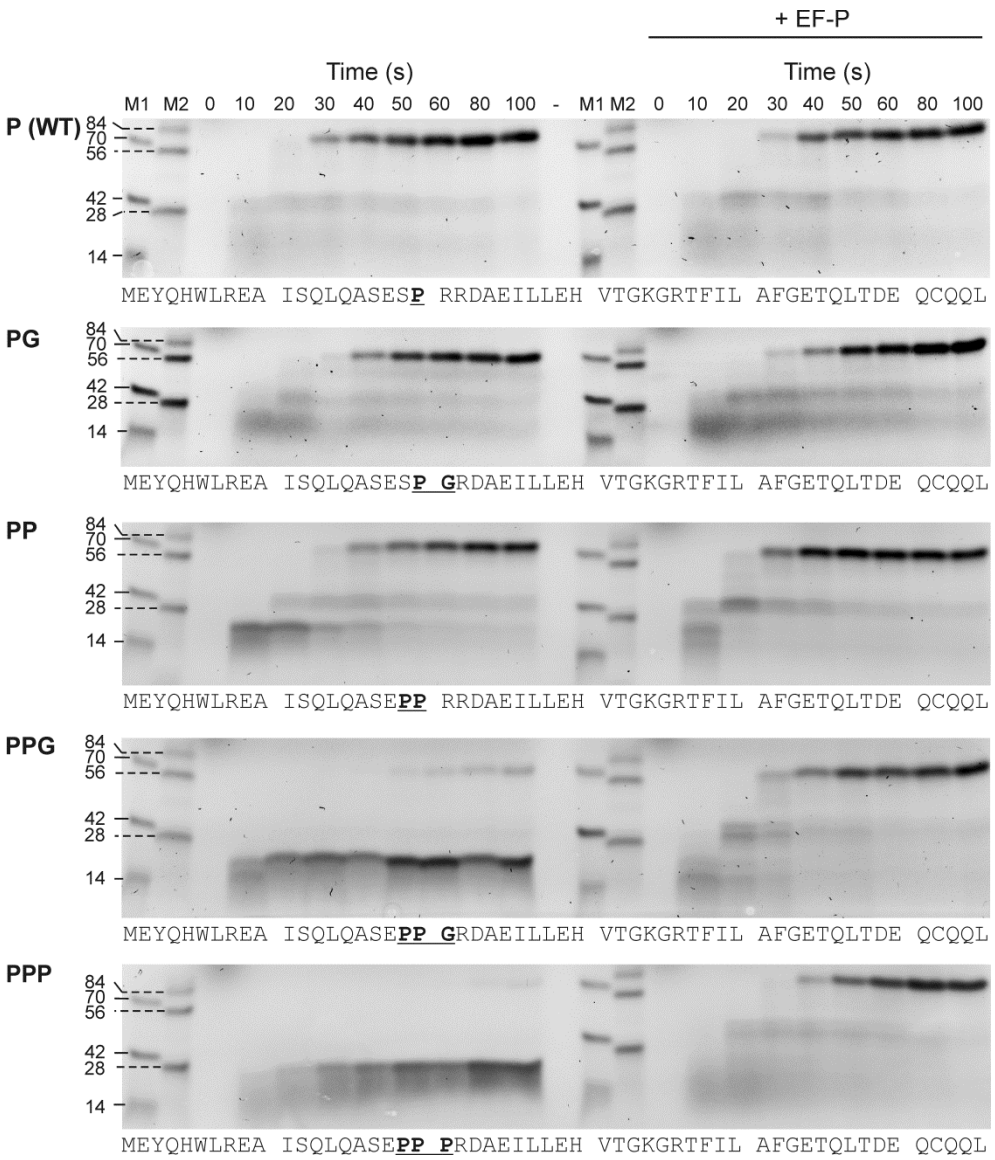

Fig. 11: EF-P prevents ribosome stalling on PPG and PPP sequences engineered into PrmC.

Translation of the N-terminal domain of PrmC (75 amino acids) with wild-type (wt) or mutant sequences containing PG, PP, PPG or PPP in the absence (left time course) or presence (right time course) of EF-P. Peptides were separated by SDS-PAGE and visualized by the fluorescence of BOF attached to the N-terminus of the peptides. M1 and M2 are peptide markers for PrmC fragments of the indicated number of amino acids.

2.1.2.6 Ribosomes stall at PP/G and can be rescued by EF-P

To identify the exact stalling position upon translation of a PPG motif the translation of PPG containing prmC was repeated in the absence of EF-P with radioactively labeled [^{3}H]Gly-tRNA^{Gly} and [^{14}C]Pro-tRNA^{Pro} (section 2.1.2.5, Materials & Methods). This allows quantifying the amount of proline and glycine residues in relation to each other at a specific time point of translation (90 s). To determine the ratio of proline and glycine residues bound to the P- and A-site tRNAs, stalled ribosome-nascent chain complexes were purified by size exclusion chromatography (SEC) (Fig. 12 A). To determine the amino acid composition of the nascent peptide, the peptide was hydrolyzed from its tRNA and separated from single amino acids by HPLC (Materials & Methods). The ratio Gly:Pro

bound to the ribosome was 0.47 which corresponds to one glycine and two proline residues and is in good agreement with a ribosome stalling at the PPG sequence (Fig. 12B). Notably, a faint band corresponding to 14% of expected full-length product was quantified on the translation gel after 100 s (Fig. 11). Considering that the entire peptide contains four Gly residues, the Gly:Pro ratio of 0.47 would correspond to 14% PPGGGG (full-length product), 38% PPG and 48% PP bound to the ribosome. In the nascent peptide the Gly:Pro ratio was 0.26 (Fig. 12B) and clarifies the distribution of Pro and Gly residues bound to P- and A-site tRNAs: considering the 14% full-length peptide formed at 100 s the Gly:Pro ratio in the remaining stalling peptide is 0:2 corresponding to two proline and no glycine residues. Thus, ribosome stalling occurs with a peptidyl-ProPro-tRNA^{Pro} in the P site and Gly-tRNA^{Gly} in the A site. These data show that EF-P facilitates peptide bond formation involving the poor substrates Pro and Gly in a larger sequence context thereby alleviating translational stalling at polyproline sequences.

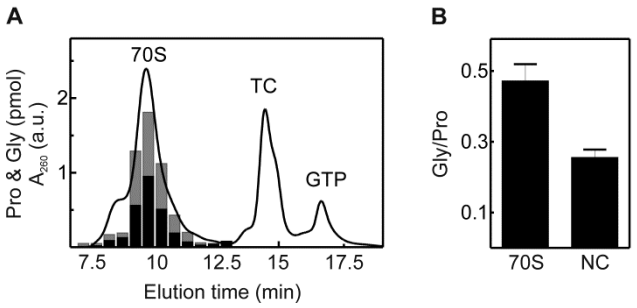

Fig. 12: Identification of the stalling site in PrmC

A) Chromatographic separation of a ribosome-nascent chain complex stalled during synthesis of PPG containing PrmC from TC and free aa-tRNA by gelfiltration. Elution profile (black line); retention of ribosome-bound [^{14}C]Pro (grey bars) and [^{3}H]Gly (black bars). B) Gly/Pro stoichiometry on the ribosome (70S) and in the nascent chain (NC). According to the sequence PPG the stoichiometry Gly/Pro should be 0.5 or less if Gly is not incorporated. The experiment was performed and analyzed together with Ingo Wohlgemuth.

To test whether stalled ribosomal complexes could be rescued by EF-P, translation of PrmC containing a PPP motif was monitored in the absence of EF-P, in the presence of EF-P and with delayed addition of EF-P, after robust stalling had occurred (Fig. 13). In the absence and presence of EF-P translation proceeded as seen in Fig. 11, with robust stalling in the absence of EF-P and efficient translation of full-length peptide in the presence of EF-P. The delayed addition of EF-P alleviated ribosome stalling, such that a considerable amount of full-length product was synthesized within 20 s. In line with the observation that peptidyl-tRNA drop-off decreases for longer peptides (Heurgue-Hamard et al, 1998), the ~20 amino acids-long peptidyl-tRNA^{Pro} appears to remain bound to the ribosome. Hence, binding of EF-P to the stalled ribosomal complex restores translation. This also shows that the ribosomes do not undergo inactivation upon stalling.

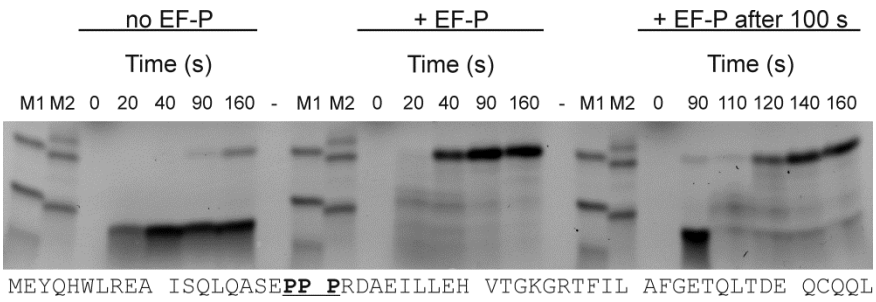

Fig. 13: Rescue of stalled ribosomes by EF-P

Translation products of mutated prmC encoding a PPP motif were separated on SDS-PAGE. The translation was performed in the absence and presence of EF-P as well as with a delayed addition of EF-P after 100 s of reaction without EF-P, as indicated.

2.1.2.7 EF-P enhances synthesis of E. coli proteins containing polyproline motifs

Proline-induced ribosome stalling is strongly affected by the amino acid sequence context (Peil et al, 2013; Starosta et al, 2014; Tanner et al, 2009; Woolstenhulme et al, 2013). Hence, the question arises whether native proteins containing polyproline stretches evolved sequences which reduce stalling at polyproline motifs or whether their synthesis relies on EF-P. Sequence analysis of *E. coli* K12 genes revealed that ~ 100 *E. coli* proteins contain three or more consecutive prolines and ~180 contain at least one PPG motif. To test whether EF-P is required for efficient synthesis of these proteins, the synthesis of TonB, YafD (75 amino acid long N-terminal fragment), Rz1 and AmiB (1-159 aa) (Fig. 14) as well as EspfU (1-154 aa), FlhC (1-94 aa) and Flk (1-87 aa) was investigated (Fig. 15), all containing polyproline motifs. Translation and analysis were performed as described for PrmC (section 2.1.2.5) but individual peptide markers were used for each protein.

In all cases translation in the absence of EF-P stalled at positions corresponding to the polyproline or PPG motifs. The pausing time correlated with the length of the polyproline stretch with moderate, transient pausing at PP, PPP or PPG (TonB, YafD, EspfU) and strong stalling at 5-8× Pro (Rz1 or AmiB) which did not permit formation of any full-length product (Fig. 14).

EF-P prevented ribosome stalling or strongly decreased the pausing time (Fig. 14 and Fig. 15, right panel). Translational pausing at positions other than the polyproline motifs was independent of EF-P. These data show that EF-P is specifically required to prevent ribosome stalling at polyproline stretches in the tested proteins and thus leads to efficient synthesis of full-length native proteins *in vitro*.

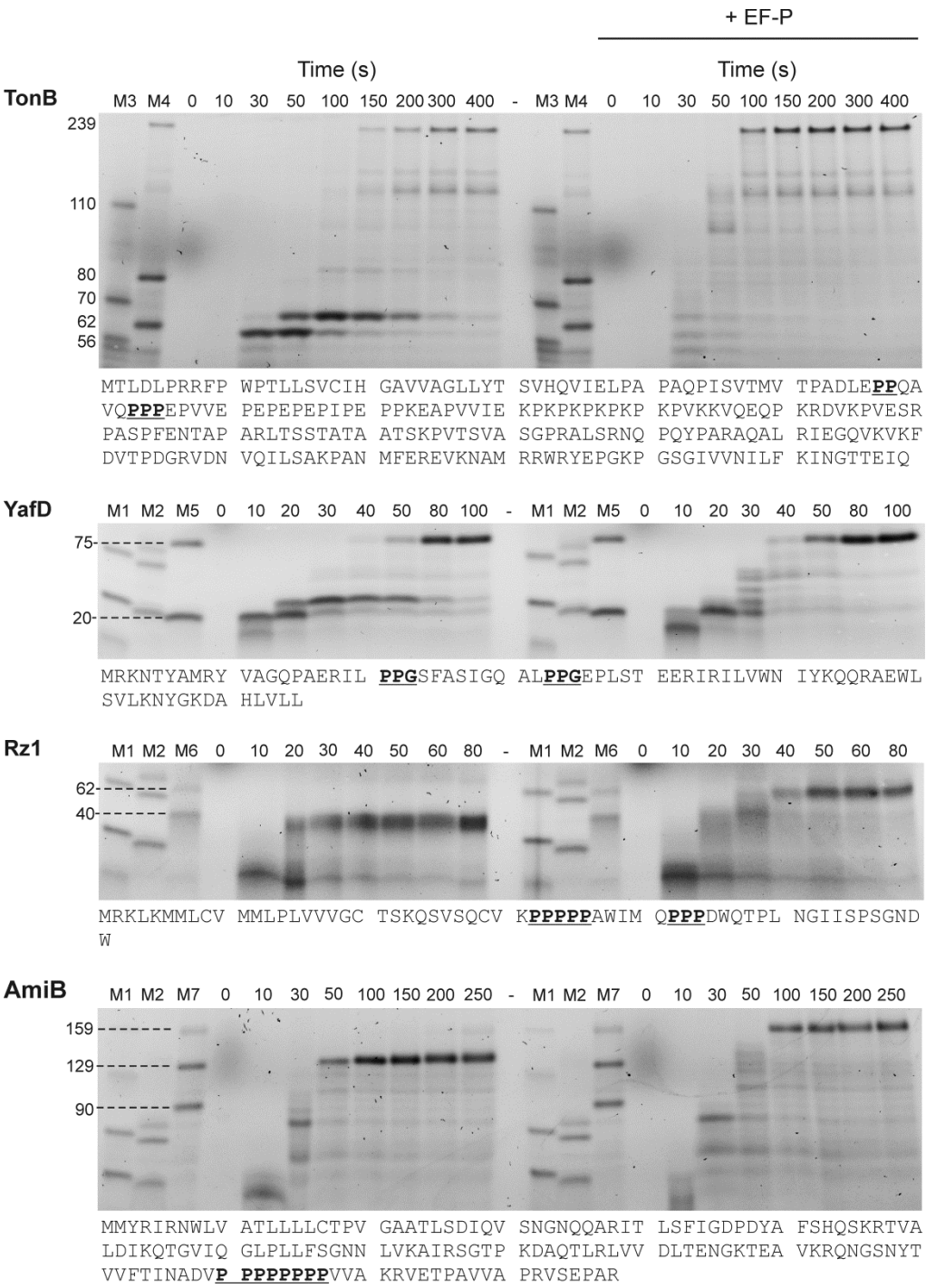

Fig. 14: EF-P alleviates PPP/PPG-induced stalling during synthesis of native *E. coli* proteins

Translation products of TonB (239 aa), YafD (75 aa from the N-terminus), Rz1 (62 aa), and AmiB (159 aa from the N-terminus) were separated by SDS-PAGE. M3, and M4, peptide markers containing TonB fragments of the indicated lengths. M5, M6, and M7, peptide markers of the indicated lengths of YafD, Rz1, and AmiB sequences, respectively. The sequence of the respective protein is shown below each gel.

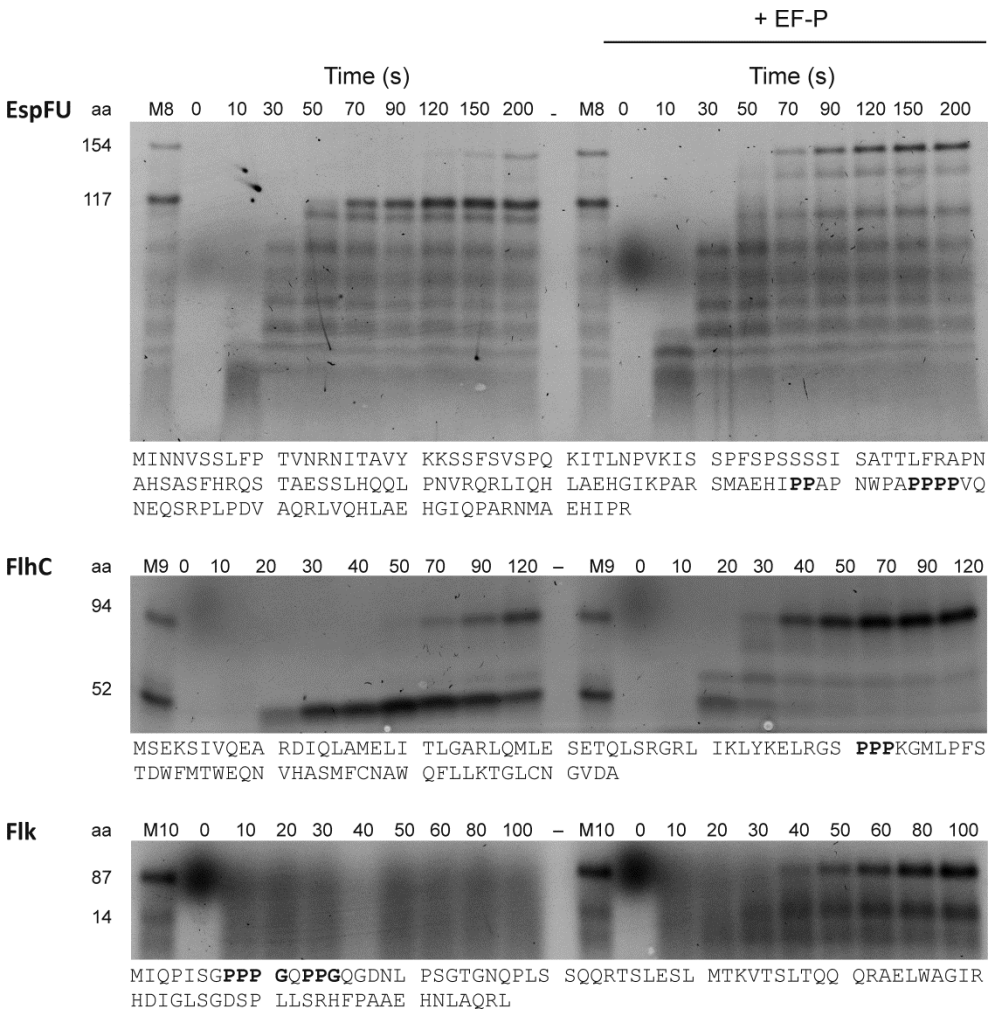

Fig. 15: *In-vitro* translation of proteins containing polyproline stretches

Translation products of EspfU (1-154 aa), FlhC (1-94 aa) and Flk (1-87 aa) were separated on SDS-PAGE. M8, 9, 10 and 11 correspond to peptide markers of the indicated length of EspfU, FlhC and Flk respectively. The sequence of the respective protein is shown below each gel.

2.1.2.8 Stalling is mainly caused by the Pro moiety of Pro-tRNA^{Pro}

Peptidyl transfer to Pro-tRNA^{Pro} is similar for the Pro codons CCA, CCU and CCG when exposed in the A site but two times slower for CCC (Pavlov et al, 2009). Additionally, tRNA isoacceptors have different abundance (Dong et al, 1996). Thus, proline-induced stalling might be codon-dependent i.e. caused by variable codon-anticodon interactions or caused by starvation of the tRNA isoacceptor corresponding to the mRNA codon exposed in the A site. To investigate these possibilities, four prmC constructs were generated containing a PPP motif encoded by a cluster of one of the four Pro-codons. If proline-induced stalling depends on the Pro codon or the tRNA isoacceptor, the synthesis pattern should differ in the absence of EF-P. If the EF-P function depends on one of these factors the translation of the full-length product should differ for the prmC constructs. The time-resolved *in-vitro* translation of these constructs in the presence and absence of EF-P revealed an almost identical pattern of stalling and full-length product formation (Fig. 16A). In order to extract the rates of

product formation, bands referring to stalling and full-length products were quantified densiometrically (Fig. 16B,C). Stalling-products in the absence of EF-P were formed at similar rates with all codons (0.04 ± 0.004 s^{-1}), indicating that the stalling efficiency was independent of the codon encoding proline. In the presence of EF-P, also the full-length products were formed at similar rates with all codons (0.03 ± 0.07 s^{-1}) suggesting that EF-P recognized all isoacceptors of $tRNA^{Pro}$.

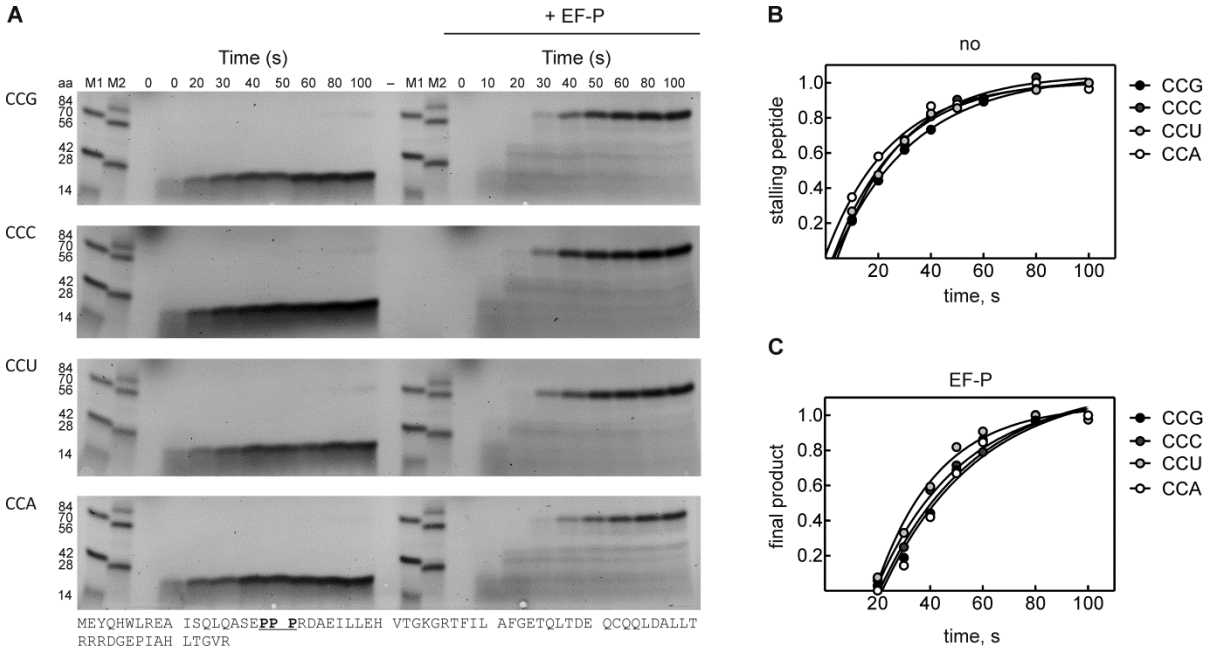

Fig. 16: *In-vitro* translation of PrmC containing a PPP motif encoded by different Pro-codons

A) Translation products of PrmC containing a PPP motif, with Pro being encoded by three CCG, CCC, CCU or CCA codons in the presence and absence of EF-P. M1 and M2 are PrmC peptide markers of the indicated lengths. B,C) Translation kinetics monitored in (A), visualized by quantification of stalling peptides without EF-P (B) and full-length products in the presence of EF-P (C). The density of product bands were normalized to the total density in the respective line and shown relative to the band intensity at 100 s.

To analyze the influence of the tRNA identity on peptide bond formation with proline, $tRNA^{Phe}$ was misaminoacylated with proline (Materials & Methods) and the reactivity of Pro-$tRNA^{Phe}$ in fMet-Pro-Pmn (fMP-Pmn) formation was analyzed (Fig. 17). To avoid interference of the misaminoacylated tRNA in decoding (Pavlov et al, 2009) PTCs with f[^{3}H]Met-[^{14}C]Pro-$tRNA^{Phe}$ or f[^{3}H]Met-[^{14}C]Pro-$tRNA^{Pro}$ in the P-site were mixed with subsaturating Pmn and fMP-Pmn formation was monitored (Fig. 17, Materials & Methods). Due to low quantities of misaminoacylated tRNA, the PTCs were used without purification. However, the usage of unpurified complexes did not influence translation kinetics measured in the absence of EF-P, as rates of both controls (purified or unpurified PTCs containing fMet-Pro-$tRNA^{Pro}$) were virtually identical (0.015 ± 0.001 s^{-1} and 0.014 ± 0.001 s^{-1}, respectively) and were consistent with rates determined previously (section 2.1.2.1). Surprisingly, fMet-Pro-Pmn formation with $tRNA^{Phe}$ followed two exponential kinetics with a dominant phase (k_{obs}= 0.02 s^{-1}, 81%) and a minor phase (k_{obs}= 0.7 s^{-1}, 19%) which could be explained by inhomogeneity of the complexes. The weighted average rate, corresponding to the overall half-time of the reaction

(k_{obs}= 0.14 s^{-1}) was 10-fold faster than that of the control reaction fMP-Pmn with $tRNA^{Pro}$, showing that $tRNA^{Phe}$ increased the rate of peptide bond formation with proline. However, the rate of fMP-Pmn formation from $tRNA^{Phe}$ was still 30-fold slower than the rate of fMF-Pmn formation (k_{obs}= 4.2 s^{-1}), suggesting that the poor reactivity of Pro-$tRNA^{Pro}$ is at least in part caused by the amino acid. Peptide bond formation with Pro-$tRNA^{Phe}$ as A-site substrate is ~7-fold slower than with Pro-$tRNA^{Pro}$ (Pavlov et al, 2009). Thus, the reduced reactivity of Pro-$tRNA^{Pro}$ compared to Pro-$tRNA^{Phe}$ as P-site substrate is compensated by its increased reactivity as A-site substrate. These results suggest that the main reason for stalling at PPP motifs is not the tRNA identity but the amino acid. Addition of EF-P accelerated both phases of fMP-Pmn formation with misaminoacylated tRNA by about 4-fold. However, compared to an 85-fold increase in the rate with $tRNA^{Pro}$ this effect is small. Furthermore, the weighted average rate in the presence of EF-P (k_{obs}= 0.5 s^{-1}) was two-fold slower than EF-P-catalyzed fMP-Pmn formation with $tRNA^{Pro}$ (k_{obs}= 1.1 s^{-1}). This might be rationalized by a reduced affinity of EF-P to $tRNA^{Phe}$.

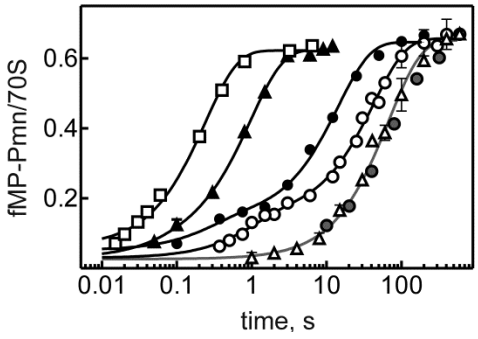

Fig. 17: Influence of the tRNA identity on peptide bond formation

Tripeptide formation between fMet-X-$tRNA^{Y}$ (0.15 µM) and subsaturating Pmn (1 mM), with X-$tRNA^{Y}$ being:
Pro-$tRNA^{Phe}$, unpurified PTC (white circles);
Pro-$tRNA^{Phe}$, unpurified PTC + EF-P (black circles);
Pro-$tRNA^{Pro}$, unpurified PTC (grey circles);
Pro-$tRNA^{Pro}$, purified PTC (white triangles);
Pro-$tRNA^{Pro}$, purified PTC + EF-P (black triangles);
Phe-$tRNA^{Phe}$, purified PTC (white squares).

Table 2: Influence of tRNA identity on the rate of peptide bond formation

X,Y	k_{obs}, s^{-1}		acceleration
	no EF-P	EF-P	by EF-P
Pro-$tRNA^{Pro}$	0.014 ± 0.05	1.1 ± 0.1	79
Pro-$tRNA^{Phe}$	0.14 ± 0.05	0.5 ± 0.2	3.6
	[0.02 ± 0.003 (81%); 0.7 ± 0.3 (19%)]	[0.07 ± 0.007 (85%); 2.8 ± 1.5 (15%)]	(3.5; 4)
Phe-$tRNA^{Phe}$	4.2 ± 0.3		

fMet-X-$tRNA^{Y}$ (0.15 µM) vs. subsaturating Pmn (1 mM) ± EF-P (3 mM). Reaction performed in buffer A at 37 °C.

2.1.3 Release

In addition to being a poor substrate in the peptidyl transferase reaction, proline reduces the efficiency of RF-catalyzed translation termination (Hayes et al, 2002; Mottagui-Tabar et al, 1994; Tanner et al, 2009). Furthermore, Pro is statistically underrepresented at the -1 position of UAA stop codons in *E. coli* (Arkov et al, 1993). To investigate whether EF-P influences termination efficiency at UAA stop codons following a proline codon, posttranslocation complexes with f[^{3}H]Met-[^{14}C]Pro-$tRNA^{Pro}$ in the P site and UAA codon in the A site were mixed with release factor 1 (RF1) in the absence and presence of EF-P (Fig. 18). The termination reaction was monitored by nitrocellulose

filtration (Materials & Methods). In the presence and absence of EF-P the kinetics of peptide release followed single exponential behavior (Fig. 18). The rate of peptide release by RF1 ((1.9 ± 0.3) $\times 10^{-3}$ s^{-1}) was increased by EF-P ((5.8 ± 0.7) $\times 10^{-3}$ s^{-1}) approximately three-fold. Comparable results were obtained with yeast eIF5A, which stimulates translation termination by two-fold (Saini et al, 2009). Compared to the almost 90-fold effect of EF-P on translation elongation, its influence on termination appears negligible. This interpretation is in line with reduced termination efficiency with C-terminal proline *in vivo*, i.e. with EF-P present (Hayes et al, 2002; Tanner et al, 2009). Thus, ribosomes trapped at Pro-stop cannot be released by EF-P but require the SmpB/tmRNA rescue mechanism (Hayes et al, 2002; Tanner et al, 2009).

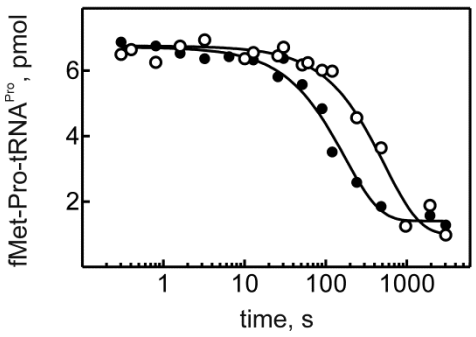

Fig. 18: EF-P in termination

RF1-catalyzed peptide release at posttranslocation complexes with fMet-Pro-tRNA^{Pro} in the P site and UAA stop codon exposed in the A site in the absence (open symbols) and presence (closed symbols) of EF-P.

2.2 Investigation of the catalytic mechanism of EF-P

The findings described in the previous sections raise two central questions: first, what makes proline a particularly poor substrate for peptide bond formation and second, how does EF-P facilitate peptidyl transfer with proline? In the following these question will be addressed by different approaches:

In section 2.2.1, the functions of EF-P in stabilizing the peptidyl-tRNA and accelerating peptide bond formation with poor substrates are further characterized and the importance of EF-Ps modification is investigated. In principle, EF-P can be considered as being composed of two functional parts, the EF-P body and the modification. Hence, functions performed by unmodified EF-P can be assigned to the body, while the functional difference of modified and unmodified EF-P can be assigned to the modification. Thus, comparison of the catalysis by modified and unmodified EF-P may allow drawing conclusions about these functional parts.

In section 2.2.2 the mechanism of EF-P is investigated. In addition to stabilization of the peptidyl-tRNA, the catalysis by EF-P may stem from positioning of the substrates/catalytic groups in an active conformation or from an active participation in the reaction chemistry, i.e. by donating functional groups into the active site. These questions are addressed by experiments that evaluate temperature

and pH dependences which should give insights in the activation parameters and involvement of EF-P in the chemistry step.

Section 2.2.3 deals with the question of whether the poor reactivity of Pro-tRNA^{Pro} in peptide bond formation is due to its intrinsic reactivity or induced by the ribosome. To investigate these possibilities the stereo-electronic properties of proline are modified by different substituents on the prolyl ring and subsequently compared to the changed reactivity in peptide bond formation and hydrolysis/aminolysis in solution.

2.2.1 The function of the EF-P body and the modification

2.2.1.1 EF-P modification increases its catalytic proficiency

In *E. coli* EF-P is posttranslationally modified at Lys34 which points into the direction of the peptidyl transferase center (Fig. 3E and Fig. 4, section 1.2) (Ambrogelly et al, 2010; Aoki et al, 2008; Peil et al, 2012; Roy et al, 2011; Yanagisawa et al, 2010). The modification is crucial for the factor's function (Bearson et al, 2011; Charles & Nester, 1993; Iannino et al, 2012; Navarre et al, 2010; Park et al, 2012; Peng et al, 2001).

To investigate the functional importance of the modification, the catalysis by EF-P in its modified and unmodified form was characterized. For this purpose, expression constructs containing either the gene encoding EF-P alone or EF-P together with different combinations of genes coding for EF-P-modifying enzymes (EpmA, B, C) were used (kindly provided by Frank Peske and modified by Christina Kothe, MPI-BPC, Göttingen; Materials & Methods). When EF-P is overexpressed alone, the protein remains mostly unmodified, presumably due to insufficient amounts of the modifying enzymes. Accordingly, only upon co-expression of EF-P with EpmA and EpmB the ratio of EF-P and its modifying enzymes is restored, which leads to efficient lysylation of EF-P (Ambrogelly et al, 2010; Bailly & de Crecy-Lagard, 2010; Doerfel et al, 2013; Park et al, 2012; Roy et al, 2011; Yanagisawa et al, 2010). Hydroxylation of Lys34 of EF-P is achieved by the additional co-expression of EpmC (Peil et al, 2012). Unmodified, lysylated and lysylated/hydroxylated EF-P were purified by affinity chromatography using an N-terminal histidine tag (Materials & Methods) and the modification state was verified by mass spectrometry (carried out by Ingo Wohlgemuth, MPI-BPC, Göttingen, Fig. S1). Comparison of lysylated/hydroxylated EF-P obtained by recombinant overexpression and by native purification from *E. coli* revealed that the modification state and the catalytic proficiency of the factor were independent of the purification method (Fig. S1, Fig. 19C). No difference between lysylated and lysylated/hydroxylated EF-P in facilitating fMPPG synthesis was observed (Fig. 19C), in agreement with the absence of a phenotype for the EpmC gene deletion in *S. typhimurium* (Bullwinkle et al, 2013); therefore the function of EF-P hydroxylation was not further investigated. Instead, all assays were performed either with unmodified or lysylated/hydroxylated EF-P. Functional

activity of unmodified EF-P was tested in the *in-vitro* translation system (described in section 2.1.2.5) and further characterized using the tetrapeptide formation approach (described in section 2.1.2.3).

In the *in-vitro* translation assay, unmodified EF-P facilitated synthesis of PrmC with an internal PPG motif, albeit less efficiently compared to modified EF-P (Fig. 19A, B). Pausing at PPG prior to continuation of synthesis of the full-length protein was longer in the presence of non-modified EF-P (+10 s) than with the modified EF-P. After overcoming the stalling, full-length peptide formation was essentially the same with unmodified and fully modified EF-P (0.029/0.03 ± 0.004 s^{-1}, respectively) which is in agreement with the notion that synthesis of proline-free sequences is independent of EF-P.

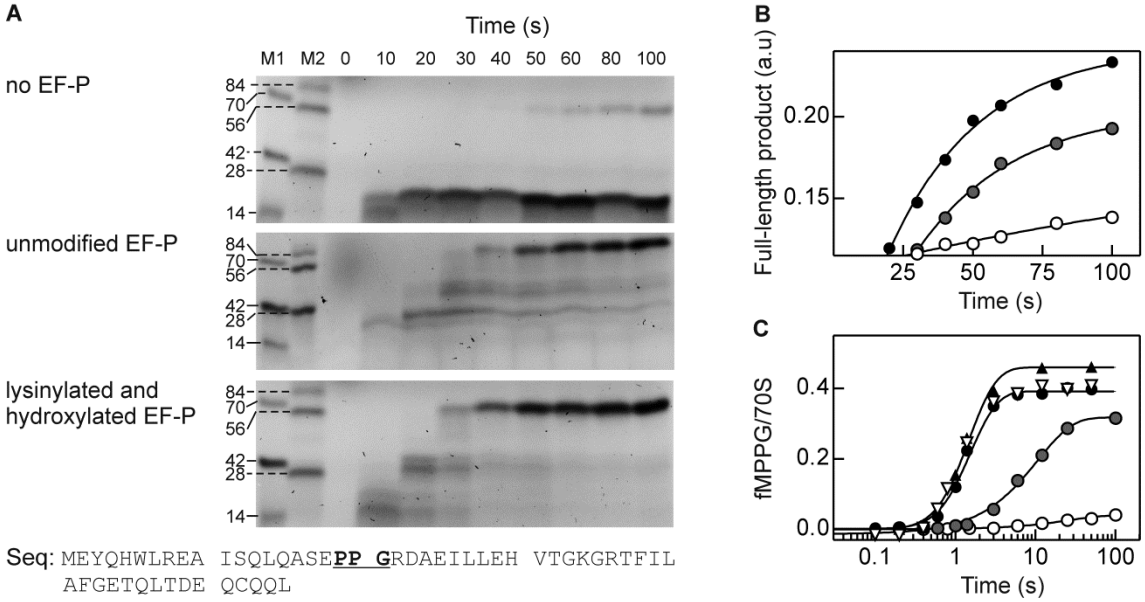

Fig. 19: Effect of the EF-P modification on the translation of the PPG motif

A) Synthesis of PrmC (75 aa from N-terminus) containing a PPG sequence. Synthesized peptides were separated by SDS-PAGE and visualized by fluorescence imaging. B) Quantification of full-length product seen in (A) obtained without EF-P (white circles), with unmodified EF-P (grey circles) and fully modified EF-P (black circles). The density of the product band was normalized to the total density in the respective lane and presented in arbitrary units (a.u.). C) fM-PPG synthesis without EF-P (white circles), with unmodified EF-P (grey circles), with lysylated EF-P (black triangles) and lysylated/hydroxylated EF-P (overexpressed: black circles, native: white triangles).

To identify the reason for the reduced activity of unmodified EF-P, the synthesis of the tetrapeptide fMPPG was investigated with modified and unmodified EF-P (Fig. 19C). This assay provides the precise quantification of the contribution of unmodified EF-P, as the translated sequence comprises the *bona fide* stalling site. Furthermore, the influence on tRNA stabilization/drop-off can be investigated. The reaction was performed as described in section 2.1.2.3 by mixing ICs with EF-G and TC(P,G) and monitors the time-resolved formation of the tetrapeptide. The rate of fMPPG synthesis in the presence of unmodified EF-P (0.12 ± 0.03 s^{-1}) was intermediate between the rates obtained without and with modified EF-P (0.02 ± 0.01 s^{-1} and 0.56 ± 0.04 s^{-1}, respectively) confirming a reduced activity of unmodified EF-P (Fig. 19C). Notably, unmodified EF-P strongly increased the yield of fMPPG peptide compared to the uncatalyzed reaction from ~10% to 74% of full-length product

obtained with modified EF-P. This indicates that unmodified EF-P is able to prevent peptidyl-tRNA drop-off from the ribosome. Apparently, the EF-P body can stabilize the peptidyl-tRNA in the P site (Fig. 19), while the modification additionally increases the catalytic effect of EF-P.

To characterize the functional contribution of the EF-P body and the modification in more detail, the EF-P concentration dependence of unmodified and modified EF-P on fMPPG formation was investigated (Fig. 20, Table S3). The concentration dependence of the rates as well as of the reaction end level yielded hyperbolic curves (Fig. 20C, D) that could be fitted to the Michaelis Menten formula extended by an offset that reflects the EF-P-uncatalyzed reaction $Y_{(EF-P)} = \frac{Y_{max}*[EF-P]}{K_{1/2}+[EF-P]} + C$ (Fersht, 1999).

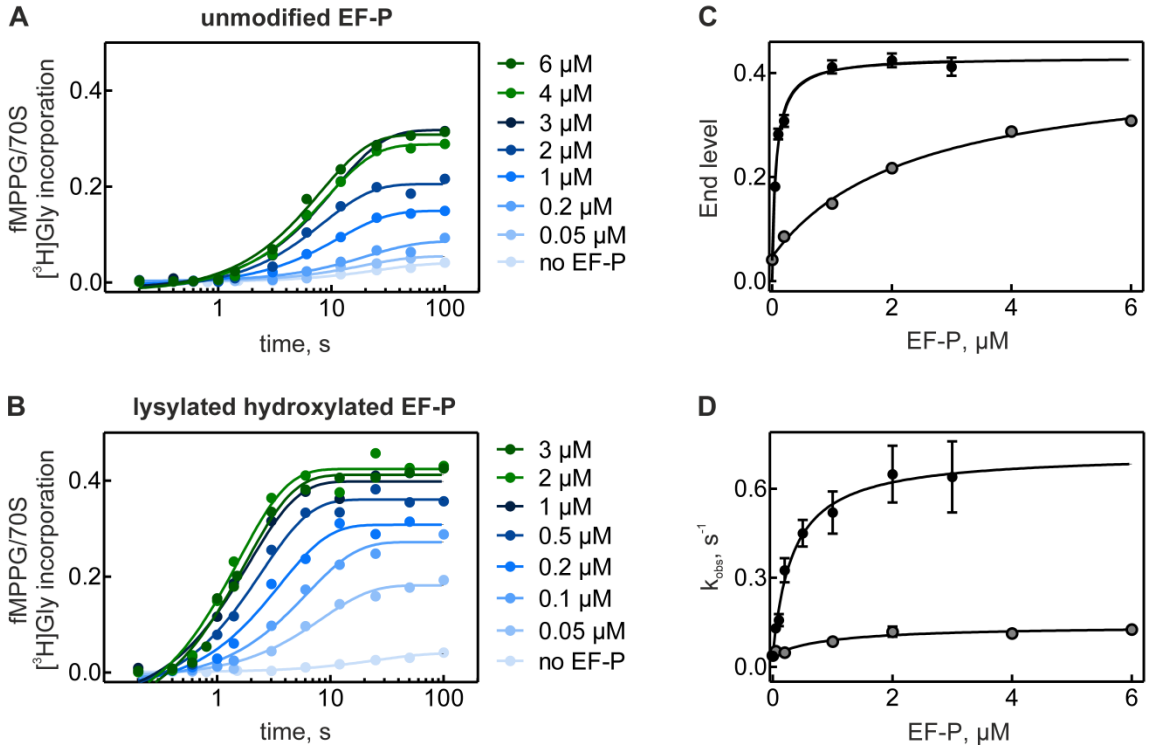

Fig. 20: Impact of the EF-P modification state on its catalytic proficiency

A,B) Time courses of synthesis of the tetrapeptide fMPPG with increasing amount of unmodified (A) und lysylated /hydroxylated (B) EF-P. C) Yield of fMPPG peptide as a function of EF-P concentration with unmodified (grey circles) or modified (black circles) EF-P. D) Rate of fMPPG synthesis as a function of the concentration of unmodified (grey circles) and modified EF-P (black circles). Error bars represent SD. For exact values see Table S3.

Table 3: EF-P dependence of fMPPG synthesis

EF-P	End level		rate	
	max end level/70S	K_M, µM	k_{cat}, s^{-1}	K_M, µM
unmodified EF-P	0.37 ± 0.03	2.4 ± 0.5	0.12 ± 0.03	-
modified EF-P	0.39 ± 0.02	0.08 ± 0.02	0.65 ± 0.02	0.27 ± 0.04

fMPPG synthesis with modified and unmodified EF-P.

As observed in the previous experiments, the maximal yield of fMPPG tetrapeptide was basically the same for unmodified and modified EF-P (Fig. 20C, Table 3). However, the EF-P concentration at which

50% of the maximum yield was reached was 30-fold higher with unmodified EF-P (Table 3). Furthermore, the maximal rate obtained with fully modified EF-P was approx. five-fold faster than that obtained with unmodified EF-P (Fig. 20D, Table S3). The K_M obtained by fitting of the rate-EF-P could only be determined for modified EF-P because rate-acceleration with unmodified EF-P was too little. Comparison of the K_M for the reaction rate and the end-level reveals that higher EF-P concentration is required for saturating the rate of the reaction compared to the end level.

Upon tetrapeptide formation multiple steps are monitored (fM → fMP → fMPP → fMPPG) (Fig. 21).

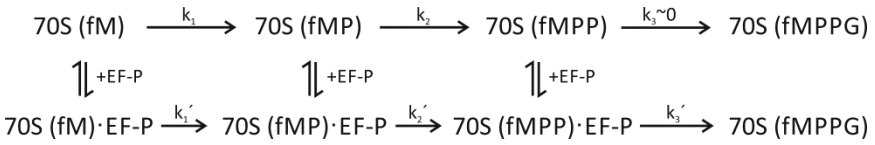

Fig. 21: Model for fMPPG formation

EF-P is an activator which catalyzes every step of peptide bond formation and thus it has to be saturating for all steps to monitor k_{cat}. The last step however is particularly slow and causes ribosome pausing /peptidyl-tRNA dissociation. To yield the maximal amount of product it might thus only be required to saturate the last very slow step which might explain why the K_M is different when rate or product yield is monitored. Thus, modification of EF-P increased the apparent affinity of the factor to the stalling complex 30-fold. Furthermore, the k_{cat} is increased five-fold. The differences on the K_M and k_{cat} together led to a > 100 fold difference of the k_{cat}/K_M demonstrating that EF-P modification increases the catalytic proficiency of the factor.

2.2.1.2 Slow peptide bond formation competes with the translocation process

Upon tetrapeptide formation (fM-PPG), fMet-Pro-Pro-tRNA^{Pro} dissociated from stalled ribosomes in the absence of EF-P prior to glycine incorporation (section 2.1.2.3). EF-P prevented peptidyl-tRNA dissociation, presumably by stabilizing the P-site tRNA (section 2.1.2.4). tRNA dissociation could be caused by a spontaneous dissociation of short peptidyl-tRNAs (from the P-site) as a result of the extended time window with poor substrates (Karimi et al, 1998; Pavlov et al, 2009). However, peptidyl-tRNA dissociation was induced by the presence of an A-site tRNA (Fig. 22).

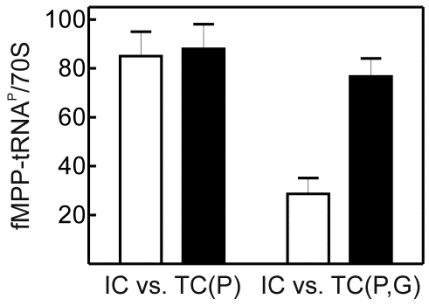

Fig. 22: A site-bound tRNA speeds up the dissociation of fMet-Pro-Pro-tRNA^{Pro} from ribosomes

The amount of fMet-Pro-Pro-tRNA^{Pro} bound to ribosomes was quantified by nitrocellulose filtration 100 s after initiation complexes primed on an mRNA coding for fMPPG were mixed with EF-G, and either TC(P) only or TC(P) and TC(G). The presence of the A-site tRNA (Gly-tRNA^{Gly}) facilitated the dissociation of the P-site tRNA. The reaction was performed in the absence (white bar) and presence (black bar) of EF-P.

Because tetrapeptide formation requires three consecutive elongation cycles, the reaction mixture contained EF-G to promote translocation. Thus, an alternative reason for the peptidyl-tRNA drop-off is an active release mechanism; as it was described for peptidyl-tRNA dissociation catalyzed cooperatively by IF1 and IF2 (Karimi et al, 1998) or by RRF, EF-G and RF3 (Heurgue-Hamard et al, 1998). To investigate whether EF-G induces the peptidyl-tRNA dissociation and whether EF-P is able to counteract this influence, fM-PPG formation in the presence and absence of EF-P was monitored at varying concentrations of EF-G (Fig. 23A, B).

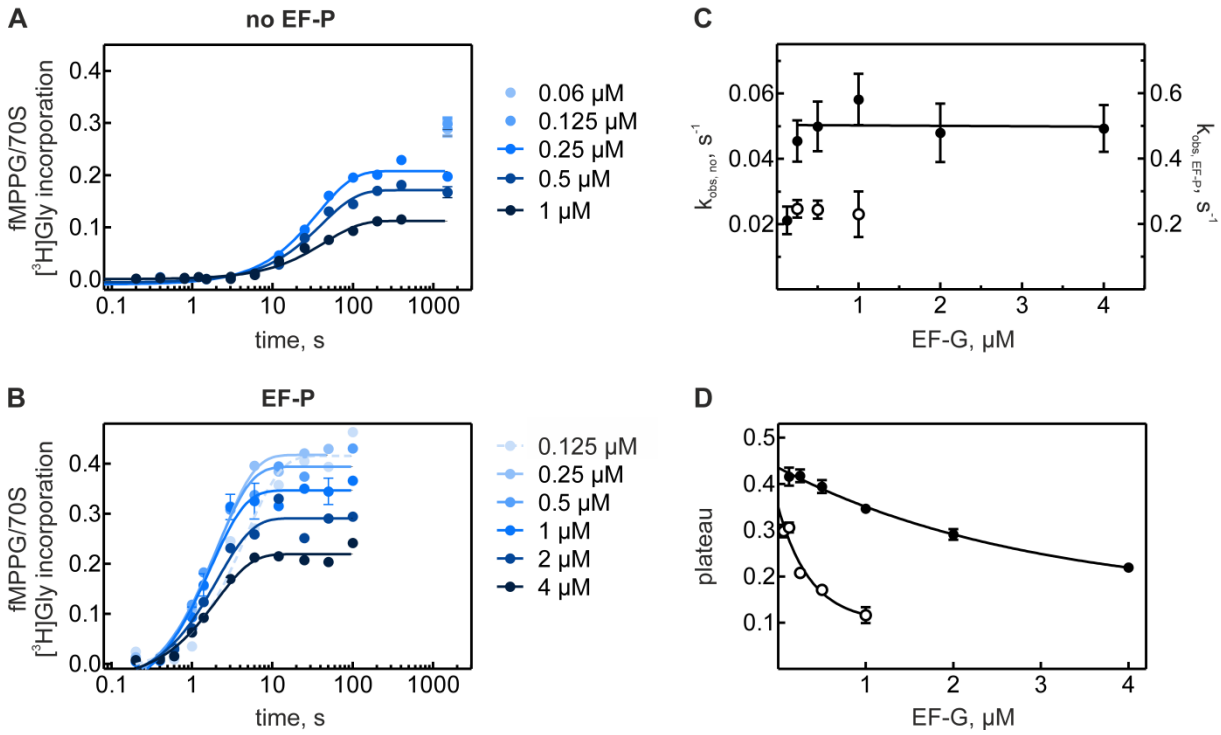

Fig. 23: Impact of the interplay of EF-P and EF-G on peptide synthesis

A,B) Time courses of tetrapeptide fM-PPG translation with increasing amount of EF-G in the absence (A) and presence (B) of modified EF-P. C) EF-G concentration dependence of fM-PPG synthesis rate without (open circles) and with modified EF-P (closed circles). Trends represent visual guides. Error bars represent SD. D) Yield of fM-PPG peptide as a function of EF-G concentration without (open circles) and with modified EF-P (closed circles). Error bars represent SD of three replicates.

Except for concentrations ≤0.125 µM EF-G the rate of product formation was independent of EF-G in the presence and absence of EF-P, indicating that translocation does not dominate the reaction kinetics (Fig. 23C,Table **S4**). Below 0.25 µM EF-G translocation presumably became rate limiting for fM-PPG synthesis. Increasing concentrations of EF-G considerably reduced the amount of final product in the presence and absence of EF-P (Fig. 23D) suggesting that at high EF-G concentrations peptide-bond formation and EF-G induced tRNA dissociation are competitive reaction pathways (see below). As seen from the steeper slope in Fig. 23D, the reaction in the absence of EF-P is more sensitive to the EF-G concentration. Furthermore, the different yield of

final product in the absence and presence of EF-P at a certain EF-G concentration shows that EF-P counteracts EF-G-induced peptidyl-tRNA drop-off to certain extent.

Based on the current data peptidyl-tRNA dissociation cannot be deduced; one likely scenario involves unconventional translocation by EF-G: the ribosome stalls with fMetProPro-tRNA^{Pro} in the P site and Gly-tRNA^{Gly} in the A site (section 2.1.2.6). Due to very slow peptide bond formation EF-G might induce non-canonical translocation prior to the peptidyl transfer and would thus transfer the peptidyl-tRNA to the E site from where it dissociates. This latter idea is supported by the fact that the presence of an A-site tRNA increased the dissociation of the P-site tRNA (Fig. 22). Notably, there are examples showing that EF-G can induce translocation in a ribosome complex with an aminoacyl-tRNA in the A site (Semenkov et al, 2000). On the basis of these observations, reduction of peptidyl-tRNA dissociation by EF-P may be explained by a combination of two scenarios: First, EF-P accelerates the rate of peptide bond formation (section 2.1.2) and thereby reduces the time window in which dissociation could occur. Second, as EF-P binds both, the tRNA and the ribosome (Blaha et al, 2009) EF-P might function as a kind of anchor for the tRNA opposite to the EF-G binding site, thus physically counteracting premature translocation. Based on the crystal structure, Blaha *et al*. suggested that EF-P may stabilize the A-minor interactions of two G-C base pairs in the anticodon stem loop of tRNA^{fMet} with ribosomal residues A1339 and G1338 of 16S rRNA which stabilise tRNA^{fMet} and the breaking of which is a prerequisite for translocation (Blaha et al, 2009; Selmer et al, 2006). If the same contacts form between EF-P and tRNA^{Pro}, this stabilization would explain how EF-P inhibits the futile translocation of peptidyl-tRNA prior to peptide bond formation.

2.2.1.3 Increasing $MgCl_2$ concentrations reduce peptidyl-tRNA dissociation

To further investigate the phenomenon of peptidyl-tRNA dissociation and its implications on EF-P function, the yield of final product was quantified depending on the $MgCl_2$ concentration. $MgCl_2$ stabilizes peptidyl- and aminoacyl-tRNAs in the P and A site, respectively (Gromadski et al, 2006; Katunin et al, 1994; Konevega et al, 2004; Semenkov et al, 2000; Thompson et al, 1981). If indeed tRNA stabilization was the reason for the increased level of final product formation in the presence of EF-P, this might be also accomplished by increased $MgCl_2$ concentrations. Because translation kinetics are strongly affected by $MgCl_2$ (Johansson et al, 2012; Lucas-Lenard & Lipmann, 1967; Manchester & Alford, 1979; Wohlgemuth et al, 2010) only the final yield of fM-PPG formation was determined (Endpoints at 80 and 400 s with and without EF-P, respectively). The final product level was essentially independent of $MgCl_2$ in the presence of EF-P (Fig. 24). By contrast, in the absence of EF-P the product level increased linearly with increasing $MgCl_2$ concentrations up to the level of the EF-P-catalyzed reaction (Fig. 24, Table S5). This indicates that stabilization of the peptidyl-tRNA facilitates fM-PPG formation, supporting the notion that EF-P positions the peptidyl-tRNA.

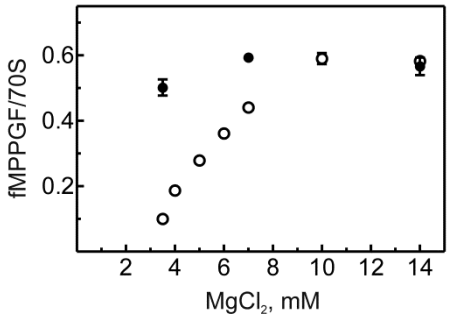

Fig. 24: $MgCl_2$ increases the yield of fMPPG tetrapeptide formation

Yield of fMPPG tetrapeptide formation as a function of $MgCl_2$ concentration in the absence (open symbols) and presence (closed symbols) of EF-P. Error bars represent SD of three experiments.

2.2.1.4 EF-P selectively accelerates peptide bond formation with poor substrates.

To access the EF-P effect kinetically more direct, single peptide bond formation was investigated. Furthermore, the focus of the investigation was changed from substrate stability to reactivity. With Gly-tRNA^{Gly} as A-site substrate the rate of peptidyl transfer depends on the P-site substrate (section 2.1.2.2): the reaction with fMet-Pro-tRNA^{Pro} (4.2 ± 0.3 s^{-1}) was approximately 7-fold slower than with fMet-tRNA^{fMet} (28 ± 3 s^{-1}). Moreover, a PPG motif in a protein sequence led to robust ribosome stalling while PG was readily translated (Fig. 11, section 2.1.2.5). Hence, the reason for stalling is unlikely to be an additive effect upon the consecutive incorporation of poor substrates but may be rather explained by a reduced reactivity of the C-terminal amino acid in the nascent chain caused by neighboring amino acids. To investigate whether the reactivity of a peptidyl-tRNA with a C-terminal proline could be further reduced by an alteration of the amino acid preceding proline, Pro-Gly peptide bond formation was monitored with another Pro preceding the C-terminal Pro (Materials & Methods). Because fMet-Pro-Pro-tRNA^{Pro} was used as P-site substrate instead of fMet-Pro-tRNA^{Pro} (Fig. 25), rate differences could be attributed to the changed reactivity of the P-site substrate. Peptidyl transfer from fMet-Pro-Pro-tRNA^{Pro} to Gly-tRNA^{Gly} (fMPP-G; 0.013 ± 0.001 s^{-1}) was ~300 fold slower than for fMet-Pro-tRNA^{Pro} (fMP-G; 4.2 ± 0.3 s^{-1}) demonstrating a strong influence of the sequence context in the nascent peptide. Thus, the neighboring residue may reduce the intrinsic reactivity of the C-terminal amino acid or may sterically inactivate the reaction by inducing an unfavorable conformation of the Pro-tRNA or of the catalytic environment. The EF-P body stabilizes the peptidyl-tRNA (sections 2.1.2.3 and 2.2.1.1) and thus may be sufficient to position the tRNA in an active conformation antagonizing potential steric constraints induced by the nascent chain. To test this hypothesis, the experiment was repeated in the presence of unmodified or modified EF-P (Fig. 25). To monitor the effect on the catalysis, rather than on EF-P binding, saturating concentrations of EF-P were used. Unmodified and modified EF-P accelerated peptide bond formation in either reaction (fMP-G and fMPP-G). Notably, about a half of the catalytic acceleration can be attributed to the modification: the acceleration from no EF-P to unmodified EF-P and from unmodified EF-P to

modified EF-P was ~2.7-fold for fMP-G and ~10-fold for fMPP-G (Table 4), demonstrating that the latter reaction was more sensitive towards EF-P function.

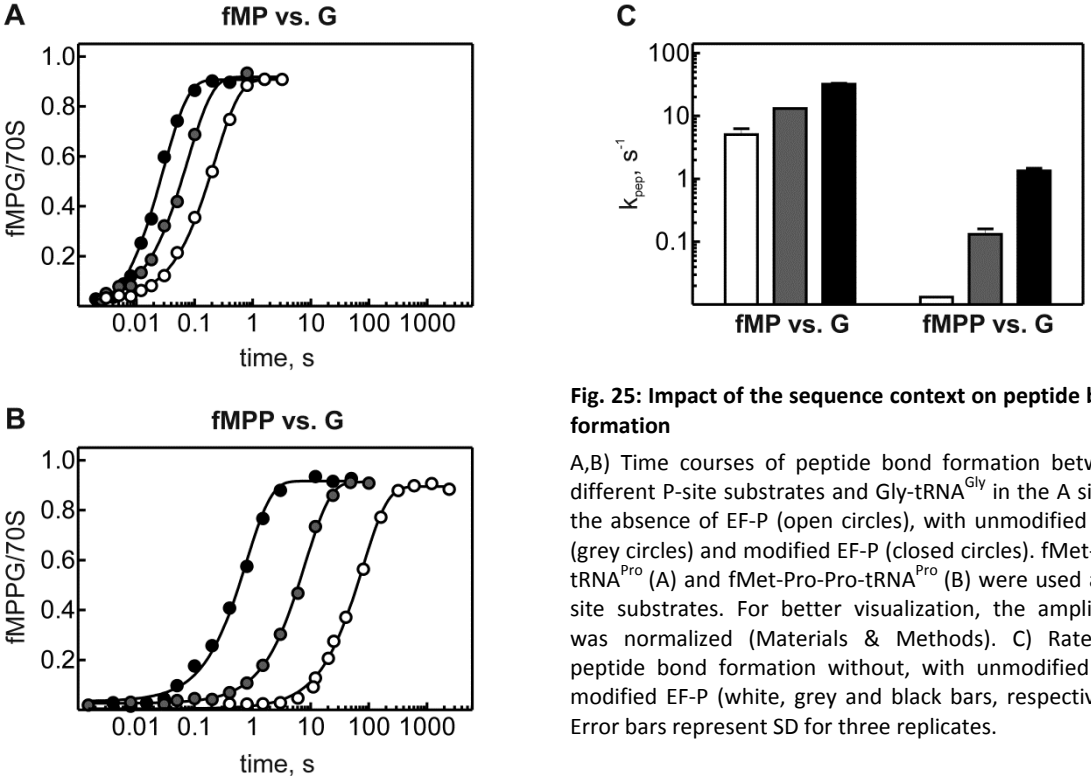

Fig. 25: Impact of the sequence context on peptide bond formation

A,B) Time courses of peptide bond formation between different P-site substrates and Gly-tRNA^{Gly} in the A site in the absence of EF-P (open circles), with unmodified EF-P (grey circles) and modified EF-P (closed circles). fMet-Pro-tRNA^{Pro} (A) and fMet-Pro-Pro-tRNA^{Pro} (B) were used as P-site substrates. For better visualization, the amplitude was normalized (Materials & Methods). C) Rates of peptide bond formation without, with unmodified and modified EF-P (white, grey and black bars, respectively). Error bars represent SD for three replicates.

Table 4: Peptidyl transfer to glycine as a function of the P-site substrate

	k_{obs}, s^{-1}				
	no EF-P		unmodified EF-P		modified EF-P
fM vs. G[a]	28 ± 3				44 ± 5
fMP vs. G	4.2 ± 0.3	$\xrightarrow{x\,3.1}$	13.1 ± 0.5	$\xrightarrow{x\,2.5}$	33 ± 3
fMPP vs. G	0.013 ± 0.002	$\xrightarrow{x\,9.2}$	0.12 ± 0.02	$\xrightarrow{x\,10.8}$	1.3 ± 0.2

IC/PTC (0.2 µM) vs. TC(G, 10 µM) in the absence of EF-P, in the presence of unmodified EF-P (6 µM) or lysylated/hydroxylated EF-P (3 µM). Reaction performed in buffer B at 37 °C. [a] Taken from Fig. 8, section 2.1.2.2.

The rate differences obtained for modified and unmodified EF-P (in this assay and for tetrapeptide formation (section 2.2.1.1)) cannot be explained solely by a modification-dependent increase of the affinity of EF-P to the ribosome (section 2.2.1.1), because they are measured at saturating EF-P concentrations. Thus, the modification improves the catalytic proficiency of EF-P further to tRNA stabilization by the EF-P body.

2.2.1.5 Impact of the EF-P modification on peptidyl transfer

To investigate the maximal catalytic effect of the EF-P modification, peptidyl transfer from fMet-tRNA^{fMet} to Pmn was monitored in the absence or presence of unmodified or modified EF-P. The reaction was performed as described (section 2.1.2.1, Materials & Methods) with the difference that saturating Pmn concentrations were used. As mentioned, Pmn does not require decoding for

productive binding to the ribosome (Katunin et al, 2002; Sievers et al, 2004). Thus, saturating Pmn concentrations should allow monitoring the maximal effect of EF-P on the chemistry of peptide bond formation. The rate of peptide bond formation was similar without and with unmodified EF-P (4 ± 0.2 and 4.7 ± 0.3 s^{-1}, respectively), indicating that unmodified EF-P had only marginal effects on the reaction chemistry. Modified EF-P accelerated the rate approx. 10-fold (45 ± 6 s^{-1}) which is comparable to its 6-fold acceleration of the reaction with subsaturating Pmn. The slight difference might be caused by Pmn binding in case of subsaturating Pmn concentrations.

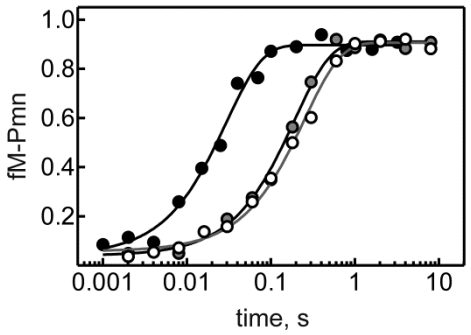

Fig. 26: Impact of EF-Ps modification on fMet-Pmn formation

Time courses of peptide bond formation between fMet-$tRNA^{fMet}$ and Pmn in the absence of EF-P (open circles), in the presence of unmodified EF-P (grey circles) and in the presence of modified EF-P (closed circles).

2.2.2 Variation of physico-chemical parameters

The lysyl-moiety of modified EF-P protrudes into the peptidyl transferase center and may come within a hydrogen bond distance (~ 2Å) of the C-terminal amino acid of the peptidyl-tRNA (Lassak et al, 2015). In general, the ε-amino group of lysine often participates in hydrogen bonding and can act as a general base in catalysis. Although the unperturbed pK_a of the amino group of lysine in polypeptides is close to 10, it is sensitive to environmental effects that can lower it substantially (down to 5.3) (Isom et al, 2011; Schmidt & Westheimer, 1971). Thus, the EF-P modification might act either indirectly by positioning the CCA end of the tRNA and/or the C-terminal amino acid in the nascent chain and/or by direct covalent general base catalysis. To investigate the catalytic contribution of EF-P, peptide bond formation in the presence and absence of EF-P was investigated at different temperatures and pH. A change of the rate-parameter dependence might indicate whether EF-P is involved in the chemistry step and if yes, how.

2.2.2.1 pH-dependence of peptide bond formation with a native A-site substrate

Nucleophiles (in this case, aminoacyl-tRNA) are only reactive in their deprotonated form, which renders their reactions pH dependent (Fahnestock et al, 1970). However, the formation of most dipeptides is independent of pH (Beringer et al, 2005; Bieling et al, 2006; Johansson et al, 2011). These contradictory observations can be explained by a rate-limiting and pH-independent accommodation step kinetically masking peptide bond formation (Pape et al, 1998; Rodnina et al, 1994; Wohlgemuth et al, 2010). Nevertheless, peptidyl transfer can be kinetically accessed – and

thus the involvement of EF-P in this process studied – when the reaction is slower than the rate of tRNA accommodation (Beringer & Rodnina, 2007b). The formation of fMet-Gly-tRNA^{Gly} was reported to be pH-dependent in the pH range of 6.5-8.5. Furthermore, its rate/pH profile revealed the presence of one ionizing group involved in catalysis that was assigned to the α-amino group of Gly-tRNA (Johansson et al, 2011).

This raises the question of whether catalysis by EF-P is pH-dependent. If EF-P was involved in general base catalysis, EF-P should change the pH dependence. To test this, the rate of fMet-Gly dipeptide (fM-G) formation was measured at pH values ranging from 6.6-8.5 in the presence and absence of EF-P (Fig. 27A,B; Table S7). Reactions were performed as described (section 2.1.2.2, Materials & Methods).

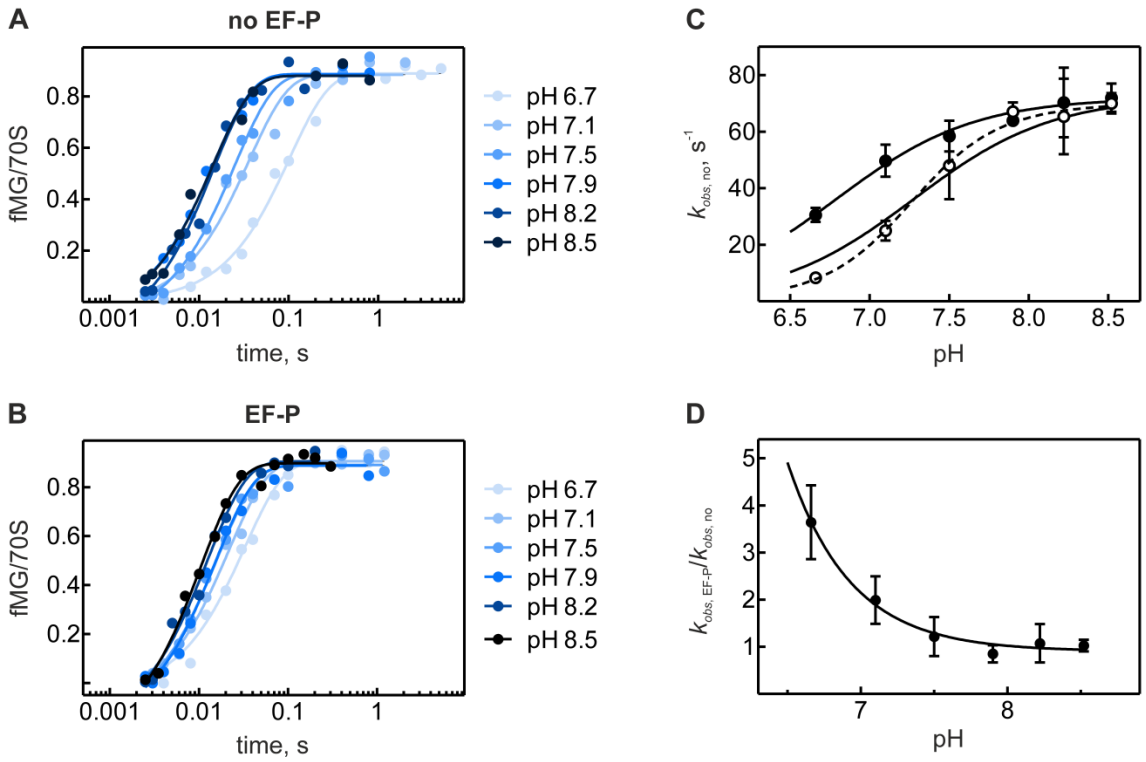

Fig. 27: pH dependence of fM-G formation

A,B) Time courses of peptidyl transfer between fMet-tRNA^{fMet} and Gly-tRNA^{Gly} in the absence (A) and presence (B) of EF-P as a function of pH at 37 °C. For better visualization, amplitudes were normalized (Materials & Methods). C) Dependence of the reaction rate on pH without (open circles) and with EF-P (closed circles). For values see Table S7. Error bars represent SD from up to five replicates. Data were fitted to a model with one ionizing group; a fit to a model with two ionizing groups is shown in dashed lines. D) Acceleration of fMG formation by EF-P as a function of pH.

In the absence of EF-P the rate of fM-G dipeptide formation was pH-dependent and increased with pH, consistent with the assertion that the chemistry step was monitored. However, at higher pH values the rate reached a maximum of ~70 s^{-1}. In the presence of EF-P the reaction was pH-dependent as well, but reached a maximal value at a slightly lower pH compared to the EF-P-uncatalyzed reaction (Fig. 27C, Table S7). Both the EF-P catalyzed and uncatalyzed reactions appeared to have the same maximal rate (70 ± 4 s^{-1}) which led to an apparent reduction of the EF-P

effect at higher pH (Fig. 27D). The pH-dependence of k_{pep} was fitted to a model assuming one ionizing group (Materials & Methods):

$$k_{pep\,(pH)} = \frac{k_{pep}^{max}}{1 + 10^{(pK_a - pH)}} \quad (10)$$

The estimated pK_a values were 7.2 ± 0.4 without EF-P and 6.8 ± 0.1 with EF-P. The value in the absence of EF-P is in good agreement with the published pK_a for Gly-tRNA^{Gly} (~7.4) as A-site substrate (Johansson et al, 2011). Notably, fM-G formation without EF-P was much better described by a model with two ionizable groups (R^2= 0.98 compared to 0.94 with one proton) with pK_{a1}= 7.7 ± 0.7 and pK_{a2}= 6.9 ± 0.8 (equation 12), indicating a simultaneous influence of the nucleophile and an additional ionizing group.

$$k_{(pH)} = \frac{10^{-pK_{a1}-pK_{a2}} \times k_{max}}{10^{-pK_{a1}-pK_{a2}} + 10^{-pH-pK_{a1}} + 10^{-2pH}} \quad (12)$$

The maximal rate observed for fM-G formation could either correspond to the maximal rate of peptide bond formation (Johansson et al, 2011) or to a preceding step (decoding/accommodation of the A-site substrate) which became rate-limiting at high pH (Pape et al, 1998; Rodnina et al, 1994). Accordingly, two interpretations are possible: i. EF-P could accelerate peptide bond formation to its maximal rate by lowering the pK_a of the attacking nucleophile (from 7.2 to 6.8) and thus, catalyze the reaction chemistry. ii. The intrinsic rate of peptide bond formation could be kinetically masked by a reaction that becomes limiting at high pH, resulting in a kinetically limited apparent pK_a, whereas the intrinsic pK_a of the nucleophile is the same with and without EF-P. This caveat in the interpretation hampers a straightforward interpretation in terms of the catalytic mechanism of EF-P.

To distinguish between these possibilities, a pH dependence of fMPG tripeptide formation from fMet-Pro-tRNA^{Pro} and Gly-tRNA^{Gly} was performed (Fig. 28, Table S8, Materials & Methods). If the rate of 70 s^{-1} reflected decoding/accommodation of Gly-tRNA^{Gly}, it should not become rate limiting for the formation of the fMPG tripeptide, which was almost 10-fold slower than fMG formation determined at pH 7.5 in the absence of EF-P (section 2.1.2.2). As for fM-G formation, the rate of fMP-G formation increased with pH in the absence of EF-P (Fig. 28). In the presence of EF-P, rates measured above pH 7 were pH-independent, with an average rate of 38 ± 3 s^{-1}. Consequently, the rate acceleration by EF-P decreased for higher pH. At pH 8.7 the rates with and without EF-P were similar (35 and 40 s^{-1}, respectively), suggesting that both reactions have the same maximal rates in this assay as well. Notably, the maximal rates for fM-G and fMP-G formation were different (70 ± 4 s^{-1} and 38 ± 3 s^{-1}, respectively), which might indicate that the slower fMP-G formation indeed monitors the chemistry step of peptidyl transfer. Alternatively, the accommodation of Gly-tRNA^{Gly} might be influenced by the P-site substrate, as already reported earlier for Phe-tRNA^{Phe} (Rodnina et al, 1994).

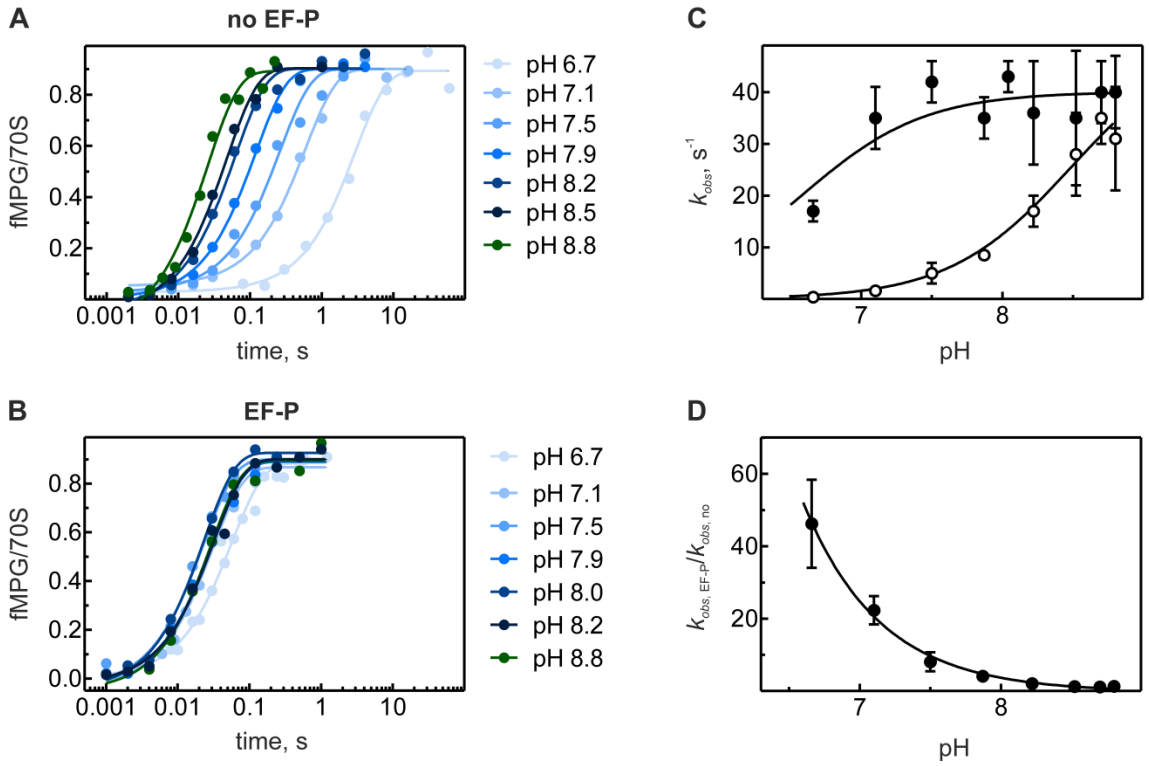

Fig. 28: Peptidyl transfer from fMet-Pro-tRNA^{Pro} to Gly-tRNA^{Gly} at different pH

A,B) Time courses of peptidyl transfer from fMet-Pro-tRNA^{Pro} to Gly-tRNA^{Gly} in the absence (A) and presence (B) of EF-P as a function of pH at 37 °C. For better visualization, amplitudes were normalized (Materials & Methods). C) Dependence of the reaction rate on pH in the absence (open circles) and presence of EF-P (closed circles), see also Table S8. Error bars represent SD from up to six replicates. D) Acceleration of fMP-G formation by EF-P as a function of pH.

The data were fitted to a model with one ionizing group (equation 10, Materials & Methods), which resulted in pK_a values of 8.5 ± 0.1 in the absence and 6.6 ± 0.2 in the presence of EF-P. Thus, EF-P shifted the pH-sensitive kinetic window to lower pH values. If the maximal rate reflects the reaction chemistry, this would indicate that EF-P catalyzed the reaction chemistry in a way which led to earlier deprotonation of the attacking nucleophile. However, the pK_a value of the ionizing group that is seen in the absence of EF-P is too high to correspond to that of Gly-tRNA^{Gly}; this makes the assignment of the rate-limiting reaction step uncertain (see Discussion, section 3.4.3).

2.2.2.2 Activation parameters

Compared to model reactions in solution, the ribosome catalyzes peptidyl transfer entropically, presumably by positioning the substrates (Johansson et al, 2008; Sievers et al, 2004; Wohlgemuth et al, 2008). To investigate how EF-P augments the peptidyl transferase activity, the temperature dependence of fMP-G formation was measured with and without EF-P (as described in section 2.2.2.1 and Materials & Methods) (Fig. 29A, B, Table S9). The reaction between fMet-Pro-tRNA^{Pro} and Gly-tRNA^{Gly} was chosen for three reasons: in the absence of EF-P the monitored reaction step was (i) pH-dependent, (ii) not limited by a pH-independent step at pH 7.5 and 37 °C, and (iii) sensitive to

EF-P (section 2.2.2.1). As expected, the reaction rates increased with increasing temperature in the presence and absence of EF-P (Fig. 29C). For the reaction without EF-P the corresponding Arrhenius plot (log(k) vs. 1/T) was linear (Fig. 29D), indicating that there is no change in the rate-limiting step. In the presence of EF-P the Arrhenius plot was linear below 30 °C and almost parallel to the plot of the EF-P-uncatalyzed reaction. Above this temperature the Arrhenius plot deviates from its linear behavior (Fig. 29D), indicating a change in the rate-limiting step. This step probably corresponds to the pH-independent step monitored previously (Fig. 28C). Accordingly, activation parameters were determined without the rate obtained at 37 °C. The free energy of activation ($\Delta G^{\neq}$), the enthalpy of activation ($\Delta H^{\neq}$) and the activation entropy ($T\Delta S^{\neq}$) were determined according to equations 4-6 (Materials & Methods) (Table 5). Apparently, EF-P catalyzed the reaction entropically with an energetic contribution ($\Delta\Delta G^{\neq}$) of -1.5 ± 0.2 kcal/mol.

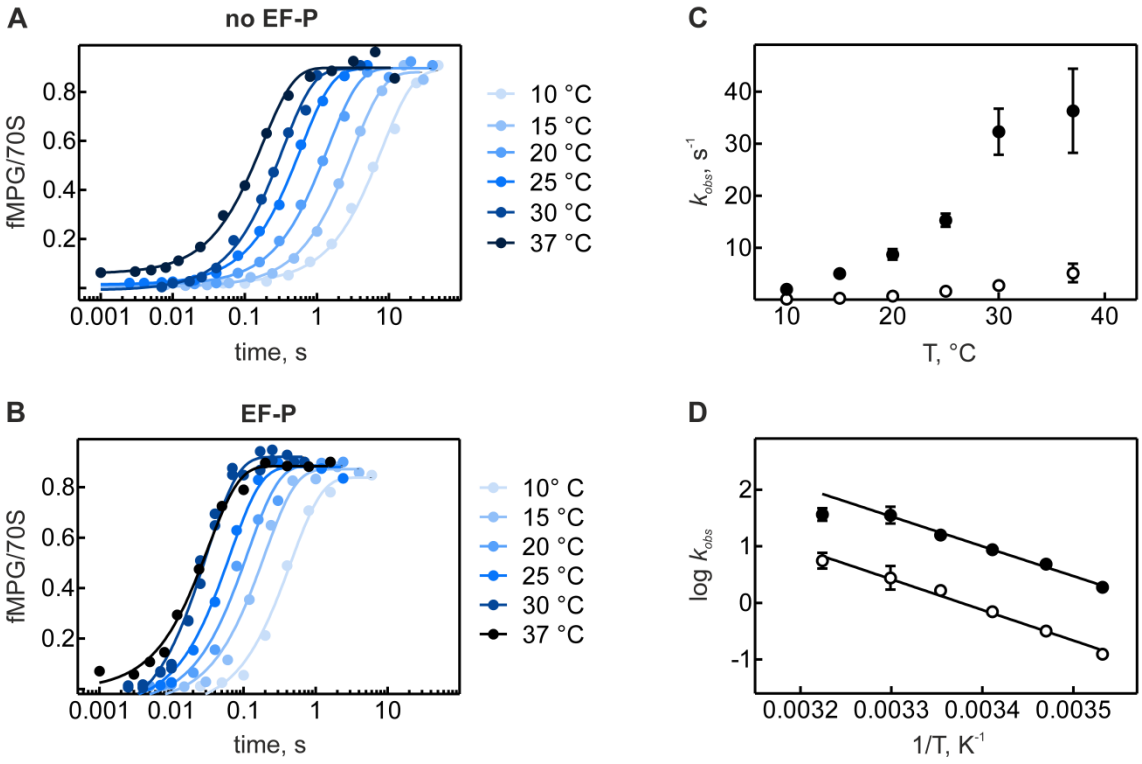

Fig. 29: Temperature dependence of fMP-G formation at pH 7.5

A,B) Time courses of peptidyl transfer between fMet-Pro-tRNA^{Pro} and Gly-tRNA^{Gly} in the absence (A) and presence (B) of modified EF-P as a function of temperature. The pH was adjusted at the respective temperature. For better visualization, amplitudes were normalized (Materials & Methods). C) Correlation of the reaction rate with the temperature without (open circles) and with modified EF-P (closed circles). Error bars represent SD. D) Arrhenius plot for fMP-G formation in the presence (closed circles) and absence (open circles) of EF-P.

Table 5: Activation parameter of fMP-G formation at pH 7.5

fMP-G	$\Delta G^{\neq}$ kcal/mol	$\Delta H^{\neq}$ kcal/mol	$T\Delta S^{\neq}$ kcal/mol
no	17.3 ± 0.6	24 ± 1	6.7 ± 0.5
EF-P [a]	15.6 ± 1	25 ± 1	9.5 ± 0.7

Activation parameters were calculated according to equation 4-6 (Materials & Methods) for 25 °C (298.15 K). [a] The value at 37 °C was excluded from the fitting

The Arrhenius plot of the EF-P catalyzed reaction at pH 7.5 deviates from a linear behavior (Fig. 29D) indicating that above 30 °C a different step becomes rate limiting. This is in agreement with the lack of pH dependence of the EF-P-catalyzed reaction at this temperature and pH value (7.5) (section 2.2.2.1).

To circumvent this problem, a temperature dependence was performed at pH 6.5 (Fig. 30A, B, C; Table S10). At this pH the rate of fMP-G formation in the presence of EF-P was in the linear part (Fig. 28) and thus the chemistry step is presumably rate limiting. As for the reaction at pH 7.5, the rate increases with temperature. Notably at 10 °C and 15 °C the kinetics in the absence of EF-P showed a biphasic behavior (Fig. 30A). This might be explained by two interconvertible populations of ribosome complexes. However, because the reason for the heterogeneity is not known, these data were excluded from analysis. At pH 6.5, the reactions with and without EF-P yield linear Arrhenius plots (Fig. 30D) and the corresponding activation parameters reveal that EF-P again contributed entropically to catalysis, with an overall catalytic contribution ($\Delta\Delta G^{\neq}$) of -3 ± 0.2 kcal/mol (Table 6).

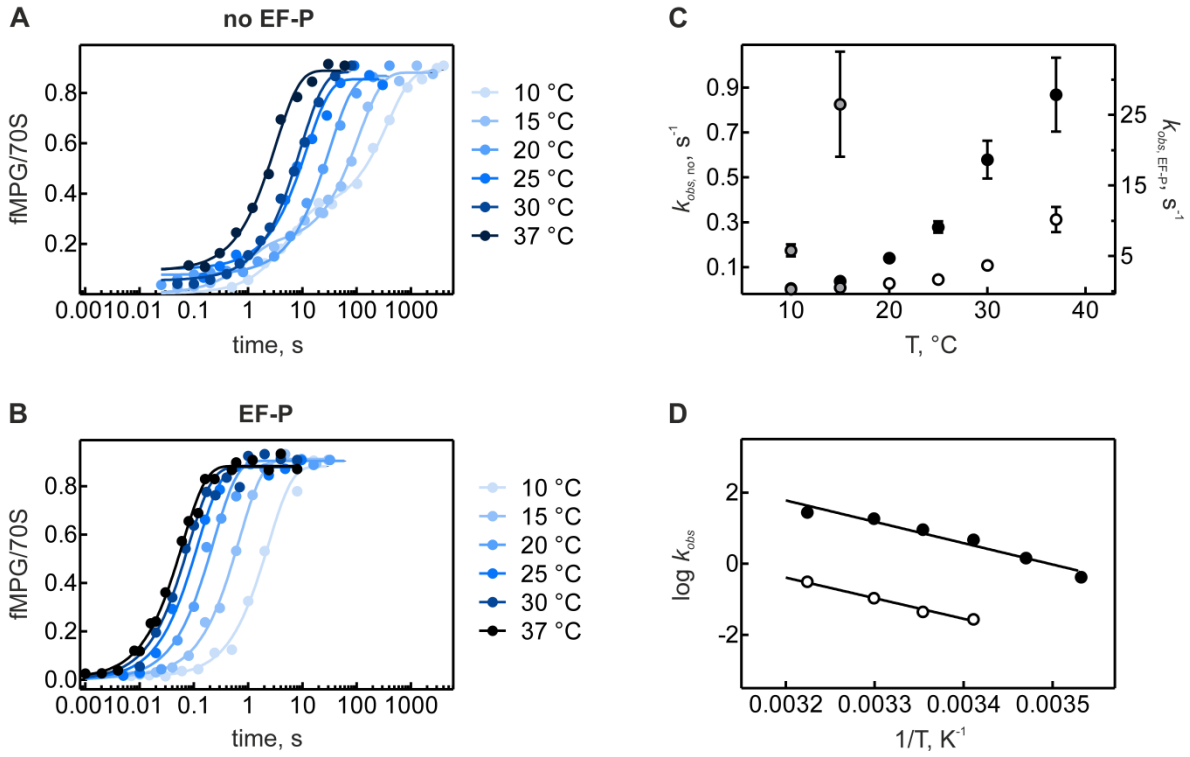

Fig. 30: Temperature dependence of fMP-G formation at pH 6.5

A,B) Time courses of peptidyl transfer between fMet-Pro-tRNA^{Pro} and Gly-tRNA^{Gly} in the absence (A) and presence (B) of modified EF-P as a function of the temperature. For better visualization, amplitudes were normalized (Materials & Methods). C) Correlation of the reaction rate with the temperature without (open circles) and with modified EF-P (closed circles). Grey circles correspond to the rates obtained by double exponential fitting of the reaction without EF-P at 10 and 15 °C. Error bars represent SD. D) Arrhenius plot for fMP-G formation in the presence (closed circles) and absence (open circles) of EF-P.

Table 6: Activation parameter of fMP-G formation at pH 6.5

fMP-G	$\Delta G^{\neq}$, kcal/mol	$\Delta H^{\neq}$, kcal/mol	$T\Delta S^{\neq}$, kcal/mol
no [a]	19 ± 1	26 ± 2	7 ± 1
EF-P	16.3 ± 0.7	27 ± 3	11 ± 2

Activation parameters were calculated according to equation 4-6 (Materials & Methods) for 25 °C (298.15 K). [a] The values obtained at 10 and 15 °C were excluded from the fitting.

2.2.3 Variation of the substrate

To determine to which extent EF-Ps catalysis is due to substrate positioning or due to direct participation in the reaction chemistry, it is important to understand what makes Pro-tRNA^{Pro} a poor substrate for the peptidyl transferase center. The main cause of stalling seems to be neither the tRNA nor the Pro codons but the amino acid itself (section 2.1.2.8) (Pavlov et al, 2009; Tanner et al, 2009).

2.2.3.1 Substitution on the prolyl ring modulates steric and electronic properties of proline

To dissect potential structural and electronic features causing the low reactivity of proline and thereby identify properties targeted by EF-P function, the impact of proline-analogs (Pro*, P*, Fig. 31) on translation was investigated. Pro analogs differ from proline in their structural preferences and the pK_a values of their amino- and carboxyl-groups (Table S11, Table S12). On the basis of a nucleophilic substitution mechanism for peptide bond formation the different pK_as should result in different intrinsic reactivities of the Pro derivatives (Fersht, 1999).

The conformation of the X-Pro bond (*cis* or *trans*), with X being any amino acid, influences the electron density distribution within the analogs. In combination with a slow isomerization rate as for proline, this leads to conformer-specific carboxyl pK_a values (Bedford & Sadler, 1974; Hunston et al, 1985). Furthermore, the electronegativity of the substituent influences the proline pucker (Improta et al, 2001) which itself correlates with the *cis-trans* conformation (Shoulders & Raines, 2009). Thus, the steric and electronic properties are highly interdependent. To identify possible properties responsible for the poor reactivity of proline, the following Pro analogs were chosen (Fig. 31): The influence of ring size was addressed by the Pro derivatives azetidine-2-carboxylic acid (Aze) and pipecolic acid (Pip) which have four and six-membered rings, respectively. 3,4-Dehydroproline (3,4-Dhp) and 4,5-(*cis/trans*)-Methanoproline (*cis*-/*trans*-MePro) are conformationally arrested, in that the ring of 3,4-Dhp has a flat conformation (Flores-Ortega et al, 2007; Kang & Park, 2009) and *cis*-/*trans*-MePro simulate particular pucker arrangements (Hanessian et al, 1997). Finally, the C_γ substituted Pro-analogs 4-(R/S)-Fluoroproline (4-(R/S)-Flp), 4-(R/S)-Hydroxyproline (4-(R/S)-Hyp),

4-(R/S)-Methylproline (4-(R/S)-Mep) deviate from proline in their *cis-trans* equilibria and pucker preferences (Bretscher et al, 2001; DeRider et al, 2002; Improta et al, 2001; Panasik et al, 1994).

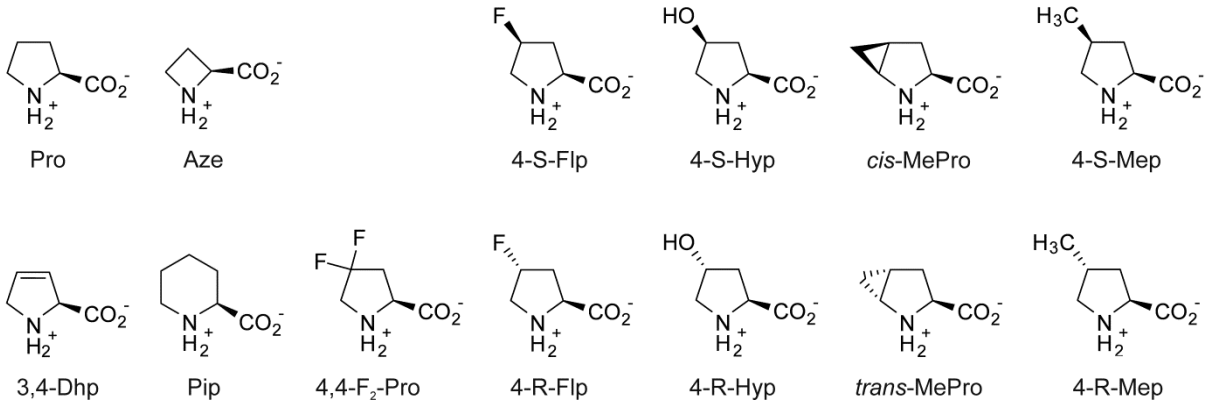

Fig. 31: Structure of proline and proline analogs

Pro: Proline, Aze: Azetidine-2-carboxylic acid, Pip: Pipecolic acid, 3,4-Dhp: 3,4-Dehydroproline, (*cis/trans*)-MePro: 4,5-(*cis/trans*)-Methanoproline, 4-(R/S)-Flp: 4-(R/S)-Fluoroproline, 4,4-F_2-Pro: 4,4-Difluoroproline , 4-(R/S)-Hyp: 4-(R/S)-Hydroxyproline, 4-(R/S)-Mep: 4-(R/S)-Methylproline.

2.2.3.2 Pro derivatives were accepted by the translation machinery

To investigate whether the different Pro analogs are accepted by the translation machinery, all analogs were charged on $tRNA^{Pro}$ by prolyl-tRNA synthetase (Pro-RS) (Maretial & Methods). This shows their similarity to proline, indicating that they are appropriate Pro mimics to study proline incorporation. Because large quantities of tRNA were required, it was transcribed *in vitro*. The transcript was as active as native $tRNA^{Pro}$ (Fig. S2), indicating that the lack of tRNA modifications in the transcript did not diminish translation efficiency or hamper recognition by EF-P. Misaminoacylated Pro*-$tRNA^{Pro}$s were recognized by EF-Tu and ternary complexs (EF-Tu·GTP·Pro*-$tRNA^{Pro}$) were stable enough to be isolated by size-exclusion chromatography (Fig. S3). Furthermore, all Pro*-$tRNA^{Pro}$s were active as A-site substrates as quantified by fMet-Pro* dipeptide formation.

2.2.3.3 Substitutions in the prolyl ring strongly modulate rate of peptide bond formation

To investigate the kinetics of proline incorporation and to get further insight how EF-P accelerates peptide bond formation with proline residues, incorporation of Pro analogs was characterized in the different approaches used previously for proline: (i) to investigate the chemical step of peptidyl transfer rather than preceding steps like A-site binding and accommodation of aa-tRNA or conformational changes the formation of fMP*-Pmn was monitored (as described for proline in section 2.2.1.4, Materials & Methods); (ii) to account for additional effects of a native A-site substrate fMP*-G formation was monitored (section 2.1.2.2, Materials & Methods) and finally, the translation of the tetrapeptide fM-P*P*G with Pro*-$tRNA^{Pro}$ serving as A- and P-site substrate was investigated (section 2.1.2.3, Materials & Methods) (Fig. 32A, B, C, respectively).

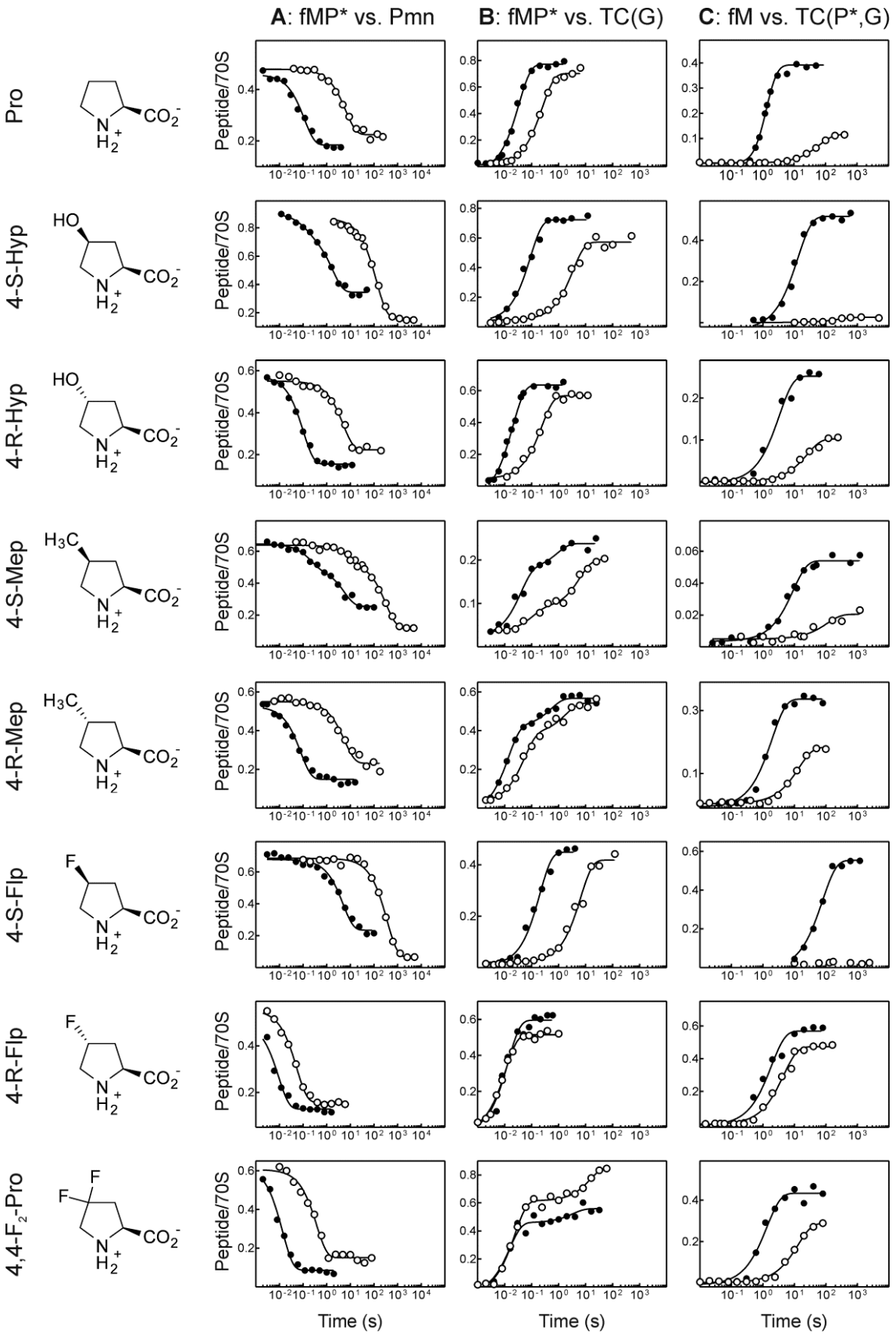

Fig. 32: Impact of prolyl ring substitutions on translation

Time courses of different kinetic approaches performed without (open circles) and with EF-P (closed circles). Formation of fMP*-Pmn (A), fMP*-G (B), the tetrapeptide fM-P*P*G (C).

All analogs tested could be incorporated into peptides, however, rates of product formation differed substantially (Fig. 32,Table S14). In the absence of EF-P rates of fMP*-Pmn formation with different analogs spanned seven orders of magnitude (~0.00006-21 s^{-1}). Thus, the substituents in the prolyl ring dramatically altered the reactivity of proline and caused large rate differences, with 4-R-Flp being the fastest (21 s^{-1}) and *cis*-MePro being the slowest substrate (~0.00006 s^{-1}). Interestingly, proline adopted a middle position (0.14 s^{-1}), showing that substitution at the prolyl ring did not per se interfere with the translation apparatus. Considering the smaller kinetic range for proteinogenic amino acids other than proline (k_{pep}~8-100 s^{-1}; measured in the same experimental setup) (Wohlgemuth et al, 2008), this dynamic range is surprising. Notably, the rate of 4-R-Flp (21 s^{-1}) was comparable to that with Phe or Val (16 s^{-1} for each). Except for 4-S-Mep the time courses could be fitted to single-exponential kinetics that could be attributed to the chemical step (Fig. 32A). Double-exponential kinetics can be rationalized by two ribosome populations (Katunin et al, 2002). EF-P accelerated peptide pond formation with all Pro analogs (Fig. 32A). Even the reactions with 4-R-Flp and 4,4-F_2-Pro with rates comparable to that of proteinogenic amino acids other than Pro were accelerated by EF-P. Calculation of the free energy from the rate acceleration revealed an averaged catalytic contribution of -2.5 ± 0.5 kcal/mol by EF-P. Notably, EF-P accelerated slower reactions slightly stronger than faster reactions (from 6- to 90-fold rate-acceleration for 4-R-Flp (k_{pep} = 21 s^{-1}) and 4-S-Hyp (k_{pep} = 0.007 s^{-1}), respectively, (Table S14), leading to more uniform rates. Thereby EF-P did not alter the reactivity trends of the Pro derivatives. Notably, the effect for *cis*-MePro might be underestimated because the reaction was too slow to be measured with high precision.

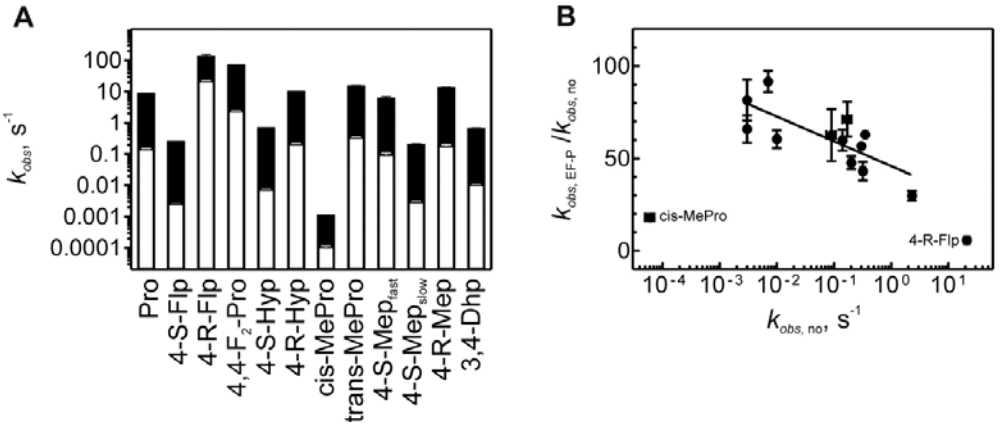

Fig. 33: Similar contribution of EF-P to catalysis

A) fMP*-Pmn formation without (white bars) and with (black bars) EF-P. B) EF-P induced rate acceleration (defined as the ratio ($k_{obs,\ EF\text{-}P}/k_{obs,no}$)) as a function of the EF-P-uncatalyzed rate. Average rates and SD from up to four replicates plotted.

The same reactivity trends were observed upon fMP*-G formation (Fig. 32B). However, the kinetic range was slightly narrower compared to fMP*-Pmn formation (four orders of magnitude), most probably due to rate-limiting aa-tRNA accommodation (see below). Apart from 4-S/R-Mep, 4,4-F_2-Pro

and *trans*-MePro reactions followed single-exponential kinetics. Two exponential traces could be rationalized by two populations of ribosomal complexes or multiple sampling of the ternary complex. EF-P accelerated the reaction of all analogs –except of those which were faster than ~70 s^{-1}– to different extend (Table S14). Notably, the rate ~70 s^{-1} matched the maximal rate of fM-G formation (section 2.2.2.1), suggesting that it represents Gly-$tRNA^{Gly}$ accommodation into the A site. This indicates that, at least for some Pro analogs, the rate of peptidyl transfer was limited by tRNA accommodation and thus the observed rate acceleration by EF-P was artificially reduced.

Upon tetrapeptide formation the reactivity of the Pro analogs is reflected in their incorporation rate and in the final product yield, due to the competitive site-reaction of peptidyl-tRNA dissociation (section 2.2.1.2). For all Pro analogs, the final product level and the observed rates were in good agreement with their respective reactivities observed in the previous assays (Fig. 32C, Table S14). For Pro derivatives which have been poor substrates in the previous assays (*cis*-MePro, 4-S-Flp and 4-S-Hyp) no final product was formed in the absence of EF-P. Pro analogs which have been good P-site substrates performed equally well in this more complex approach. EF-P generally accelerated the reaction and prevented dissociation of the peptidyl-tRNA, leading to increased product levels of final product for all Pro-derivatives, although it remained minmal for *cis*-MePro and 4-S-Mep.

The substituent effects propagated through all assays tested and thus through all steps of several elongation cycles showing their robustness and *in-vivo* relevance.

2.2.3.4 The ribosome-catalysed reaction is more sensitive to substituent effects than the in-solution reaction

Several explanations could rationalize the observed rate differences obtained with different Pro analogs: Because the nucleophilic attack on carbonyl esters is sensitive towards steric and electronic effects introduced by substitutions at the non-leaving acyl group (Fersht, 1999), the rates may reflect intrinsic reactivities of the different fMet-Pro*-tRNAs. Alternatively, the position and/or chemical nature of the substitution might interfere with the ribosomal active site. Finally, intrinsic analog-specific reactivities could be modulated by the ribosome e.g. by restricting the conformation of the peptidyl chain in the active site.

To distinguish between the influence of intrinsic and ribosome-specific effects the reactivity of the Pro analogs was determined off the ribosome. Provided that the reactions on and off the ribosome are mechanistically comparable, this should allow monitoring only the intrinsic reactivity differences. As model reaction the nucleophilic attack on the ester bond of fMet-Pro*-$tRNA^{Pro}$ by aqueous glycinamide was monitored, with glycinamide optimally reflecting the nucleophilicity of an aa-tRNA (Schroeder & Wolfenden, 2007). In addition, the hydrolysis of peptidyl-tRNA was determined as a less complex and kinetically well accessible model reaction (Fig. 34). The peptidyl-tRNAs, containing

radioactive fMet, were incubated in the presence or absence of 0.2 M glycinamide serving as N-nucleophile at 37 °C. The decomposition into radioactive peptide and unlabeled tRNA was monitored by nitrocellulose filtration (section 5.4, Materials & Methods).

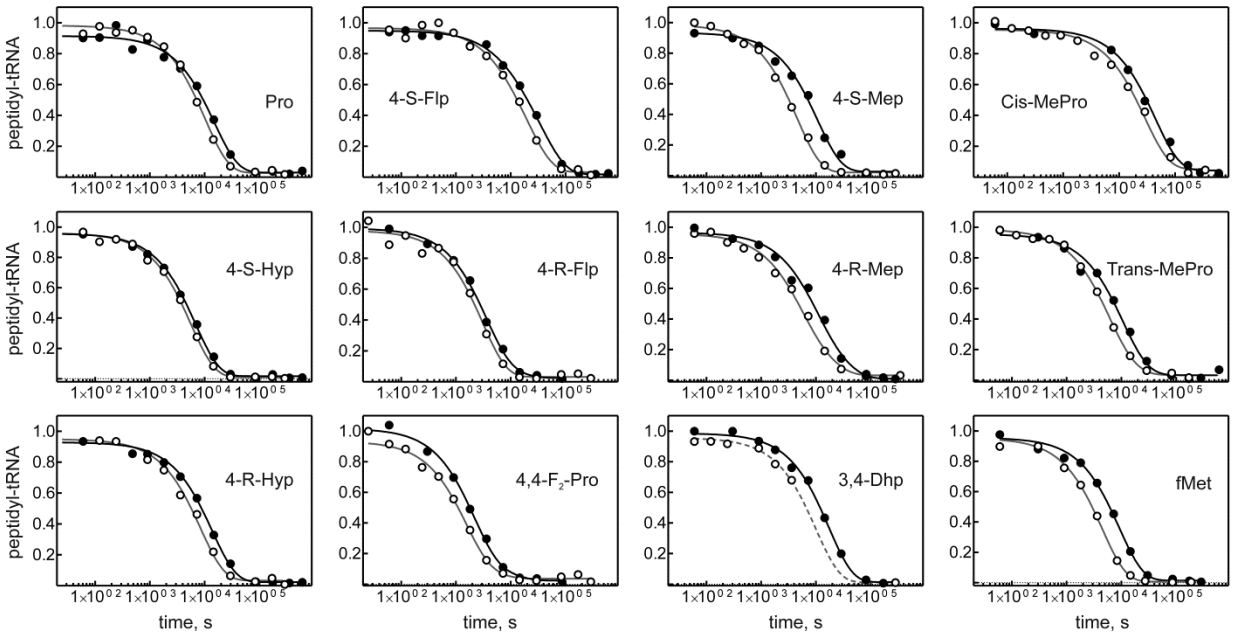

Fig. 34: Decay of peptidyl-tRNA fMet-Pro*-tRNA^{Pro}

Hydrolysis of peptidyl-tRNA fMP*-tRNA^{Pro} (closed circles) and decomposition of peptidyl-tRNAs in the presence of 0.2 M unprotonated glycinamide (open circles). Pro* as indicated in each panel. For rates see Table 7.

Table 7: Rates of fMet-Pro*-tRNA^{Pro} decay

Pro*	k_{hydrol} $\times 10^5$ s^{-1}	k_{aminol} $\times 10^5$ s^{-1}	k_{decay} $\times 10^5$ s^{-1}
Pro	6.3 ± 0.5	3.7 ± 0.5	10 ± 0.5
4-S-Flp	3 ± 0.3	2 ± 0.4	5 ± 0.4
4-R-Flp	23 ± 1	9 ± 3	32 ± 3
4,4-F_2-Pro	31 ± 1	28 ± 5	59 ± 5
4-S-Hyp	14 ± 1	4 ± 1	18 ± 1
4-R-Hyp	6.3 ± 0.1	7 ± 2	13 ± 2
cis-MePro	1.7 ± 0.2	1.8 ± 0.3	3.5 ± 0.3
trans-MePro	8.4 ± 0.3	6.6 ± 0.6	15 ± 0.6
4-S-Mep	3.7 ±0.9	-	-
4-R-Mep	3.8 ±0.04	10 ± 1	14 ± 1
3,4-Dhp	5.6 ± 0.2	(4.4 ± 1)	(10 ± 1)
fMet	11 ± 0.6	11 ± 1	22 ± 1

Rates of fMet-Pro*-tRNA^{Pro} (0.5 µM) decomposition in the absence (k_{hydrol}) or presence (k_{decay}) of glycinamide (1 M; 0.2 M unprotonated) in 20 mM HEPES-HCl pH 7.5 at 37 °C, 100 mM KCl and 7 mM $MgCl_2$. The rate of aminolysis (k_{aminol}) was determined according to $k_{aminol} = k_{decay}-k_{hydrol}$.

The rate of aminolysis (k_{aminol}) was determined according to $k_{aminol} = k_{decay} - k_{hydrol}$. Consistent with other model systems (Bruice et al, 1970), substituent effects on aminolysis and hydrolysis showed the same tendencies (Table 7, Fig. 34), indicating a sensitivity of both reactions. Decomposition rates of all peptidyl-tRNAs were almost evenly distributed over the kinetic range, with peptidyl-tRNAs with Pro*= 4,4-F_2-Pro and 4-R-Flp being the most reactive and *cis*-MePro being the

most unreactive species. Notably, the kinetic range of hydrolysis/aminolysis rates was strikingly small compared to that on the ribosome, with a maximal difference of 18 to 16-fold, respectively (Table 7). However, the rates of hydrolysis/aminolysis in solution (*k*) and that of peptide bond formation on the ribosome (k_{pep}) correlate linearely in a log-log plot (Fig. 35), demonstrating that the substituents similarely effect the ribosomal and in-solution reactions. In other words, the reactivity determining features are inherent characteristics of the substrates. Notably, the slope of the plot is not 1 as it would be expected for an equal sensitivity towards Pro substitutions on and off the ribosome but ~0.2. This indicates a dramatically increased sensitivity of the ribosomal reaction towards intrinsic reactivity differences compared to both in-solution reactions. Possible reasons might be the different environment of the ribosome and/or conformational constraints within the peptidyl transferase center which amplify unfavorable conformational preferences of the substrates.

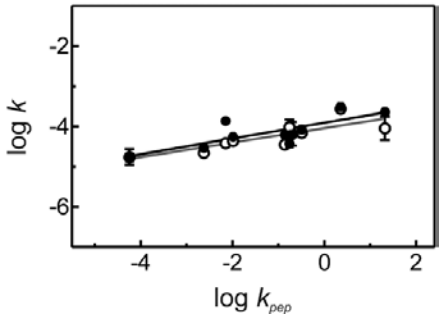

Fig. 35: Correlation between substituent effects on the ribosomal and in-solution reactions.

Hydrolysis (closed circles)/aminolysis (open circles) of peptidyl-tRNA in solution and peptide bond formation on the ribosome for all Pro derivatives. Average rates and SD from three replicates are plotted. For some points SD is too small to be visible. P values are 0.007 and 0.003 for the correlation with hydrolysis and aminolysis, respectively.

2.2.3.5 The reactivity does not correlate with the electrophilicity of the P-site substrate

If reactivity differences were primarily caused by a changed electrophilicity of the P-site substrate, the rate of peptidyl transfer should correlate with the pK_a of the respective analog. Because the conformation of the X-Pro bond modulates the carboxyl pK_a determined in model peptides (Table S11) and the Pro analogs have a characteristic *cis-trans* ratio (Table S12), an weighted average pK_a was calculated based on the isomer specific pK_a values and the respective *cis-trans* equilibria of each Pro* (Table S11). The resulting impirical pK_a values of the Pro analogs were in the range of 2.8-3.6 and did not correlate with the rate differences in peptide bond formation on the ribosome (Fig. 36). Moreover, the carboxyl- pK_a of other amino acids such as valine, phenylalanine and alanine, the k_{pep} of which are > 100-fold faster than for Pro (Wohlgemuth et al, 2008), is similar as well (Table S13). Overall, this indicates that the electrophilicity of proline does not explain its poor reactivity as P-site substrate.

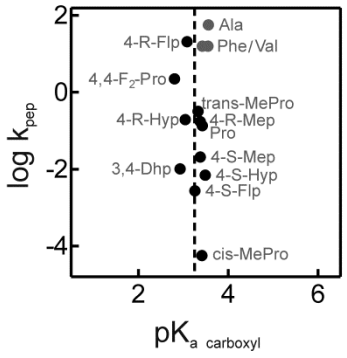

Fig. 36: The electrophilicity of the P-site substrate does not correlate with the reaction rate.

Correlation of the rate of peptidyl transfer with the electrophilicity of Pro derivatives. Rates of fMet-Pro*-Pmn formation were replotted from Table S14. The pKa values were calculated from the cis and trans pKa of the respective Pro*, taking the cis-trans equilibrium into account. Rates of fMet-Xaa-Pmn formation, with Xaa= Ala, Val and Phe were replotted from (Wohlgemuth et al, 2008).

2.2.3.6 Isomery

The five-membered prolyl ring is subject to conformational restrictions which are accompanied by rapidly interconverting *exo* and *endo* puckers and a tendency to form *cis* isomers. Thus, the steric properties of proline might render its poor reactivity.

Comparison of the rate of peptide bond formation of four R/S-analog pairs revealed that the R isomer is generally more reactive than the S isomer (Fig. 37A). Although R/S configurations relate to the analogs only, the interrelated isomer and pucker preferences could be of relevance for the EF-P mechanism. R-(Flp, Hyp) and *trans*-MePro adopt the *trans* conformation more frequent than their S or *cis* counterparts (Table S12). However, a more qualitative comparison does not show any obvious correlation between the rate of peptide bond formation and the *trans* preference (Fig. 37B).

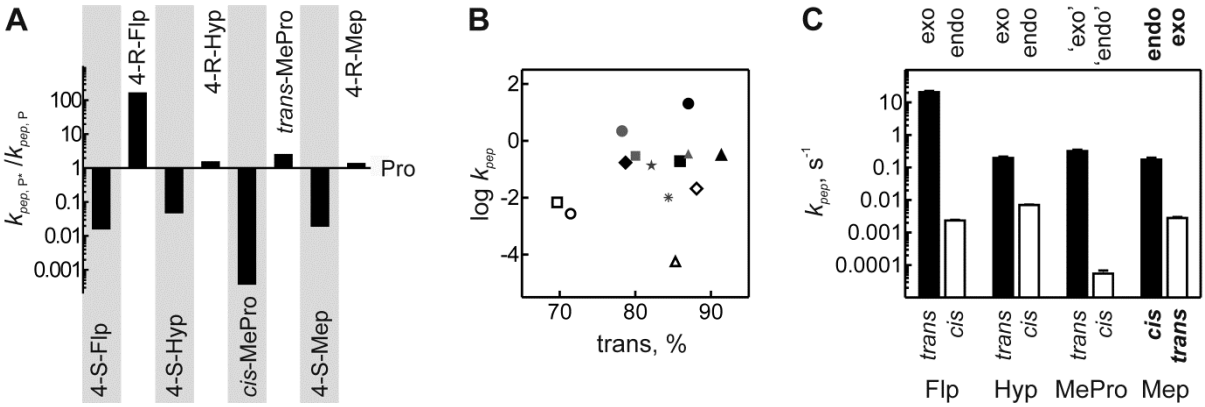

Fig. 37: Peptide bond formation is faster with R analogs

A) Relative rates of fMP*-Pmn formation for Pro* normalized to Pro. B) Influence of *trans* content of the X-P* bond on the rate of fMP*-Pmn formation. 4-(R/S)-Hyp (squares), 4-(R/S)-Flp (circles), 4-(R/S)-Mep (diamonds), *cis/trans*-MePro (triangles). S isomers (open symbols), R isomers (closed symbols). Pro, 3,4-Dhp and 4,4-F_2-Pro in grey asterisk, star and circle, respectively. C) Effect of the stereochemistry of Pro*on k_{pep} of the reaction with Pmn. Plotted are the k_{pep} values for each pair of analogs that differ only in their substituent orientation at the C_γ atom, in the R- (black bars) or S- (white bars) configuration. Isomer and pucker preference are as indicated. *Cis*- and *trans*-MePro are covalently arrested pucker mimics. The average values and SD are calculated from up to four replicates. For exact values, see Table S12 and Table S14.

Although there is no strict coupling, *trans*-stereoisomers tend to prefer the *exo* pucker conformation (Hinderaker & Raines, 2003; Milner-White et al, 1992; Vitagliano et al, 2001). *Cis*-MePro is an

exception in that it mimics the *endo* pucker conformation but has a *trans*-X-Pro* bond content comparable to other R-substituted analogs. Because *cis*-MePro was an exceptionally poor substrate, the pucker conformation rather than the *cis-trans* preference might determine the rate of peptide bond formation (Fig. 37C). Alternatively, the observed reactivity differences could originate from the orientation of the substituent. The electron donating methyl group in 4-(R/S)-Mep leads to a higher content of *cis*-X-P* bonds and *endo* pucker in the R- compared to the S-analog. However, 4-R-Mep was more reactive in peptide bond formation compared to 4-S-Mep, supporting the notion that R-analogs are better substrates than their S-counterparts, irrespective the pucker conformation. Notably, an unfavorable positioning of S-substrates due to a clash with the ribosome is unlikely to cause the poor reactivities, because the trends in solution are similar.

A way to test whether the conformational freedom of the prolyl ring influences the rate of peptide bond formation is to vary the ring size. Aze and Pip are 4 and 6 membered Pro derivatives; respectively and the conformational freedom of the prolyl ring is decreased in Aze (flat conformation) and increased in Pip (mainly chair, boat conformations). Upon peptidyl transfer from fMet-Pro*- $tRNA^{Pro}$ to Pmn, with Pro* being either Pro, Aze or Pip the latter two show double-exponential kinetics (Fig. 38), suggesting that the complexes formed with Aze and Pip were heterogeneous for unknown reason. In case of Aze the slower rate could correspond to *cis-trans* isomerization. The weighted average rates, taking the relative contribution of both rates into account, of Aze and Pip were in the same order of magnitude as proline (0.14, 0.3 and 0.35 s^{-1} for Pro, Aze and Pip, respectively, Table 8) indicating that conformational restrictions inherent to the five-membered ring were not a dominant underlying characteristic of Pro-mediated stalling.

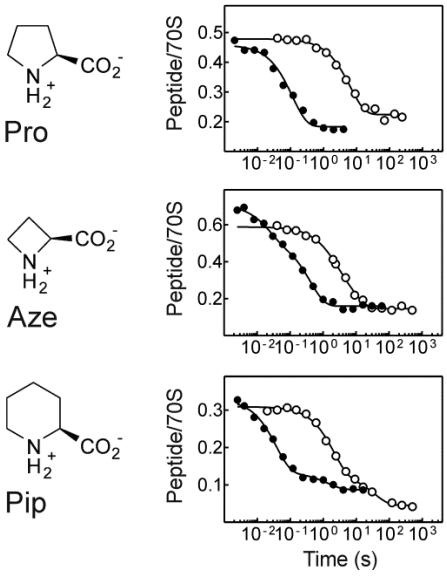

Fig. 38: Impact of ring size on peptide bond formation

fMP*-Pmn formation in the presence (closed circles) and absence (open circles) of EF-P with P* being either Pro, Aze or Pip as indicated.

Table 8: Influence of the ring size on the rate of peptidyl-transfer

aa	rate 1, s^{-1}	rate 2, s^{-1}	Weight average rate, s^{-1}
	- EF-P		
Pro	0.14 ± 0.1		0.14 ± 0.1
Aze	0.12 ± 0.04 (60%)	0.55 ± 0.26 (40%)	0.3 ± 0.1
Pip	0.5 ± 0.06 (68%)	0.03 ± 0.01 (32%)	0.35 ± 0.05
	+ EF-P		
Pro	8.2 ± 0.8		8.2 ± 0.8
Aze	2.4 ± 0.3 (66%)	45 ± 13 (34%)	17 ± 5
Pip	27 ± 3 (81%)	0.7 ±0. 3 (19%)	22 ± 3

Furtheremore, the rate of *cis-trans* interconversion of peptide bonds preceeding Aze and Pip is increased (0.1-1 s^{-1}) compared to Pro (10^{-4}-10^{-3} s^{-1}) (Kern et al, 1997), further indicating that *cis*- or

trans-conformations of the X-P bond influence the rate of peptide bond formation only slightly, if at all. EF-P accelerates the reaction of all substrates to a similar extend (~60 fold), which might indicate that a shared characteristic is targeted.

2.2.3.7 Impact of Pro analogs on activation parameters

To further understand the substituent effects and to dissect EF-Ps contribution, the thermodynamic impact of Pro derivatives on peptidyl transfer was investigated. The analog pair 4-(S/R)-Flp was chosen because R- and S-Flp have the same substituent but large opposite substituent effects. The rate of peptidyl transfer from fMet-(R/S)-Flp-tRNA^{Pro} to Pmn (10 mM) was monitored at different temperatures at pH of 7.5 in the presence and absence of EF-P (Fig. 39A-D, Table S15). The reaction was performed and analyzed as described (Materials & Methods).

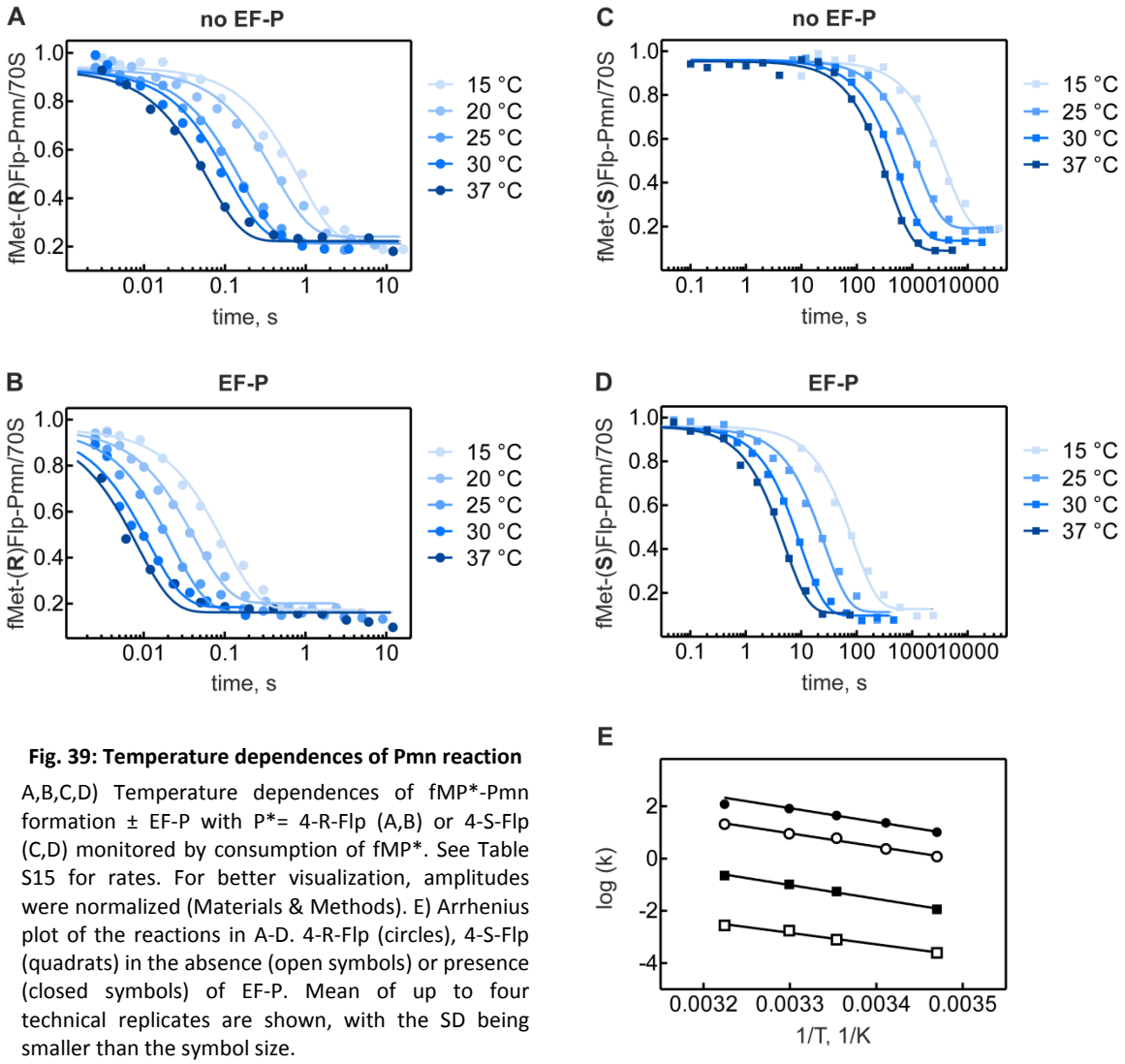

Fig. 39: Temperature dependences of Pmn reaction

A,B,C,D) Temperature dependences of fMP*-Pmn formation ± EF-P with P*= 4-R-Flp (A,B) or 4-S-Flp (C,D) monitored by consumption of fMP*. See Table S15 for rates. For better visualization, amplitudes were normalized (Materials & Methods). E) Arrhenius plot of the reactions in A-D. 4-R-Flp (circles), 4-S-Flp (quadrats) in the absence (open symbols) or presence (closed symbols) of EF-P. Mean of up to four technical replicates are shown, with the SD being smaller than the symbol size.

All reactions followed the Arrhenius law (Fig. 39E) and the activation parameters were calculated according to equations 3-6 (Materials & Methods). Due to experimental restrictions in quantifying rates >100 s^{-1} with high precision, the rate for 4-R-Flp in the presence of EF-P at 37 °C was excluded

from the fitting (Materials & Methods). The Arrhenius-plots of the four reactions revealed almost parallel linear relationships which resulted in similar activation enthalpies for all four reactions ($\Delta H^{\neq}_{average}$ = 22.5 ± 2 kcal/mol, Table 9). Accordingly, rate differences were of entropic origin: The activation entropy was more favorable in 4-R-Flp than in 4-S-Flp (Table 9). In the presence of EF-P the activation entropy was more favorable for 4-R-Flp ($T\Delta\Delta S^{\neq}_{EFP\ -\ no\ EFP}$= 2.4 kcal/mol) and 4-S-Flp ($T\Delta\Delta S^{\neq}_{EFP\ -\ no\ EFP}$ = 6.6 kcal/mol) compared to the EF-P uncatalyzed reactions (Table 9), supporting the idea that the rate acceleration by EF-P is entropically driven (see section 2.2.2.2). EF-P improved the free energy of activation ($\Delta\Delta G^{\neq}$) by -1.2 kcal/mol for 4-R-Flp and -2.5 kcal/mol for 4-S-Flp.

Table 9: Activation parameter for fMP*-Pmn formation with P* = 4-(R/S)-Flp

Pro*	$\Delta G^{\neq}$, kcal/mol	$\Delta H^{\neq}$, kcal/mol	$T\Delta S^{\neq}$, kcal/mol
4-R-Flp, no EF-P	16 ± 1	22 ± 2	6 ± 0.6
4-R-Flp, EF-P [a]	15 ± 1	24 ± 1	8.4 ± 0.7
4-S-Flp, no EF-P	22 ± 1	20 ± 2	- 2.2 ± 0.2
4-S-Flp, EF-P	19 ± 1	24 ± 1	4.4 ± 0.3

Activation parameters were calculated for 25 °C according to equations 4-6 (Materials & Methods). [a] The value at 37 °C was excluded from the fitting

3 DISCUSSION

3.1 The biological role of EF-P

The first part of this study dealt with the investigation of the function of EF-P in translation, which was not established at the beginning of this thesis. We showed that EF-P specifically accelerates peptide bond formation with proline and glycine residues, thereby preventing ribosome stalling and facilitating efficient synthesis of proteins containing polyproline motifs (section 2.1.2) (Doerfel et al, 2013). At the same time Ude and colleagues came to the same conclusions (Ude et al, 2013); subsequently, the function of EF-P was confirmed by several other groups (Bullwinkle et al, 2013; Peil et al, 2013; Starosta et al, 2014; Woolstenhulme et al, 2013). After our results on EF-P were presented, also eIF5A was found to facilitate peptide bond formation with consecutive prolines (Gutierrez et al, 2013), suggesting that the function is conserved in prokaryotes and eukaryotes. The function of EF-P in translation elongation depends on β-lysylation of Lys34 but not on hydroxylation (section 2.2.1.1) (Bullwinkle et al, 2013; Doerfel et al, 2013; Ude et al, 2013). This is corroborated by similar, albeit somewhat milder, phenotypes caused by deletions of genes encoding EpmA or EpmB compared to deletion of the EF-P gene (Marman et al, 2014; Zou et al, 2012), while deletion of EpmC in *S. typhimurium* causes no noticeable phenotype (Bullwinkle et al, 2013).

3.1.1 EF-P inactivation causes pleiotropic *in-vivo* phenotypes

Consistent with the determined function, quantitative mass spectrometric analysis of the proteome of Δ*efp* strains of *S. typhimurium* and Δ*efp* strains of *E. coli* revealed that an above-average number of downregulated proteins contain PPP and PPG motifs (Hersch et al, 2013). Furthermore, the majority of proteins containing PPP as well as specific XPPY motifs are down-regulated in Δ*efp*, Δ*epmA*, Δ*epmB* in *E. coli* and the expression can be restored by complementing the cells with modified EF-P *in vivo* (Peil et al, 2013). Some of the identified down-regulated proteins readily explain phenotypes observed in cells lacking modified EF-P. Deletion of EF-P, EpmA and/or EpmB genes modulate a variety of cellular functions including cell viability, growth, virulence, motility, and sensitivity to low osmolarity, detergents, and antibiotics (Abratt et al, 1998; Balibar et al, 2013; Bearson et al, 2011; Charles & Nester, 1993; Iannino et al, 2012; Kaniga et al, 1998; Marman et al, 2014; Navarre et al, 2010; Peng et al, 2001; Zou et al, 2012). About 7% of annotated *E. coli* genes encode motifs of three or more consecutive prolines or PPG motifs. Notably, proteins of the basal transcription-translation machinery are underrepresented, while metabolic enzymes, transporters and regulatory transcription factors are frequent among proteins containing PPP or PPG motifs (Doerfel et al, 2013). Consistently, quantitative comparison of the wild type and Δ*efp* proteome of *S. typhimurium* by stable isotope labeling of proteins in cell culture (SILAC) revealed that metabolic

proteins and two-component regulatory systems that regulate cell motility and chemotaxis are overrepresented among proteins that are down-regulated in cells lacking EF-P (Hersch et al, 2013). Transcriptional repressors were not identified (Hersch et al, 2013), presumably because they escaped the dynamic range of current mass spectrometers due to their low abundance. The pleiotropic phenotypes observed in Δ*efp*/Δ*epmA*/Δ*epmB* strains can be rationalized by EF-Ps function in accelerating proline incorporation.

3.1.1.1 Susceptibility to external stimuli

A prominent group of misregulated proteins in cells lacking functional EF-P are membrane proteins (Balibar et al, 2013; Navarre et al, 2010; Zou et al, 2012). Membrane proteins play important roles in many metabolic pathways and are essential for antibiotic-induced lethality (Girgis et al, 2009; Kohanski et al, 2008; Silver, 2011; Tamae et al, 2008; van Stelten et al, 2009). Consistently, an altered membrane permeability caused by the lack of functional EF-P may explain the increased susceptibility to external stressors in Δ*efp* strains (Hersch et al, 2013; Zou et al, 2012). This idea is supported by *in-vitro* data showing that internal polyproline motifs in TonB led to robust stalling and that efficient translation is restored by EF-P (section 2.1.2.7) (Doerfel et al, 2013; Ude et al, 2013). TonB supplies energy for the function of TonB-dependent transporters that import siderophores (ferric chelates), vitamin B12, nickel ions and carbohydrates (Noinaj et al, 2010). Reduced iron uptake due to a TonB deficiency may contribute to reduced growth phenotypes observed in Δ*efp* strains (Doerfel et al, 2013). Another interesting example is CadC whose translation depends on EF-P *in vitro* and *in vivo* (Ude et al, 2013). CadC regulates translation of the lysine/cadaverine antiporter CadB and the lysine decarboxylase CadA. CadA generates the polyamine cadaverine (Cad) which inhibits the activity of porins (OmpF and OmpC) (Miller-Fleming et al, 2015). Furthermore, translation of Rz1 - an outer membrane lipoprotein involved in host lysis by bacteriophages (Berry et al, 2012; Berry et al, 2008) - stalls at a polyproline motif in its periplasmic domain and efficient synthesis depends on EF-P *in vitro* and *in vivo* (section 2.1.2.7) (Doerfel et al, 2013; Ude et al, 2013).

3.1.1.2 Motility

Δ*efp*, Δ*epmA*, Δ*epmB* strains of *S. typhimurium* (Bearson et al, 2011; Hersch et al, 2013; Zou et al, 2012) and *B. subtilis* (Kearns et al, 2004) show reduced motility. This observation may be explained by the reduced synthesis of proteins involved in cell motility, the expression of which is decreased in Δ*epmA S. typhimurium* (Bearson et al, 2011; Hersch et al, 2013). Consistently, FlhC and Flk which regulate expression of flaggelar proteins require EF-P to be efficiently synthesized *in vitro* (section 2.1.2.7) (Doerfel et al, 2013; Ude et al, 2013).

3.1.1.3 Virulence

In several pathogenic organisms deletion of genes encoding EF-P and its modifying enzymes is connected with a reduction of the virulence potential (Charles & Nester, 1993; Iannino et al, 2012; Kaniga et al, 1998; Navarre et al, 2010; Peng et al, 2001). This may be explained by the altered expression of virulence factors containing polyproline motifs. In *A. tumefaciens* deletion of the EF-P encoding *chvH* gene causes avirulence by reducing the cellular level of the virulence factor VirE2. Consistent with the presence of a PPP motif in VirE2, this phenotype can be rescued by introduction of *E. coli* EF-P (Peng et al, 2001). In some cases the altered virulence potential may be explained by an impaired pathogen-host interaction due to altered expressions of membrane associated proteins. In *B. abortus* deletion of the EF-P-encoding gene leads to a penetration defect which causes avirulence (Iannino et al, 2012). In *S. flexneri* deletion of genes encoding for EF-P or EpmA reduces expression of several virulence effector proteins including IpaA, -B, and -C and IcsA involved in pathogen-host interaction and leads to reduced mRNA levels of virB and virF encoding master virulence regulators (Marman et al, 2014). Consistently, the sequence of IpaA contains LPTPP and TPPL which lead to weak ribosome stalling *in vivo* and *in vitro* (Peil et al, 2013). This indirect evidence for the involvement of EF-P in virulence is further supported by *in vitro*-investigations: EspFU, which requires EF-P for efficient synthesis *in vitro* (section 2.1.2.7)(Doerfel & Rodnina, 2013), is a key player during the infection of eukaryotic hosts by enterohaemorrhagic *E. coli* (EHEC) (Campellone et al, 2004; Sallee et al, 2008). The fact that virulence proteins contain polyproline motifs in combination with different modification pathways in eukaryotes and bacteria opens the possibility to generate new antimicrobials which target EF-P or its modifying enzymes (Doerfel et al, 2013).

3.1.2 Potential regulation by the EF-P modification state

As discussed in the previous section, the expression of a variety of proteins depends on proper EF-P function, resulting in far-reaching consequences for the cellular fitness in the absence of EF-P. Because the cellular level of spermidine- the basis for eIF5A modification- is tightly controlled by the metabolism in eukaryotes, the modification status of eIF5A was proposed to function as a late response which transmits environmental changes by regulation of the cell proliferation (Miller-Fleming et al, 2015). In yeast, spermidine was proposed to serve mainly for eIF5A modification (Chattopadhyay et al, 2008; Chattopadhyay et al, 2003). In *E. coli*, the modification of EF-P is based on lysine, which in other contexts is involved in regulatory processes: The lysine-dependent gene regulation mechanism of the lysC riboswitch (Caron et al, 2012; Smith-Peter et al, 2015) or the necessity of lysine to induce CadC expression (Ude et al, 2013) demonstrates the potential of lysine to regulate the modification status of EF-P. Considering that EF-P requires posttranslational modification to acquire its full catalytic proficiency, the EF-P modification pathway may allow

regulation of translation, e.g. in a manner similar to that in eukaryotes. This might explain why polyproline or PPG sequences are found with high frequency in metabolic enzymes (Doerfel et al, 2013). On the other hand, in *S. oneidensis* and *P. aeruginosa* EF-P is modified with a sugar derivative (Lassak et al, 2015), which may thus connect translation to the energy status in the cell.

3.2 What makes proline slow in peptide bond formation?

EF-P is a specialized translation elongation factor which promotes the synthesis of polyproline stretches that are otherwise poor substrates in peptide bond formation and would cause ribosome stalling (see above). Having thus determined the function of EF-P in bacterial translation, the question arises how EF-P promotes synthesis of polyproline motifs. Similarely to the reduced termination efficiency and slow peptide bond formation caused by proline (Hayes et al, 2002; Pavlov et al, 2009; Tanner et al, 2009), proline-induced stalling is mainly caused by the amino acid (section 2.1.2.8). Thus, as it will be discussed in the following sections, the analysis of the catalytic mechanism of EF-P is linked to the question what makes polyproline motifs poor substrates for protein synthesis.

3.2.1 Poor reactivity of proline

Proline is the only proteinogenic amino acid with a ring spanning the α-carbon and the amino group. However, substitutions on the pyrrolidine-ring dramatically alter the reactivity of Pro in both directions (sections 2.2.3.3 and 2.2.3.4). Some Pro analogs even show reactivities similar to other proteinogenic amino acids. This indicates that imino acids are not per se unreactive in peptide bond formation. Notably, substituent effects are immense on the ribosome and only small in solution; however the residual trend is similar (Fig. 35, section 2.2.3.4). Because steric and electronic properties of proline are highly interdependent (Improta et al, 2001; Shoulders & Raines, 2009) interpretations of their impact on peptide bond formation have to be made with caution. The electrophilicity of the carbonyl-carbon of different Pro analogs and other proteinogenic amino acids such as Val, Phe or Ala is similar (section 2.2.3.5). This indicates that the electrophilicity of proline does not explain its poor reactivity as P-site substrate or its stalling properties on the ribosome and suggests that the steric properties of proline lead to stalling. Consistently, when analog pairs such as Flp, Hyp and MePro were compared, peptidyl transfer was faster for the analog that preferred *exo* and *trans* conformations; however, when all analog pairs were considered no clear correlation was observed (section 2.2.3.6). This could indicate that there is not only one particular conformation that is favorable for nucleophilic attack, but that the peptidyl-tRNA can acquire one out of an ensemble of possible conformations. To conclude, there is no simple explanation based on electrophilicity and preferences for single conformations. However, the entropic character of substituent effects (section 2.2.3.7) in combination with their dramatic effect on the ribosome-catalyzed reaction suggests that

an unfavorable positioning of the peptidyl-Pro-tRNA^{Pro} is exaggerated in the ribosomal active site compared to the reaction in solution and thus is a major determinant for proline´s reduced reactivity. For the future it will be interesting to cocrystallize peptidyl-Pro-tRNA^{Pro} and modified EF-P in complex with the ribosome and to use such structures for detailed molecular dynamic simulations. Our biochemical data may provide orthogonal information and serve as benchmark for such studies.

3.2.2 Proline in proteins and in the cell

Proline is a poor substrate for the peptidyl transferase center which can induce ribosome stalling but at the same time is important for protein structure and function. Thus, presumably the same properties of proline lead to a necessity of minimizing translational stalling and yet keeping the necessary functionality. Although EF-P might reduce the evolutionary pressure, stalling motifs should be avoided as long as they are not functionally relevant. Interestingly, the frequency of proline is declining in taxa from all domains of life (Jordan et al, 2005). Furthermore, not all polyproline-containing proteins depend on EF-P *in vivo* (Hersch et al, 2013), but stalling at polyproline sequences appears to be strongly influenced by the sequence context (Elgamal et al, 2014; Starosta et al, 2014; Woolstenhulme et al, 2013). Accordingly, engineered PPP/PPG sequences can lead to very strong stalling upon *in-vitro* translation of a model protein, whereas stalling at the same sequences occurring in endogenous proteins was less severe (compare stalling at PPG in PrmC or YafD, section 2.1.2.5 and 2.1.2.7). This indicates that the sequences of endogenous proteins may already be slightly optimized for translation of such motifs (Doerfel et al, 2013). As demonstrated, all Pro analogs could be incorporated into peptides (section 2.2.3), indicating the possibility of their potential biotechnological application. Keeping in mind the characteristics of different substituents, e.g. in stabilizing peptide structure and functional flexibility this opens the intriguing possibility of tuning proteins in structure and function.

3.2.3 Sequence context effects of Pro-induced stalling

The rate of fMPP-G formation was reduced ~300-fold compared to fMP-G formation (Fig. 25, section 2.2.1.4). Notably, not only the A-site substrate but also the C-terminal amino acid in the nascent chain and the P-site tRNA were identical in the two reactions. Hence, the rate differences must have been caused by Pro at the -1 position in the nascent peptide, thus demonstrating that proline-induced stalling is affected by the amino acid sequence context. This 300-fold reactivity difference of fMet-Pro-Pro-tRNA^{Pro} compared to fMet-Pro- tRNA^{Pro} as P-site substrate indicate that stalling at PPP motifs is not due to the accumulation of moderate peptidyl-transferase effect over several consecutive steps, but a cumulative effect. (A rate-reduction due to different accommodation rates is unlikely, because fMP-G formation was not rate limited by accommodation at pH 7.5 (Fig. 28, section 2.2.2.1)). A context effect is corroborated by the identification of several amino acids (X,Y) that

increase ribosome stalling at XPPY motifs (Elgamal et al, 2014; Hersch et al, 2014; Peil et al, 2013; Starosta et al, 2014; Woolstenhulme et al, 2013). Similarly, the efficiency of translation termination was influenced by the second and last amino acids in the nascent chain with ProPro being most severe (Björnsson et al, 1996; Hayes et al, 2002; Mottagui-Tabar et al, 1994). Two possible explanations may account for the observed sequence context dependence in Pro-induced stalling: One possibility is that the Pro-residue at the -1 position may reduce the intrinsic reactivity of the C-terminal proline. As a result, the P-site substrate may have a reduced propensity to act as electrophile for peptide bond formation. This possibility is corroborated by the fact that neighboring amino acids influence stereo-electronic properties of proline (Owens et al, 2007; Renner et al, 2001). However, the reaction rate does not correlate with the carboxyl-pK_a of the P-site substrate (Fig. 36), arguing against the idea that a changed electrophilicity is the major source for the sequence dependency of Pro-induced stalls. Another, more likely explanation can be deduced based on steric considerations: the nascent chain extended by one amino acid might change the conformation/orientation of the C-terminal Pro residue or that of the peptidyl-tRNA in the peptidyl transferase center. Because unmodified EF-P stabilizes the peptidyl-tRNA (see below, sections 2.1.2.3 and 2.2.1.1) and accelerates fMP-G and fMPP-G formation only to the half extend compared to modified EF-P (Fig. 25, section 2.2.1.4) the low reactivity of the peptidyl-Pro-tRNA^{Pro} has most likely been partially caused by a mispositioning of the tRNA. This mispositioning seemed to be amplified by two consecutive prolines (section 2.2.3.6), possibly inducing an unfavorable conformation of the nascent chain and thereby further distorting the position of the tRNA as well as the reactive ester bond. Notably, a recent structure of human pre-termination complex with a stalling peptide containing two C-terminal proline residues revealed that the conformation of the active site residue *Hs* U4493 corresponding to *E. coli* U2585 was drastically changed, presumably due to a clash with the penultimate proline residue (Matheisl et al, 2015). Although this structure was obtained in another organism is shows that two C-terminal proline residues in the nascent peptidyl-chain can have wide reaching consequences on the conformation of the nascent chain as well as residues of the ribosomal active site.

3.3 EF-P binds to the ribosome in a tRNA^{Pro}-specific fashion

EF-P specifically accelerates peptide bond formation with proline. This raises the question where this specificity of EF-P comes from. The crystal structure of ribosome-bound EF-P shows that it is bound between the E and P sites of the ribosome (Blaha et al, 2009); this implies that the E site has to be empty to allow EF-P binding. The propensity for a vacant ribosomal E site increases with ribosomal pausing which in turn would then become a prerequisite for EF-P binding. As proline is a poor A- and P-site substrate (Johansson et al, 2011; Muto & Ito, 2008; Pavlov et al, 2009; Rychlik et al, 1970;

Wohlgemuth et al, 2008) the specificity of EF-P to proline could be just coincidental due to prolines ability to robustly stall ribosomes. However, this is not the case, as EF-P had only marginal effects on other stalling sequences *in vivo* (Hersch et al, 2013; Woolstenhulme et al, 2013) and specifically rescues stalled complexes with a peptidyl-$tRNA^{Pro}$ (Doerfel et al, 2013; Peil et al, 2013; Starosta et al, 2014; Ude et al, 2013). EF-P may thus specifically recognize $tRNA^{Pro}$ or the mRNA codon exposed in the E site. Alternatively, EF-P could bind unspecifically to any stalled complex with an empty E site, but the reaction with other amino acids could be insensitive to EF-P. On the ribosome, EF-P interacts with the P-site $tRNA^{fMet}$ (Blaha et al, 2009) and may be able to contact the mRNA in the E site (Choi & Choe, 2011); however the region of EF-P that point towards the mRNA is unresolved in the crystal structure (Blaha et al, 2009) indicating structural flexibility at this site. Notably, the structure was obtained with $tRNA^{fMet}$ and not $tRNA^{Pro}$, and also the codon in the E site was not a Pro codon but a Lys codon (AAA), which might have prevented specific interactions of EF-P with the codon and the tRNA. EF-P had a reduced catalytic effect when misaminoacylated fMet-Pro-$tRNA^{Phe}$ was used instead of $tRNA^{Pro}$ (Fig. 17, section 2.1.2.8). Notably, for the reaction of these two P-site substrates the codon exposed in the E site was identical (AUG), suggesting that the tRNA and not the mRNA codon reduced the EF-P effect with misaminoacylated Pro-$tRNA^{Phe}$. Additionally in both cases, the C-terminal amino acid (Pro) was the same. Thus, although the amino acid (Pro) would have been sensitive towards EF-P function, the possible effect of EF-P was reduced with $tRNA^{Phe}$. These data could be explained by a reduced affinity of EF-P to $tRNA^{Phe}$ which would indicate that specific recognition of $tRNA^{Pro}$ is required for EF-P to be fully effective. This would require $tRNA^{Pro}$ to contain specific recognition elements. If so, EF-P would have coevolved with $tRNA^{Pro}$ to increase specificity. Notably, tRNA modifications are not important for EF-P recognition, as the usage of the *in-vitro* transcribed $tRNA^{Pro}$ did not alter EF-P function (section 2.2.3.2 and 5.2).

3.4 How does EF-P catalyze peptide bond formation?

3.4.1 EF-P body stabilizes and positions the peptidyl-tRNA

EF-P prevents the dissociation of a peptidyl-tRNA with short nascent chains from the P site (sections 2.1.2.3 and 2.2.1.1), most probably by direct interaction. This is corroborated by structural investigations showing interaction surfaces between the P-site $tRNA^{fMet}$ and unmodified EF-P (Blaha et al, 2009). Moreover, the fact that EF-P seems specific for $tRNA^{Pro}$ further supports the idea of a direct contact that is responsible for tRNA stabilization (section 2.1.2.8). Because tRNA stabilization/positioning is accomplished to the same extent by unmodified EF-P i.e. by the EF-P body (section 2.2.1.1) tRNA stabilization might reflect the main function of the EF-P body. In the crystal structure $tRNA^{fMet}$ adopts virtually identical conformations and positions in the presence and absence

of unmodified EF-P (Blaha et al, 2009). Because fMet-tRNA^{fMet} is more stably bound to the P site compared to peptidyl-tRNA (Lancaster & Noller, 2005) it might not require additional positioning and/or stabilization. Consistently, unmodified EF-P only slightly accelerates fMet-Pmn formation (section 2.2.1.5). In contrast, unmodified EF-P accelerated the synthesis of fMP-G and fMPP-G 3-fold and 10-fold, respectively. The reactivity of the P-site substrate decreases from fMP- to fMPP-tRNA, which is consistent with an increase of conformational constraints of the nascent chain due to its increasing proline content which might be transmitted to the tRNA. Thus, the positioning effect by unmodified EF-P might be of greater relevance for substrates which are more mispositioned compared to others.

3.4.2 The modification of EF-P contributes to catalysis

Compared to unmodified EF-P, modified EF-P further accelerates the rates of peptidyl transfer (sections 2.2.1.1, 2.2.1.4, 2.2.1.5 and 2.1.2.2) as well as translation of longer peptides (section 2.1.2.3) and has an increased capacity to overcome ribosome stalling (section 2.1.2.5). Notably, rate differences were preserved at saturating EF-P concentrations and thus cannot solely be explained by a reduced affinity of the unmodified factor (sections 2.2.1.1 and 2.2.1.4). This is corroborated by similar phenotypes caused by deletion of the modifying enzymes and deletion of EF-P (Marman et al, 2014; Zou et al, 2012) and the fact that the unmodified EF-P K34A variant provided in trans cannot rescue *efp* deletion strains of *E.coli* (Ude et al, 2013). Hence, it can be assumed that in addition to the stabilization and alignment by the body of EF-P its posttranslational modification contributes to the catalytic effect. A molecular model suggests that the β-lysyl-moiety of modified EF-P reaches into the ribosomal active site and is located in the close proximity (2 Å) of the C-terminal proline attached to a P site-bound tRNA (Fig. 40, (Lassak et al, 2015)).

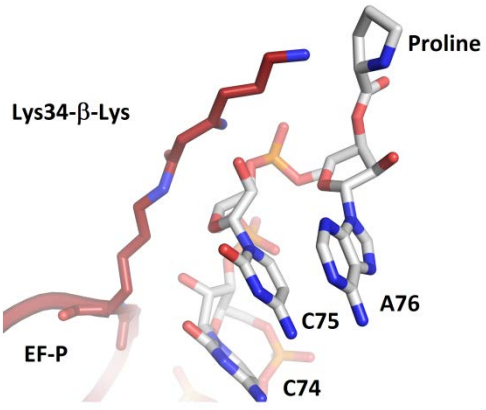

Fig. 40: Model of lysylated EF-P with aminoacyl-tRNA

Close-up view of ribosome bound EF-P. Model of Lys 34 of EF-P modified with R-β-lysine (red) and the CCA-end of Pro-tRNA (grey) bound to the ribosomal P site. The model was recreated from Lassak et al, 2015 and generated in PyMOL (https://www.pymol.org), based on PDB: 3HUY.

However, shorter modifications in eukaryotes and other phylogenetic groups of bacteria argue against a conserved function of EF-P/eIF5A involving a direct interaction of the modification with the peptidyl chain. Therefore, the modification was proposed to primarily stabilize the CCA end of the peptidyl-tRNA (Doerfel et al, 2013; Lassak et al, 2015). However, a lack of conservation in the length

of the modification does not exclude the possibility that the β-lysyl moiety of *E. coli* EF-P actively participates in the chemistry step of peptidyl transfer.

3.4.3 EF-P function does not involve general acid or base catalysis

To investigate whether EF-P participates in general acid-base catalysis, the rate of peptidyl transfer was monitored at different pH values. The experiments show that EF-P shifts the pH optimum of peptidyl transfer from fMet-tRNA^{fMet} or fMet-Pro-tRNA^{Pro} to Gly-tRNA^{Gly} (fM-G and fMP-G, respectively) to lower pH ranges (sections 2.2.2.1). The pK_a value for fM-G formation in the absence of EF-P (7.2) is in good agreement with the pK_a determined previously (7.4) (Johansson et al, 2011)); although both values are smaller than the pK_a of Gly-tRNA^{Gly} in solution (7.8) (Johansson et al, 2011). Johansson and colleagues explain the discrepancy between the pK_a of Gly-tRNA^{Gly} on the ribosome and in solution was explained by a ribosome-induced down-shift of the pK_a (Johansson et al, 2011). However, an alternative explanation is a change of the rate-limiting step at high pH. In the latter case the maximal rate of fM-G formation (70 s^{-1}) would correspond to a pH-insensitive step that leads to an apparent, kinetically down-shifted pK_a (Fersht, 1999). For the current dataset, the latter interpretation is more likely, because the rate of fMP*-G synthesis with Pro derivatives serving as P-site substrates was likewise limited at 70 s^{-1} (Fig. 32, section 2.2.3.3). The fact that both reactions have the same upper rate limit is in good agreement with the rate-limiting accommodation of Gly-tRNA^{Gly} which kinetically masks peptide bond formation. Accordingly, the down-shifted pK_a observed in the presence of EF-P is determined kinetically as well.

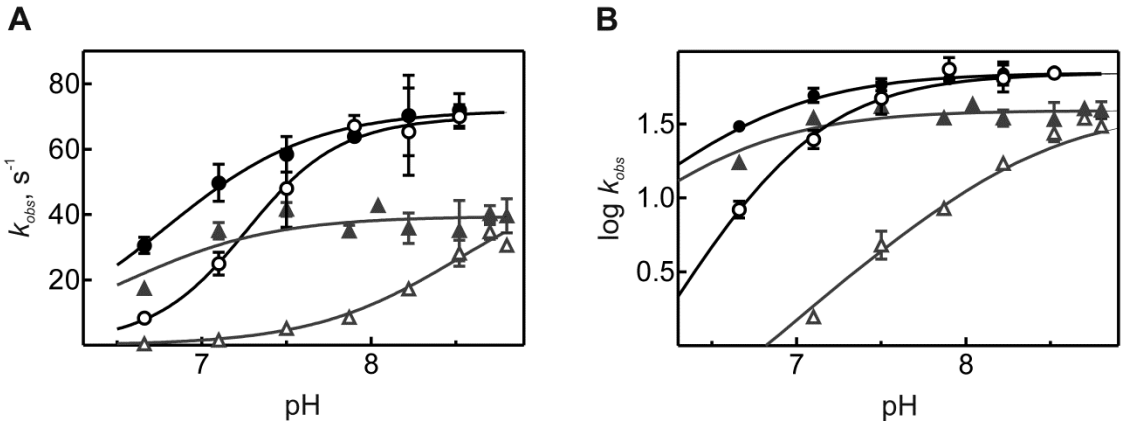

Fig. 41: pH dependent fM-G and fMP-G formation.

Linear (A) and logarithmic plot (B) of pH-dependent fM-G and fMP-G formation (circles and triangles, respectively), determined in the absence (open symbols) and in the presence of modified EF-P (closed symbols). Except for fM-G without EF-P, the pH dependencies were fitted to a model with one ionizing group.

The maximal rate of fMP-G formation from fMet-Pro-tRNA^{Pro} and Gly-tRNA^{Gly} was reduced compared to that of fM-G formation (38 ± 3 s^{-1} and 70 ± 4 s^{-1}, respectively; Fig. 41A). Assuming a rate of Gly-tRNA^{Gly} accommodation of 70 s^{-1} (see above), this might suggests that fMP-G formation actually monitors the chemistry of peptide bond formation. However, the Arrhenius plot for fMP-G formation

determined at pH 7.5 in the presence of EF-P deviates from linearity above 30 °C indicating a change in the rate-limiting step (Fig. 29D, section 2.2.2.2), thus arguing against a rate limiting chemistry step at 37 °C. Accordingly, as for fM-G formation, the pK_a measured for fMP-G formation in the presence of EF-P (pK_a = 6.6) seems to be set kinetically. Due to the small biochemically accessible range in which the reaction with EF-P was pH-dependent, the initial slope of the log(k)-pH dependence was not well defined (Fig. 41B), which precluded the determination of the number of ionizing groups involved in catalysis. The pK_a value determined in the absence of EF-P was 8.5 and thus too high to correspond to the α-amino group of Gly-$tRNA^{Gly}$. Furthermore, because the maximum rate at high pH values may represent a rate-limiting step other than the chemistry step, the real pK_a of the latter reaction might be even higher than 8.5, further aggravating the discrepancy to the literature value of Gly-$tRNA^{Gly}$ (pK_a = 7.8, (Johansson et al, 2011)). The slope of 0.9 for the log(k)-pH plot (Fig. 41B) indicates that only one ionizing group was titrated. Thus, the reaction depends on the deprotonation of one group which is presumably not the attacking nucleophile. This observation could be interpreted as a pH-dependent conformational change within the ribosomal active site. The conformation of active site residues is modulated by pH (Beringer et al, 2005; Hesslein et al, 2004; Xiong et al, 2001) and accordingly, observed pK_as have been assigned to pH-dependent conformational changes of the peptidyl transferase center (Bieling et al, 2006; Katunin et al, 2002; Muth et al, 2001; Okuda et al, 2005). Because the reaction in the absence of EF-P is not limited by the reaction chemistry, the change of the pH dependence by EF-P is most probably not the result of the acid-base catalysis of the chemistry step. Instead, EF-P might influence local rearrangements of the ribosomal active site. Additionally, EF-P positions the peptidyl-tRNA (see above) and may improve the electrostatic environment at the peptidyl transferase center (see below).

Further evidence against general acid-base catalysis by EF-P is provided by the entropic character of the contribution of EF-P to catalysis as demonstrated for fMP-G (section 2.2.2.2) and fMP*-Pmn formation (sections 2.2.3.7). Because acid-base catalysis would involve bond formation and breaking unique to the EF-P catalyzed reaction, the lack of a favorable enthalpic contribution by EF-P disfavors the idea of that EF-P donates functionally active groups (Wolfenden et al, 1999). Also the independence of the peptidyl transfer from fMP*-$tRNA^{Pro}$ to Pmn of the carboxyl-pK_a of the P-site substrate (and thus of the electrophilicity of the attacked carbonyl carbon) (Fig. 36, section 2.2.3.5) argues against general acid catalysis by EF-P.

3.4.4 A possible catalytic mechanism of EF-P

The EF-P body interacts with the tRNA body (Blaha et al, 2009) and facilitates peptide bond formation by stabilization as well as positioning of the peptidyl-tRNA in the ribosomal active site (sections 2.2.1, 2.2.1.4 and 2.2.1.5). The modification of EF-P extends the factor along the CCA end of

the peptidyl-tRNA and further increases the catalytic proficiency of the factor (sections 2.2.1, 2.2.1.4 and 2.2.1.5). The pH titrations indicate that EF-P is not involved in general acid-base catalysis but accelerates peptidyltransfer by altering a pH-dependent rate-limiting step (section 2.2.2.1). Notably, for small substrates conformational changes within the ribosomal active site can be pH-dependent and are critical for efficient peptidyl transfer (Beringer & Rodnina, 2007a; Brunelle et al, 2006; Schmeing et al, 2005b). Moreover, a recent crystal structure of a peptidyl-ProPro-tRNA^{Pro} in the P site of human ribosomes shows that the nascent chain induce a rearrangement of the ribosomal residue *Hs* U4493 (Matheisl et al, 2015). In *E. coli* the corresponding U2585 residue is critical to allow a reorientation of the ester-linkage on the peptidyl-tRNA favorable for nucleophilic attack (Schmeing et al, 2005b). Although the structure was obtained in another organism, it shows that the nascent chain containing two C-terminal Pro residues can stall the ribosome by adopting conformations that lead to rearrangements of ribosomal residues. In analogy to these findings, the peptidyl chain of the poor P-site substrate fMet-(Pro)-Pro-tRNA^{Pro} might sterically induce an unreactive orientation of the peptidyl-tRNA itself and of ribosomal residues. Notably, the reactivity of the P-site substrate decreases with fM-, fMP- and fMPP-tRNA, which would be consistent with an increase of conformational constraints (section 2.2.1.4). The analysis of linear-free-energy relationships (LFER) with proline analogs (section 2.2.3) supports the idea that an unfavorable orientation or conformation of the peptidyl-tRNA plays a major role in proline-induced stalling. EF-P accelerates the reaction with fMetPro-Pro-tRNA^{Pro} more than with fMetPro-tRNA^{Pro} (section 2.2.1.4), indicating that its function is more important for substrates with constrained peptidyl-chains. Apart from the stabilizing and positioning function of the EF-P body, modified EF-P might additionally accelerate peptide bond formation by positioning of the peptidyl-tRNA CCA end and/or the amino acid attached to the peptidyl-tRNA in a more active conformation. The analysis of the activation parameter revealed that EF-P catalyzes peptide bond formation by lowering the entropy of activation (sections 2.2.2.2 and 2.2.3.7) which is in good agreement with the induction of conformational changes. In addition to the positioning effects, a favorable entropic term may be due to an improved electrostatic environment at the peptidyl transferase center or a better orientation of water molecules involved in catalysis (Polikanov et al, 2014; Sharma et al, 2005; Trobro & Aqvist, 2005; Wallin & Aqvist, 2010). Thus, EF-P might as well support the preorganization of catalytic water molecules or the H-bond network required for efficient proton-shuttling.

4 MATERIALS AND METHODS

4.1 Equipment

Table M1: Equipment

Device	Manufacturer
Milli-Q Advantage A10	Millipore
pH meter, pH electrode	WTW
Vortex Genie 2	Scientific Industries
Water bath RE104 and E100	Lauda
Benchtop centrifuge 5415R and 5810R	Eppendorf
Centrifuge Avanti J-26 XP	Beckmann Coulter
Centrifuge Avanti J-30I	Beckmann Coulter
Ultracentrifuge Optima XPN-100	Beckmann Coulter
Galaxy mini star	VWR
Electrophoresis power supply EV261	Peqlab Biotechnologie
Mini gel electrophoresis chamber	Peqlab Biotechnologie
PCR thermocycler Peqstar	Peqlab Biotechnologie
Nanodrop 2000C	Peqlab Biotechnologie
Bio-vision imaging system	Peqlab Biotechnologie
Emulsiflex C-3 homogenizer	Avestin
FLA-9000 biomolecular imager	Fuji
Plates incubator INE600	Memmert
Incubator shaker series Innova44	New Brunswick
ÄKTA FPLC	GE Healthcare
ÄKTA Explorer	GE Healthcare
Liquid scintillation counter	PerkinElmer
RQF-3 Rapid Quench-Flow Instrument	KinTek

4.2 Software

Table M2: Software

Software	Provider
Pymol 1.3	Schrödinger
GraphPad Prism 5.0	GraphPad software
MultiGauge 2.0	Fujifilm
FluorEssence 3.5	Horiba Scientific

4.3 Chemicals and consumables

Chemicals were purchased from Sigma Aldrich, Roche Molecular Biochemicals or Merck, unless stated otherwise. Chemicals for electrophoresis (agarose, acrylamide and SDS) were obtained from Serva, GTP from Jena Bioscience, kits for DNA preparation from Macherey-Nagel and protein concentrators, nitrocellulose filters, sterile filters were purchased from Sartorius. Radioactive

compounds were obtained from Hartmann Analytic. Scintillation liquid IRGA-SAFE Plus and Quickszint 361 were obtained from PerkinElmer and Zinsser Analytics, respectively.

4.4 Reaction buffers

Most kinetics were performed either in buffer A or buffer B. Buffer A allows comparison of the new data with the literature because many studies were performed in this buffer. Furthermore, ribosomal complexes are more stable in buffer A compared to buffer B. However, buffer B is more physiological, the proofreading is better than in buffer A and the determined rates are more comparable to rates determined *in vivo*. For the experiments the buffer was chosen depending on the respective purpose of the experiment.

Buffer A: 50 mM Tris-HCl pH 7.5 at 37 °C, 70 mM NH_4Cl, 30 mM KCl and 7 mM $MgCl_2$; buffer B: 50 mM Tris-HCl pH 7.5 at 37 °C, 70 mM NH_4Cl, 30 mM KCl, 3.5 mM $MgCl_2$, 0.5 mM spermidine, 8 mM putrescine and 2 mM DTT; buffer C: 50 mM Tris-HCl pH 7.5 at 37 °C, 70 mM NH_4Cl, 30 mM KCl, 1 mM spermidine, 16 mM putrescine and 4 mM DTT, for all pH titrations the buffer was supplemented with 20 mM Bis-Tris; buffer D: 20 mM HEPES-HCl pH 7.5 at 37 °C, 100 mM KCl and 7 mM $MgCl_2$. All buffers were filtered through a 0.2 µm cellulose acetate filter (Sartorius Stedim). For temperature dependencies, the pH of the buffer was adjusted at the respective temperature.

4.5 Bacterial strains

For molecular biological work *E. coli* DH5α or TOP10 cells were used; for expression *E. coli* BL21(DE3) cells were used.

Table M3: Bacterial strains

strain	Genotype
E. coli DH5α	F^- endA1 glnV44 thi-1 recA1 relA1 gyrA96 deoR nupG Φ80d*lacZ*ΔM15 Δ(*lacZYA-argF*)U169, hsdR17(r_K^- m_K^+), λ–
E. coli TOP10 Invitrogene	F- mcrA Δ(mrr-hsdRMS-mcrBC) ϕ80lacZΔM15 ΔlacX74 nupG recA1 araD139 Δ(ara-leu)7697 galE15 galK16 rpsL(Str^R) endA1 λ^-
E. coli BL21(DE3)	$F^–$ ompT gal dcm lon $hsdS_B$(r_B^- m_B^-) λ(DE3 [lacI lacUV5-T7 gene 1 ind1 sam7 nin5])

4.6 Cloning

In general, genes encoding proteins of interest were amplified from *E. coli* genomic DNA by PCR using corresponding primers containing cleavage sides for restriction enzymes at their 5' ends and the amplified DNA fragments were digested with the respective restriction enzymes (NEB). The target vector was cleaved with the respective enzyme, dephosphorylated by arctic phosphatase (NEB), and the DNA fragment was ligated into the vector using Quick T4 DNA ligase (NEB) according to the

manufacturer's protocol. The ligation mixture was transformed into *E. coli* TOP10 cells (Invitrogen) and plated on LB agar plates containing the antibiotic, for which the vector provides resistance. Colonies were picked and grown over night in LB medium containing antibiotic and the plasmid was purified using the NucleoSpin Plasmid kit (Macherey-Nagel) according to the manufacturer's protocol. The sequence of the plasmid was determined by DNA sequencing.

To introduce point mutations into plasmids by QickChange technique (Stratagene) (Constructs 08b-j) PCR primers which spanned the target position for mutation and contained the point mutation were generated. The mutation was introduced into the plasmid by PCR amplification of the complete vector using the primers. The template, not containing the mutation is digested by Dpn1, which digests methylated DNA, for 1-2 h at 37 °C. Plasmid multiplication and purification was performed as described above.

4.6.1 Construct for overexpression of EF-P and its modifying enzymes

The vector constructs containing genes encoding EF-P and its modifying enzymes EpmA and EpmB (pET28*efp*, pET28*efp/epmA*, pET28*efp/epmA/B*) were kindly provided by Frank Peske, MPI-BPC, Göttingen. The construct pET28*efp/epmA/B/C* was cloned on the basis of pET28*efp/epmA/B* by Christina Kothe, MPI-BPC Göttingen. The cloning strategy was as follows: Genes coding for EF-P (*efp*) and its modifying enzymes EpmA (*epmA*), EpmB (*epmB*) and EpmC (*epmC*) were amplified from the *E. coli* genome (BL21(DE3) cells). The genes were first cloned separately into pET24a and a construct containing the ribosomal binding site encoded by pET24a together with the respective gene was cloned into pET28a. The *efp* gene was cloned into pET28a, adding an N-terminal 6xHis tag to EF-P as described (Yanagisawa et al, 2010). To obtain EF-P in different modification statuses, EF-P was overexpressed either alone or together with its modifying enzymes from the following constructs: pET28*efp*, pET28*efp/epmA*, pET28*efp/epmA/B* and pET28*efp/epmA/B/C* (Fig. M1). Since only EF-P need to be purified, the other genes were cloned without tag.

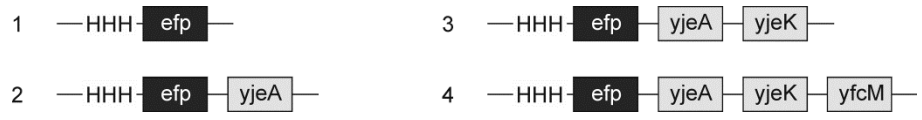

Fig. M1 EF-P constructs in pET28a

4.6.2 Generation of mRNA constructs

To generate mRNAs corresponding to proteins containing polyproline motifs the respective genes (encoding for release factor glutamine methyltransferase (PrmC; 1-75); TonB, outer membrane subunit Rz1; N-acetylmuramoyl-L-alanine amidase (AmiB, 1-159); flagellar transcriptional regulator (FlhC, 1-94); flagellar regulator (Flk, 1-87) and YafD (1-75)) were amplified from genomic DNA of *E.*

coli BL21(DE3) with primers introducing 3' Xho1 and 5' Nde1 restriction sites (Table M5). The PCR product was digested with *Nde1* and *Xho1* (New England Biolabs) and ligated into the pET24a vector (Novagen). The gene of secreted effector protein EspF(U) (1-154) from *E. coli* DH5alpha with 3' Xho1 and 5' Nde1 restriction sites was purchased from Eurofins and cloned into pET24a as described for the other constructs. Some of these constructs were cloned by Christina Kothe and Jörg Mittelstät, MPI-BPC Göttingen (see Table M4).

4.6.3 Construction of $tRNA^{Pro}$ template

The transcript of $tRNA^{Pro}$ was prepared as described (Brown et al, 1979). Two partially complementary DNA oligomers containing isoacceptor $tRNA^{Pro}$ with the anticodon CGG fused to T7 RNA polymerase promoter were obtained from IBA (primer 1 and 2,Table M5), extended by PCR and cloned into pUC19 vector using SMA1 restriction site (Himeno et al, 1989). The CCG isoacceptor was chosen because its matching codon (CCG) is the most abundant of the four Pro codons (Dong et al, 1996) and was reported to be the most efficient for proline incorporation (Pavlov et al, 2009).

4.6.4 Constructs used in this study

Table M4: Plasmids

C	Construct	Comment
01	pET28_*efp*[a]	pET28 vector for expression of N-terminally 6xHis-tagged EF-P
02	pET28_*efp/epmA/B*[a]	Like 01 but additionally for expression of EpmA and B
03	pET28_*efp/epmA/B/C*[b]	Like 01 but additionally for expression of EpmA, B and C
04	pET24a_*epmA*[a]	pET24a vector containing EpmA gene, template for cloning EpmA with ribosomal binding site (RBS) of pET24a into pET28
05	pET24a_*epmB*[a]	Like 04 but encoding EpmB instead of EpmA
06	pET24a_*epmC*[b]	Like 04 but encoding EpmC instead of EpmA
07	pUC19_$tRNA^{Pro}$	pUC19 vector containing sequence of $tRNA^{Pro}$ CGG isoacceptor fused to T7 RNA promoter
08a	pET24a_prmC[c]	pET24a vector containing sequence of PrmC, template for mRNA formation
08 b-j	pET24a_prmC_mod	Like 08a, containing pointmutations introducing PG, PP, PPG, PPGF and PPP into PrmC sequence
09-15	pET24a_XY[b]	pET24a vector containing sequence of genes coding for TonB (09), YafD (10), Rz1 (11), AmiB (12), FlhC (13), Flk (14) and EspfU (15)
16	pEX-K_EspfU1-154	pEX-K vector containing sequence of EspfU gene from *E. coli* DH5alpha (N-terminal fragment, 154 amino acids)

Constructs were [a] provided by F. Peske; cloned by [b] C. Kothe or [c] J. Mittelstät (Mittelstaet, 2012)

4.6.5 Primer

DNA oligonucleotides were obtained from IBA Life Sciences or Eurofins MWG Operon.

Table M5: DNA oligonucleotides

Primer for cloning EF-P constructs		
Name	Sequence 5'→ 3'	Template/Comment
EF-P_Nde1_F	ATTCCTCATATGGCAACGTACTATAGCAACGATTTTCG	For amplification from *E. coli* BL21(DE3) genome and cloning into pET28 by N-terminal Nde1 and C-terminal Yba1 restriction site
EF-P_Xba1_R	TGGTGGTCTAGATTACTTCACGCGAGAGACGTATTCACCAG	
EpmA_pET24_F	GAGATATACATATGAGCGAAACGGCATCCTGGCAGC	For amplification from *E. coli* BL21(DE3) genome and cloning into pET24a by N-terminal Nde1 and C-terminal Yba1 restriction site
EpmA_pET24_R	GTGGTGCTCGAGTGCCCGGTCAACGCTAAAGGCGATG	
EpmA_-Nde1_F	TGACCAGCCCGGAATACCATACGAAACGCCTG	To remove internal Nde1 site in EpmA gene
EpmA_-Nde1_R	CAGGCGTTTCATACGGTATTCCGGGCTGGTCA	
EpmA_pET28_F	CAATTCCCCTCTAGAAATAATTTTGTTTAACTTTAAGAAG	pET24a_EpmA, for cloning into pET28_efp
EpmA_pET28_R	TGGTGGGAATTCTCTTATGCCCGGTCAACGCTAAAGGC	F:EpmA including RBS, R: introduces Stop codon and EcoR1 site
EpmB_pET24a_F	GAGATATACATATGGCGCATATTGTAACCCTAAATACCCC	For amplification from *E. coli* BL21(DE3) genome and cloning into pET24a by N-terminal Nde1 and C-terminal Yba1 restriction site
EpmB_pET24a_R	GGTGGTGGTGCTCGAGCTGCTGGCGTAGCTGGAGATCCAG	
EpmB_pET28_F	CCCCTCTAGAAAGAATTCTGTTTAACTTTAAGAAGGAGATATAC	pET24a_EpmB, for cloning into pET28_efp/EpmA; F: EpmB including RBS, introduces EcoR1 site; R: introduces Stop and BamH1 site
EpmB_pET28_R	GGTGGTGGATCCCTTACTGCTGGCGTAGC	
EpmC_pET28_F	AGTTGCTAGCAAGGAGATATACATATGAACAGTACACACCACTACGAGCAGTTG	For amplification from *E. coli* BL21(DE3) genome and cloning into plasmid 02 by N-terminal Nde1 and C-terminal Pst1 restriction sites
EpmC_pET28_R	TCAACTGCAGTCAGTTGAGCGCTTCCGGCC	
Primer for tRNA transcript		
Name	Sequence 5'→ 3'	Template/Comment
1	AGTTGCTGCAGTAATACGACTCACTATACGGUGAUUGGCGCAGCCUGGUAGCGCACUUCGUUCG	For cloning of $tRNA^{Pro}$ sequence into PUC19 using SMA1 restriction sites
2	TGGTCGGTGATAGAGGATTCGAACCTCCGACCCCTTCGTCCCGAACGAAGTGCGCTACCAGGCTG	
3	GTTTTCCCAGTCACGAC	pUC19_$tRNA^{Pro}$, to generate PCR template for transcription
4	TGmGTCGGTGATAGAGGATTC	
m designates a 2'-O-methyl group to prevent nonspecific 3'mRNA extension by T7 RNA polymerase		
Primer for cloning translation constructs into pET24a		
Name	Sequence 5'→ 3'	
tonB_Nde1_F	GATTATGACTCATATGACCCTTGATTTACCTCGCCG	

tonB_Xho1_R	GACTTTCCTCGAGCTGAATTTCGGTGGTGCC
yafD_Nde1_F	TCAAAGTCACATATGCGAAAAAACACC
yafD_Xho1_R	ACATCTCGAGTTTATCAGGCTTGC
Rz1_Nde1_F	GAGTTAGCATATGCGAAAGCTGAAAATGATGC
Rz1_Xho1_R	TGCACTCGCGCCAGTCGTTCCCGGAG
AmiB_Nde1_F	GGTCATATGATGTATCGCATC
AmiB_Xho1_R	GGTCTCGAGTTAATTGCGCGCCGGTTC
FlhC_Nde1_F	CCTCATATGAGTGAAAAAAGCATTG
FlhC_Xho1_R	CCTCTCGAGTTAAACAGCCTGTACTCTC
Flk_Nde1_F	GGATACATATGATACAACCTATTTCCGGCCCTCC
Flk_Xho1_R	TCGAGACGAACCAGCCAGACCAGC

Quickchange primers to modify 08a pET24a_prmC construct

Name	Sequence 5'→ 3'
PrmC_PG_F	GAGCGAAAGCCCGGGGCGTGATGCTGAAATCC
PrmC_PG_R	GGATTTCAGCATCACGCCCCGGGCTTTCGCTC
PrmC_PP_F	CAGGCGAGCGAACCCCCGCGGCGTGATGC
PrmC_PP_R	GCATCACGCCGCGGGGGTTCGCTCGCCTG
PrmC _PPG_F	CAGGCGAGCGAACCCCCGGGGCGTGATGCTGAAATCC
PrmC _PPG_R	CAGCATCACGCCCCGGGGGTTCGCTCGCCTGAAGTTG
PrmC _PPP_F	AACCCCCGCCGCGTGATGCTGAAATCC
PrmC _PPP_R	CATCACGCGGCGGGGGTTCGCTC
PrmC _PPPG_F	CGAGCCCGCCCCCGGGGCGTG
PrmC _PPPG_R	CGGGGGCGGGCTCGCCTGAAGTTGG
PrmC _3x ccc_F	AGCGAACCCCCCCCCCGTGATGCTGA
PrmC _3x ccc_R	CAGCATCACGGGGGGGGGGTTCGC
PrmC _3x cca_F	GGCGAGCGAACCACCACCACGTGATGCTGA
PrmC _3x cca_R	CAGCATCACGTGGTGGTGGTTCGCTCGC
PrmC _3x cct_F	GGCGAGCGAACCTCCTCCTCGTGATGCTGA
PrmC _3x cct_R	CAGCATCACGAGGAGGAGGTTCGCTCGC
PrmC _3x ccg_F	GGCGAGCGAACCGCCGCCGCGTGATGCTGA
PrmC _3x ccg_R	CAGCATCACGCGGCGGCGGTTCGCTCGC

Primer for mRNA formation

Name	Sequence 5'→ 3'	Template/ Comment
T7-5 forward	TAATACGACTCACTATAG	Forward primer for all mRNAs
PrmC 14_R	AAGTTGGCTTATTGCTTCACG	pET24a_PrmC, generates template for mRNA of indicated length
PrmC 28_R	CAGCAGGATTTCAGCATCACGC	
PrmC 42_R	AAAGGCGAGGATAAAAGTACGC	
PrmC 56_R	ATCAAGTTGCTGACATTGTTCG	
PrmC 70_R	ATGAGCAATGGGTTCACCATCG	
PrmC 75_R	TCGCACCCCGGTTAAATGAG	
PrmC 84_R	AACAAATAAACGGCAACGACCAGA	
PrmC 112_R	ACGGCAAGGTTGTTCAGGCA	
PrmC 140_R	ATCTACAGCGGTAATTTCGCAGT	
PrmC 168_R	CCAGTCGCTTTGCAGAATGCG	
PrmC 196_R	TTGTTGAAGATGTGGGTCCTGCT	

PrmC 224_R	CGACTGTTCGATGATATGCACGA	
PrmC 252_R	GAGGATAAATGCTTGTCGCACCG	
TonB 56_R	TTCGAGATCAGCAGGCGTAACC	pET24a_TonB, generates template for mRNA of indicated length
TonB 62_R	CTGAACGGCTTGTGGCGG	
TonB 70_R	CTCTACCACCGGCTCCGG	
TonB 80_R	TTCGGGGATCGGCTCAGGTTC	
TonB 110_R	TGGCTGCTCCTGTACCTTTTTCAC	
TonB 160_R	CTGATTACGGCTTAATGCGCG	
TonB 239_R	GTTCGCAGGCTTGGCTGAGAGGATTTG	
YafD_20_R	TAAGATCCTTTCCGCAGGTTGTC	pET24a_YafD, generates template for mRNA of indicated length
yafD_75_R	CAATAACACCAGATGTGCATC	
Rz1_40_R	GCATTATCCACGCCGGAGG	pET24a_Rz1, generates template for mRNA of indicated length
Rz1_62_R	GTTCCCGGAGGGTGAAATAATCC	
AmiB_90_R	AGGCGTTCCAGAGCGAATC	pET24a_AmiB, generates template for mRNA of indicated length
AmiB_129_R	CACATCGGCGTTAATCGTAAAGA	
AmiB_159_R	GCGCGGTGCGACAACC	
FlhC_52_R	CGGTGGGCTTCCGCGCAGTTC	pET24a_FlhC, generates template for mRNA of indicated length
FlhC_94_R	CGCATCGACGCCATTACACA	
Flk_14_R	TGGTGGTTGCCCAGGAGG	pET24a_Flk, generates template for mRNA of indicated length
Flk_94_R	ACGAACCAGCCAGACCAG	
EspfU_117_R	TGGTGGCGCAGGCCAGTTAG	pET24a_EspfU, generates template for mRNA of indicated length
EspfU_155_R	CTCGAGGAATATGTTCAGCCATAT	

4.7 RNA

4.7.1 Short mRNA constructs

Short mRNAs were purchased from IBA Life Sciences. They are based on 002 mRNA and have a strong Shine-Dalgarno sequence (Calogero et al, 1988). The 5' → 3' sequence is GGCAAGGAGGUAAAUA followed by codons encoding the peptide of interest. The codons were chosen to be recognized by the most abundant tRNA isoacceptor (Dong et al, 1996). For Pro and Gly CCG and GGU were used respectively. Ile (AUU) served as last untranslated codon for all short mRNAs (Table M6).

Table M6: Synthetic mRNAs

Name	Sequence
fMPFI	GGCAAGGAGGUAAAUAAUGCCGUUCAUU
fMPGFI	GGCAAGGAGGUAAAUAAUGCCGGGUUUC
fMPFGI	GGCAAGGAGGUAAAUAAUGCCGUUCGGUAUU
fMPPFI	GGCAAGGAGGUAAAUAAUGCCGCCGUUCAUU
fMPPPFI	GGCAAGGAGGUAAAUAAUGCCGCCGCCGUUCAUU
fMPPGFVI	GGCAAGGAGGUAAAUAAUGCCGCCGGGUUUCGUU
fMPPPGI	GGCAAGGAGGUAAAUAAUGCCGCCGCCGGGUAUU
fMFGI	GGCAAGGAGGUAAAUAAUGUUCGGUAUU

fMFFGI	GGCAAGGAGGUAAAUAAUGUUCUUCGGUAUU
fMFFFGI	GGCAAGGAGGUAAAUAAUGUUCUUCUUCGGUAUU
fMFPGI	GGCAAGGAGGUAAAUAAUGUUCCCGGGUAUU
fMGPFI	GGCAAGGAGGUAAAUAAUGGGUCCGUUCAUU
fMVGF	GGCAAGGAGGUAAAUAAUGGUUGGUUUC
fMWPPFI	GGCAAGGAGGUAAAUAAUGUGGCCGCCGAUU
fMKEFI	GGCAAGGAGGUAAAUAAUGAAAGAAUUCAUU
fMR_2PGFI	GGCAAGGAGGUAAAUAAUGCGACCGGGUUUCAUU
fMQ_2PGFI	GGCAAGGAGGUAAAUAAUGCAGCCGGGUUUCAUU
fMEG3I	GGCAAGGAGGUAAAUAAUGGAGGGUAUU
fMDPGFI	GGCAAGGAGGUAAAUAAUGGACCCGGGUUUCAUU
Pro1Stop	GGCAAGGAGGUAAAUAAUGCCGUAAGUUAUU
No SD	AUGUUCAUCCCUUCUUAUACUACCUUCACG

4.7.2 Transcription of long mRNAs

For long mRNAs the open reading frames of the genes of interest were cloned into pET24a as described (section 4.6.2). Using the vector as a template, PCR constructs containing the T7 promoter and the Shine-Dalgarno sequence of the pET24a 5'UTR (GGGGAAUUGUGAGCGGAUAACAAUUCCCCC UCUAGAAAUAAAUUUUGUUUAACUUUAAGAAGGAGAUAUACAU) followed by the respective open reading frame were obtained (Primers are listed in Table M5). These oligonucleotides were further used as template for transcription, which was performed in transcription buffer containing 40 mM Tris-HCl pH 7.5, 15 mM $MgCl_2$, 2 mM spermidine, 10 mM NaCl, 10 mM DTT, 3 mM NTPs each, 5 mM GMP, 10% (v/v) DNA template, 5 u/ml pyrophosphatase (PPase), 1.5% (v/v) RiboLock RNase inhibitor (Fermentas) and 0.8% (v/v) T7 RNA-polymerase for 3 h at 37 °C. For peptide markers mRNA templates of desired length of each protein were generated using reverse primer listed in Table M5. The mRNAs were purified with the RNeasy Midi Kit (Qiagen) according to the manufacturer's protocol. The mRNA concentration was determined by OD_{260} measurement and calculated according to $c = OD_{260}/(\varepsilon \cdot d)$, with d is the diameter of the cuvette, ε is the extinction coefficient of the mRNA determined by nearest neighbor model.

4.7.3 Preparation of the $tRNA^{Pro}$ transcript

The $tRNA^{Pro}$ was cloned as described (section 4.6.3) and a template for transcription was amplified from the plasmid using primers 3 and 4 (Table M5). Transcription was performed by incubation of transcription template (~100 µg/ml) in 40 mM Tris-HCl pH 7.5, 15 mM $MgCl_2$, 2 mM spermidine, 10 mM NaCl, 10 mM DTT supplemented with 3 mM NTPs, 5 mM CMP, 0.01 u/µl PPase, 1.6 u/µl T7 RNA polymerase (Fermentas) and 0.6 u/µl RiboLock RNase inhibitor (Fermentas) for 3 h at 37 °C.

The transcript was purified on a HiTrapQ HP column (GE Healthcare) in 50 mM NaOAc pH 5, 10 mM $MgCl_2$ with increasing salt concentrations (up to 1.1 M NaCl). Fractions containing tRNA transcript

were pooled, phenolized and precipitated with ethanol. The tRNA pellet was resolved in H_2O and the concentration was determined by aminoacylation with [^{14}C]proline. To confirm the functionality of the tRNA transcript it was compared to native tRNA^{Pro} in all assays applied. All kinetics were virtually identical for both tRNAs, indicating that the lack of modification does neither interfere with the translation apparatus nor with the function of EF-P (Fig. S1).

4.7.4 Native tRNAs

Native tRNAs (X-tRNA^{X}, with X= fMet, Phe, Lys, Gly, Trp, Val, Arg and Glu) were prepared as described (Gromadski & Rodnina, 2004). αBodipyFL-Met-tRNA^{fMet} (BOF-Met-tRNA^{fMet}) was prepared as described (Mittelstaet et al, 2013). Other tRNAs (X-tRNA^{X}, with X = Pro, Asp, Gln) were prepared from *E. coli* total tRNA by aminoacylation with the respective ^{14}C-labeled amino acid (Kothe et al, 2006) followed by phenol extraction (Aqua-Phenol pH 4.5 RNA grade, Roth) and ethanol precipitation at -20 °C over-night. The tRNA was pelleted by centrifugation at 5000 x g for 1 h at 4 °C, the pellet was dried in speedvac apparatus (Thermo Fischer) and dissolved in water. The aminoacyl-tRNA was enriched by high performance liquid chromatography (HPLC) on a LiChrospher WP 300 column (Merck) using a gradient of 0-15% ethanol in 20 mM ammonium acetate, pH 5.0, 400 mM NaCl and 10 mM magnesium acetate and precipitated using ethanol. The precipitated aa-tRNA was dissolved in water and stored at – 20 °C.

4.7.5 Isolation of peptidyl-tRNA

Peptidyl-tRNAs were obtained by extraction from posttranslocation complexes (PTCs, see next section) with 50 mM NaOAc pH 5, 500 mM KCl, 100 mM EDTA, for 10 min at 37 °C and separation of tRNA and ribosomal subunits by ultracentrifugation at 260,000 × g for 1 h at 4 °C. Supernatant containing peptidyl-tRNA fMet-Pro*-tRNA^{Pro} was purified and handled as described for the tRNA transcript. Additional purification and concentration of the peptidyl-tRNA was obtained by using Centrifugal filter units (Merck) according to the manufacturers' protocol.

4.7.6 Aminoacylation of tRNA

Aminoacylation of tRNA^{Pro} with proline or proline analogs was performed in buffer containing 30 mM HEPES-HCl pH 7.5, 30 mM KCl, 10 mM $MgCl_2$, 1 mM DTT and 3 mM ATP. 25 µM tRNA^{Pro} was mixed with 60 µM [^{14}C]Pro or 2-5 mM Pro analog in the presence of 1 µM prolyl-tRNA synthetase (Pro-RS) and 0.5% IPPase and incubated at 37 °C for 30 min. The efficiency of aminoacylation was determined by nitrocellulose filtration with subsequent [^{14}C] radioactivity counting. For unlabeled Pro analogs the efficiency of aminoacylation was estimated indirectly by quantification of the incorporation efficiency into peptides. Pro-RS can aminoacylate tRNA^{Pro} with all Pro-analogs but with different efficiency. Recognition of aa-tRNA by EF-Tu was confirmed by different migration behavior of the ternary

complex compared to EF-Tu on native PAGE (see below) (Ohtsuki et al, 2010) and by purification of ternary complex by size-exclusion chromatography (SEC, see section 4.7.9).

Aminoacylation of 80 u/ml total tRNA (Roche) was performed in the same buffer but with 16 mM $MgCl_2$ and 5% S100 instead of synthetase and 0.3 mM of each amino acid for 40 min at 37 °C. The pH of the total tRNA was adjusted to 7.5 by 1 M Tris-HCl. Amino acid stock solutions were obtained by dissolving the respective amino acid in water at 0 °C, except for Trp and Leu which were dissolved in 0.3 M Tris-HCl at 37 °C and Glu, Asp and Phe which were dissolved in 0.1 M Tris-HCL at 50 °C. Aminoacylated tRNA was purified as described for tRNA transcript (see above).

4.7.7 Misaminoacylation of $tRNA^{Phe}$

Phe-$tRNA^{Phe}$ was hydrolysed in 1/3 volume HEPES pH 9 at 37 °C for 8 h and deacylated tRNA was ethanol precipitated at -20 °C over-night. For misaminoacylation $tRNA^{Phe}$ was preincubated with Flexizyme dFx (Murakami et al, 2006) in 100 mM HEPES KOH pH 7.5, 100 mM KCl and 600 mM $MgCl_2$ for 5 min at room temperature followed by 4 min on ice. Subsequently, 5 mM Pro-3,5-dinitrobenzyl ester (Pro-DBE) was added and the aminoacylation reaction was kept on ice for further 60 min. Misacylated tRNA was EtOH precipitated (-20 °C over-night) and purified by TC-formation with subsequent gel filtration (as described above).

4.7.8 Analysis of Pro*-$tRNA^{Pro}$ binding to EF-Tu by native PAGE

To determine the efficiency of aminoacylation of $tRNA^{Pro}$ with Pro analogs and to prove the complex formation with EF-Tu a gel shift assay was performed as described with small changes (Ohtsuki et al, 2010). To form binary complex (BC; EF-Tu·GTP) EF-Tu was preincubated with 1 mM GTP, 0.1 µg/µl pyruvate kinase and 3 mM phosphoenolpyruvate for 15 min at 37 °C in buffer containing 40 mM HEPES-KOH pH 7.6, 52 mM NH_4OAc, 8 mM $Mg(OAc)_2$. The BC was mixed with equal amounts of $tRNA^{Pro}$ from the aminoacylation mixture and incubated at 37 °C for further 10 min. TC and BC were separated by gel electrophoresis on 5% native PAGE and visualized by staining with Coomassie.

4.7.9 Purification of tRNA/TC by size-exclusion chromatography (SEC)

The aminoacyl-tRNA was added to EF-Tu·GTP to form a ternary complex (see section 4.9.2) and the EF-Tu complexed tRNA was purified by FPLC gel filtration on two Superdex 75-10/300 GL columns (GE Healthcare) run in tandem in buffer A (Gromadski & Rodnina, 2004; Rodnina et al, 1995). The ternary complex was either used immediately or the aminoacyl-tRNA was phenolized and isolated by ethanol precipitation. The TC concentration was either determined by radioactivity counting (when radioactively labeled amino acids were used) or photometrically at 260 nm (when Pro analogs were used). Using this method, the recognition of Pro*-$tRNA^{Pro}$ by EF-Tu·GTP was confirmed (see section 5.3).

4.8 Proteins

4.8.1 EF-P expression and purification

For overexpression of EF-P *E. coli* BL21(DE3) cells were transformed with the respective construct (see section 4.6.4) and the cells were cultured in LB medium supplemented with kanamycin (30 µg/ml) at 37 °C. At OD_{600} of 0.7 to 0.8 the expression was induced by the addition of IPTG (1 mM). After 3 h of further incubation the cells were harvested and pelleted for 45min at 30000 x g using a JLA8.1 Beckmann rotor (Avanti J-26 XP centrifuge (Beckman Coulter)). Pellets were resuspended in Protino buffer A (20 mM Tris-HCl, pH 8.5, 300 mM, NaCl, 5 mM, 2-mercaptoethanol, 15% glycerol) supplemented with Complete Protease Inhibitor (Roche) and a trace of DNaseI. Cells were opened using an EmulsiFlex-C3 apparatus, and the cell extract was centrifuged for 30 min at 300,000 × g using JA25.30 Beckmann rotor (Avanti J-26 XP centrifuge (Beckman Coulter)). For purification of EF-P by affinity chromatography by its N-terminal His tag the supernatant was applied to a Protino Ni-IDA gravity-flow column (Macherey-Nagel). Following the manufacturers protocol the column was washed with Protino buffer A and the protein was eluted with Protino buffer A containing 250 mM imidazole. Purified protein was concentrated and the buffer was exchanged for cleavage buffer (20 mM Tris-HCl, pH 8.4, 150 mM NaCl and 2.5 mM $CaCl_2$) by membrane filtration (Vivaspin 10,000). The His-tag was cleaved off with 2 units thrombin (GE Healthcare) per 5000 pmol EF-P at room temperature overnight. The protein was concentrated by membrane filtration (Vivaspin 10,000) and the cleaved His tag and thrombin were removed by FPLC purification of EF-P on a HiTrapQ HP column (GE healthcare) using a 50 mM - 2 M NaCl gradient in 30 mM Tris-HCl, pH 7.5. Fractions containing EF-P were pooled, concentrated and the buffer was exchanged to buffer A containing 10% glycerol by membrane filtration (Vivaspin 10,000). The concentration was determined by absorbance at 280 nm, assuming an extinction coefficient of 25,440 cm^{-1} M^{-1} (calculated on: www.biomol.net/en/tools/proteinextinction.htm).

4.8.2 Purification of native EF-P

Native EF-P was prepared as previously described (Aoki et al, 1997; Doerfel et al, 2013) by first pelleting ribosome-bound EF-P followed by purification of EF-P by FPLC with small changes. *E. coli* MRE600 cells were opened in opening buffer (20 mM Tris-HCl pH 7.6, 30mM KCl, 10 mM $MgCl_2$, 3 mM 2-mercaptoethanol, 0.5 mM PefaBloc supplemented with one crystal of DNase) using an EmulsiFlex-C3 at 1.5 bar applied pressure and 1000 bar effective pressure (two cycles) and the lysate was centrifuged for 45 min at 30000 x g in a JA25.50 Beckmann rotor (Avanti J-30I centrifuge (Beckman Coulter)). The supernatant was collected and EF-P was dissociated from ribosomes by increasing the salt concentration to 700 mM KCl which leads to dissociation of the ribosomal subunits. Ribosomes were pelleted as described (Rodnina & Wintermeyer, 1995) by centrifugation at

300,000 × g for 5 h using TI 50.2 fixed angle rotor, Optima XPN-100 Ultracentrifuge (Beckman Coulter). The supernatant was dialyzed against dialysis buffer (25 mM HEPES pH 7.4 at 4 °C, 50 mM KCl, 10 mM $MgCl_2$, 5 mM 2-mercaptoethanol, 0.5 mM PefaBloc, 5% glycerol).

For purification by ion-exchange chromatography the sample was loaded on 42 ml Sepharose Q column (Company) and the protein was eluted by a gradient from 50 to 500 mM KCl in 25 mM HEPES pH 7.4 at 4 °C, 10 mM $MgCl_2$, 5 mM 2-mercaptoethanol and 5% glycerol. Fractions containing EF-P were identified by a dot blot (section 4.8.3) using an anti-EF-P antibody (kindly provided by D. Görlich, Max Planck Institute for Biophysical Chemistry, Goettingen), pooled and concentrated by membrane filtration (Vivaspin 10,000). Further purification was obtained by two times gelfiltration on a HiLoad Superdex 26/60 75 µg column (GE Healthcare) in 25 mM HEPES pH 7.4, 200 mM KCl, 10 mM $MgCl_2$, 5 mM 2-mercaptoethanol, 5% glycerol. Fractions containing EF-P (identified by dot blot) were pooled and loaded onto 6 ml Recource Q anion exchange column (GE Healthcare). Purification was obtained by a gradient from 75-300 mM KCl in 25 mM HEPES pH 7.4, 10 mM $MgCl_2$, 5 mM 2-mercaptoethanol, 5% glycerol. Fractions were analyzed by dot blot and SDS-PAGE, and fractions containing EF-P were pooled and concentrated. For storage, the buffer was exchanged to 2 x buffer A before adding one volume of glycerol. The concentration of native EF-P was determined by comparing densiometrically quantified band intensities of the native EF-P and of overexpressed EF-P of known concentration.

4.8.3 Identification of EF-P-containing fractions by dot blot

To identify fractions containing EF-P, 1 µl fraction and 200 ng EF-P as control were spotted on nitrocellulose membrane and blocked for 1 h with NetG (1x PBS pH 7.5, 0.1% Tween 20, 0.25% gelatine) at RT. The membrane was incubated with first antibody (α EF-P, 1:20000 in NetG) for 1 h at RT, washed with NetG (3 x 15 min) and incubated with the second antibody (α rabbit IgG, 1:5000 in NetG) for 1 h at RT followed by washing with NetG. Positive spots were identified by incubating the membrane with Pierce Supersignal west pico chemiluminescence substrate 1:1 Luminol/Enhancer + Stable Peroxidase solution (Thermo Scientific) for several minutes before exposing on a chemiluminiscence film and developing it.

4.8.4 Other Proteins

Initiation factors (IF1, IF2, IF3), EF-Tu and EF-G were prepared as described (Gromadski & Rodnina, 2004; Milon et al, 2007; Rodnina et al, 1999; Rodnina & Wintermeyer, 1995; Wieden et al, 2002). Gene of prolyl-tRNA synthetase was purchased from *Keio collection* (Baba et al, 2006); overexpressed in BL21(DE3) and purified by affinity chromatography on a Protino gravity-flow column (Macherey-Nagel) using the poly-histidine tag, as described for EF-P (section 4.8.1). Pro-RS was stored in buffer A

containing 50% glycerol; the concentration was determined by absorbance at 280 nm, assuming an extinction coefficient of 54320 cm^{-1} M^{-1}.

4.9 Ribosomes

Ribosomes were prepared as described from *E. coli* MRE600 (Rodnina & Wintermeyer, 1995).

4.9.1 Initiation complexes (ICs)

Initiation complexes were prepared by incubating 1 µM 70S ribosomes with 1.5 µM initiation factors (1, 2, 3), 3 µM mRNA , 1 mM GTP and 1.5 µM of ^{3}H or ^{14}C labeled fMet-$tRNA^{fMet}$ at 37 °C in buffer A for 30 min (Wohlgemuth et al, 2008). Purification of complexes was performed by centrifugation through 400 µl sucrose cushion (1.1 M in buffer A) at 260,000 × g for 2 h. Pellets were dissolved in buffer A and stored at -80 °C. Notably, the concentration of ribosomes is limiting during the preparation which ensures that every ribosome is initiated at an mRNA. This leads to synchronized ribosomes and minimizes re-initiation and ribosomal cueing. For 30S initiation experiments 30S ribosomal subunits were activated by high magnesium (14 mM) for 30 min at 37 °C as described (Igarashi et al, 1982).

4.9.2 Ternary complexes (TCs)

If not stated otherwise ternary complexes (EF-Tu·GTP·aminoacyl-tRNA) were obtained by preincubation of 50 µM EF-Tu with 1 mM GTP, 0.1 µg/µl pyruvate kinase and 3 mM phosphoenolpyruvate (PEP) for 15 min in buffer A or B, followed by addition of 25 µM aa-tRNA and further incubation for 2 min. When Pro*-$tRNA^{Pro}$ was used as A-site substrate, the EF-Tu complexed tRNA was purified by gel filtration on tandem Superdex 75-10/300 GL columns (GE Healthcare) (Gromadski & Rodnina, 2004; Rodnina et al, 1995) and the concentration of ternary complex was determined photometrically at 280nm.

4.9.3 Post translocation complexes (PTCs)

PTCs were formed by mixing initiation complexes with a twofold excess of the corresponding ternary complex (EF-Tu·GTP·X-$tRNA^{X}$) in buffer A. To initiate translocation EF-G was added (1/10 molar ratio of ribosome concentration) after short incubation at 37 °C. After 30 s PTCs were loaded on sucrose cushion as described for initiation complexes. Concentration of PTCs was determined by double-label scintillation counting.

4.9.4 PTCs containing Pro analogs

To increase the efficiency of PTC formation with Pro-analogs, the $MgCl_2$ concentration was increased to 14 mM and the incubation time prior to EF-G addition was increased to 5 min. To determine the efficiency of complex formation with proline analogs and thereby the PTC concentration,

incorporation of the next amino acid (Phe or Gly, labeled with ^{14}C or ^{3}H, respectively) encoded by the mRNA was monitored. For most analogs the efficiency of PTC formation was between 70-90%. Complexes with 4-S-Mep, 4-R-Mep, Aze and Pip reached only 20-50% PTC.

4.10 Gel electrophoresis

4.10.1 Soldium dodecyl sulfate polyacrylamide gel electrophoresis (SDS PAGE)

For analysis of proteins, SDS-polyacrylamide gels were prepared as described (Laemmli, 1970; Weber et al, 1972) and run vertically in SDS buffer (0.1% SDS, 192 mM glycine, 25 mM Tris pH 8.3). Resolving gels contained 15% acrylamide (acrylamide/bisacrylamide 29:1), 0.1% SDS, 400 mM Tris-HCl pH 8.8 and the stacking gel contained 4% acrylamide (acrylamide/bisacrylamide 29:1), 0.1% SDS, 125 mM Tris-HCl pH 6.8.

4.10.2 Tris-Tricine PAGE

Short peptides and longer translation products were separated on Tris-Tricine PAGE. Tris-Tricine gels were performed according to Schägger and von Jagow using three gel layers with 4% T, 3% C for the stacking gel, 10% T and 3% C for the spacer gel and 16.5% T and 6% C for the separating gel; with T being acrylamide and C being bisacrylamide (Schagger & von Jagow, 1987). All gels contained 1 M Tris pH 8.45 and 0.1% SDS (separating gels additionally contained 13.5% glycerol) and were polymerized by addition of 10% ammonium persulfate solution (APS) and 1% tetramethylenediamine (TEMED). Samples were mixed with loading buffer (50 mM Tris-HCl pH 6.8, 12% (w/v) glycerol, 2% 2-mercaptoethanol, 4% SDS) and incubated for 30 min at 40 °C before loading. PAGE was carried out with two running buffer (anode buffer: 0.2 M Tris-HCl pH 8.9; cathode buffer: 0.1 M Tric-HCl, 0.1 M Tricine pH 8.25, 0.1% SDS) at 30 V for 30 min followed by 2-4 h at 120 V. Alternatively, precast 16.5 % or 10-20% Tris-Tricine gels (Criterion, BIO-RAD) were used according to the manufacturer's protocol.

4.10.3 Native polyacrylamide gel electrophoresis (native PAGE)

Protein-RNA complexes were analyzed on native PAGE. 5% native PAGE (5% Acrylamide (40% AA:AB (29:1)), 10 mM $Mg(OAc)_2$, 4% glycerol, 1 mM EDTA, 50 mM Tris pH 8.4, 50 mM boric acid) was run in buffer containing 50 mM Tris pH 8.4, 50 mM boric acid, 1 mM EDTA, 10 mM $Mg(OAc)_2$ at 4 °C for 2 h at 100 V with current below 10 mA. Gels were stained with Coomassie.

4.10.4 Denaturing polyacrylamide gel electrophoresis (UREA PAGE)

To determine the quality of mRNA, it was analyzed by denaturing PAGE. Urea gels (40% acrylamide (AA:AB 19:1), 8 M Urea in 100 mM Tris-borate/2 mM EDTA pH 8.3 (TBE)) were polymerized with 10% APS and 1% TEMED and run in TBE buffer for 15 min at 200 V prior to sample loading. Samples other than mRNA were mixed with loading dye (80% formamide, 0.1% bromphenol and 0.1% xylencyanol

in TBE) and preheated for 2 min at 95 °C. Gels were run at 50 °C at 100 V until the samples entered the gel followed by 200 V until the end. Gels were incubated in 20% acetic acid until the first running front turns yellow, stained with methylene blue staining solution (0.04% methylene blue in 80 mM NaOAc pH 5) and subsequently destained in tap water.

4.11 Kinetics

All experiments were performed in buffer A or B pH 7.5 at 37 °C if not stated otherwise. Time courses were performed either manually or in a quench flow apparatus (Fig. M2, KinTek Laboratories, Inc.).

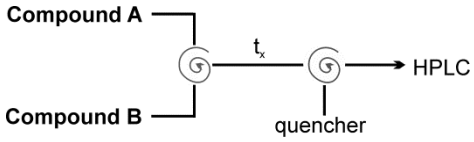

Fig. M2: Quench flow scheme

The quench flow apparatus is a mechanic mixing device which enables monitoring rapid kinetics. In a first step two reactants are mixed (which starts the reaction) and the mixture is incubated for a variable time (tx) at a temperature of interest. Afterwards a third compound is added to the mixture which can be used to stop the reaction (quencher). The dead time of the machine reflects the mixing time of approximately 2 ms. The sample is further analyzed e.g. by HPLC.

Equal volumes of two reactants are mixed rapidly and incubated for variable time before the reaction is stopped by addition of a quencher (0.5 M KOH final). The tRNA is hydrolyzed (30 min at 37 °C) and the sample is neutralized with acetic acid. If not stated otherwise, products and educts were separated on reversed phase columns (LiChrospher 100 RP-8 or Chromolith RP8 100-4.6 mm column, Merck) using 0-65% acetonitrile (ACN) gradient in 0.1% trifluoroacetic acid (TFA) and quantified by double-label scintillation counting. For reactions with Pro derivatives the quantification of products and educts was complicated by the fact that Pro analogs were not radioactive. In other words, f[^{3}H]Met and f[^{3}H]Met-Pro* were not distinguishable by scintillation counting. Therefore, the retention times of amino acids and peptides on the respective reversed phase columns was carefully determined by an exclusion procedure. In the Pmn assay with Pro derivatives (section 2.2.3.3) the decay of f[^{3}H]Met-Pro*-tRNA^{Pro} upon product formation had to be monitored because traces of contaminating ICs (f[^{3}H]Met-tRNA^{fMet}) could react with Pmn as well and the products from both reactions could not be distinguished either by radioactivity counting or by chromatographic separation.

fMet-Pmn formation (section 2.2.1.5) was quenched with 50% formic acid and fMet-Pmn was extracted with 1.5 NaOAc pH 4.5 saturated with $MgSO_4$. For this purpose 500 µl 1.5 NaOAc pH 4.5 saturated with $MgSO_4$ were mixed with the sample prior to addition of 750 µl ethyl acetate; the upper phase was collected to determine the amount of f[^{3}H]Met-Pmn by [^{3}H] radioactivity counting.

To exclude a rate-limiting binding step of EF-P to the ribosome, EF-P (3 µM) was present in both syringes. If not stated otherwise all experiments were performed with lysylated and hydroxylated EF-P. Rate constants were evaluated by exponential fitting using GraphPad or Scientist software. Data shown are the mean of at least three independent experiments; error bars represent standard deviations.

Most data were fitted to a single exponential function with the equation:

$$Y(t) = Y_{max} + (Y_0 - Y_{max}) * e^{-k_{obs}*t} \quad (1)$$

where $Y_{(t)}$ is the ratio product/(product + educt) at the time t, the Y_{max} is the maximal amount, Y_0 is the initial ratio and k_{obs} is the reaction rate. When necessary (section 2.2.3), data were fitted to a double exponential function with the equation:

$$Y_{(t)} = Y_{max} + span_{fast} * e^{-k_{fast}*t} + span_{slow} * e^{-k_{slow}*t} \quad (2)$$

where the spans are defined as: $span_{fast\ (slow)} = (Y_0 - Y_{max}) * percent_{fast\ (slow)} * 0.01$. The data evaluation was done with Graph Pad Prism software. In Figures showing an overview of temperature or pH-dependent reactions the time courses were normalized to match the same amplitude by Graph Pad Prism software for more clarity. However, all stated values are obtained from the original reaction time courses.

4.11.1 Di- and tripeptide formation with puromycin

The puromycin reaction was performed by mixing equal volumes of purified ribosomal complexes; IC or PTC (0.15 µM final) and Pmn (0.05-10 mM final) in buffer A or B at 37 °C and pH 7.5 if not stated otherwise (Katunin et al, 2002). In section 2.1.2.1 subsaturating concentrations of Pmn were used to account for effects on both affinity and catalysis. In the reactions with dipeptidyl-tRNAs, the final Pmn concentration was 1 mM (Wohlgemuth et al, 2008), whereas with fMet-tRNA^{fMet} the Pmn concentration was reduced to 100 µM, because the K_M of the reaction, 300 µM, is lower than with dipeptidyl-tRNAs (Beringer & Rodnina, 2007a). The reactions were performed in buffer A. In sections 2.2.1.5 and 2.2.3.3 high concentrations of Pmn (5-10 mM final) were used to monitor the rate of peptide bond formation and the effect of EF-P on catalysis. To improve solubility of Pmn at high concentrations (10 mM) 5% DMSO was added to buffer B. For the very fast reaction of 4-R-Flp in the presence of EF-P at 37 °C the rate was obscured by the dead time of the quench flow apparatus which is 2 ms. The rate was estimated on the basis of the initial concentration of the substrate as determined prior to mixing.

4.11.2 Di- and tripeptide formation

Purified initiation or post-translocation complexes (0.2 µM final), containing fMet-Xaa-tRNA^{Xaa} in the P site were mixed with saturating ternary complexes (EF-Tu·GTP·Yaa-tRNA^{Yaa}; 10 µM final) as

specified by the mRNA in buffer B at 37 °C (Doerfel et al, 2013). Because complexes were stored in buffer A, they were mixed 1:1 with buffer C to yield buffer B prior to the reaction.

4.11.3 Tetra- and pentapeptide formation

Purified initiation complexes (0.2 µM final) primed with mRNA encoding short peptides were mixed with ternary complexes (2 µM final each with tRNAs as specified by the mRNA sequence) in the presence of 1 µM EF-G in buffer B at 37 °C. When indicated, ternary complexes were purified by size exclusion chromatography, e.g. TCs with Proline analogs. In case of fM-PPG /fM-PPGF the observed rate comprises all kinetic steps of three/four elongation events which include accommodation of tRNAs, peptide bond formation and translocation.

4.11.4 Hydrolysis of peptidyl-tRNA

f[^{3}H]Met-Pro*- tRNA^{Pro} (0.5 µM) was hydrolyzed in buffer D at 37 °C. Peptidyl-tRNAs were precipitated in 10% TCA, 50% EtOH and collected by nitrocellulose filtration. The extent of hydrolysis of the amino acyl ester bond was quantified by ^{3}H scintillation counting (Kuhlenkoetter et al, 2011). Notably, peptidyl-tRNA and f[^{3}H]Met-tRNA^{fMet} could not be distinguished by scintillation counting. However, hydrolysis rates could be deconvoluted for most cases by the two-exponential behavior of tRNA decay. The exponentials were assigned by the comparative hydrolysis of f[^{3}H]Met-tRNA^{fMet}. In other cases the contribution of fMet-tRNAf^{Met} was so small that is was neglected.

4.11.5 Aminolysis of peptidyl-tRNA

Aminolysis of peptidyl-tRNA (0.5 µM) was performed in buffer D, containing 1 M glycinamide (Sigma-Aldrich) corresponding to 0.2 M unprotonated glycinamide at 37 °C (Schroeder & Wolfenden, 2007). Concentration of unprotonated glycinamide at pH 7.5 was calculated on basis of the published pK_a of 8.2 (Good et al, 1966). In the presence of amine, the rate of peptidyl-tRNA decomposition (k_{decay}) reflects the sum of two competing reactions, aminolysis and hydrolysis. The rate of aminolysis was calculated from the decay rate in the presence of glycinamide and the hydrolysis rate according to the equation $k_{aminol} = k_{decay} - k_{hydrol}$.

4.11.6 Termination experiments

Peptide release experiments were performed as described (Kuhlenkoetter et al, 2011). In principle, ribosomal complexes (0.25 µM final) programmed with an mRNA encoding UAA termination codon were incubated at 37 °C in buffer A (with Tris-HCl being d by HEPES-HCl pH 7.5) in the presence of RF1 (4 µM final). When intended, EF-P (3 µM final) was added. For quantification of peptide release tRNAs were precipitated in 10% TCA, 50% EtOH, intact peptidyl-tRNA was collected by nitrocellulose filtration and quantified by subsequent double-label scintillation counting.

4.11.7 *In-vitro* translation

For *in-vitro* translation ICs were prepared as described above but with BOF-Met-tRNA^{fMet} and with a long mRNA encoding the protein of interest. Binary complexes (EF-Tu*GTP) were prepared as described and mixed with total aa-tRNA. The concentration of ternary complex was increased proportionally to the length of the protein to be translated (40 µM TC for 75 amino acids, prepared with 2 mM GTP, 3 mM PEP and 2 mM DTT). As low $MgCl_2$ concentrations tend to inhibit multi-turnover assays (Johansson et al, 2012; Wohlgemuth et al, 2010), the $MgCl_2$ concentration was kept stable at 3.5 mM free $MgCl_2$ by compensating for Mg^{2+} binding to GTP and PEP (Manchester & Alford, 1979; Wohlgemuth et al, 2010). For exceptionally proline-rich proteins (TonB, AmiB, Rz1, and YafD), the total aa-tRNA was supplemented with Pro-tRNA^{Pro} (10 equivalents of Pro-tRNA^{Pro} per encoded proline). IC and TC were prepared in buffer A and mixed with an equal amount of buffer C to obtain buffer B. Ternary complex and EF-G (2 µM) were rapidly mixed with unpurified initiation complex (20 nM) and incubated at 37 °C. EF-P (3 µM, either native or overexpressed lysylated/hydroxylated) was added both to the ternary and initiation complex. Specific peptide markers were synthesized in the same way with incubation time of 10 min in the presence of EF-P (3 µM) by using mRNAs of the desired length. The reaction was stopped after varying incubation times by addition of 1/10 volume of 2 M NaOH and peptidyl-tRNAs were hydrolyzed for 30 min at 37 °C. The samples were neutralized by 1/10 volume 2 M HEPES free acid, incubated in loading buffer (50 mM Tris-HCl pH 6.8, 12% (w/v) glycerol, 2% 2-mercaptoethanol, 4% SDS) for 30 min at 40 °C and loaded onto a 10-20% or 16.5% Tris/Tricine SDS gel (Criterion, BIO-RAD) and PAGE was carried out using commercial Tris/Tricine buffer (BIO-RAD) according to the manufacturer's protocol. Alternatively Tris/Tricine SDS gel was prepared in house (section 4.10.2). Gels were incubated in water for 5 min and scanned on a FLA-9000 fluorescence imager (Fuji) at 50 µm resolution. Bodipy fluorescence was excited at 473 nm and monitored after passing a LPB (510LP) cut-off filter.

To determine Pro and Gly incorporation efficiency relative to each other at a PPG sequence in mutant PrmC (section 2.1.2.6) ternary complexes were prepared with total aa-tRNA containing [^{14}C]Pro-tRNA^{Pro} and [^{3}H]Gly-tRNA^{Gly}. Ribosome-nascent-chain complexes were purified from tRNAs, ternary complexes, EF-G, and GTP by size-exclusion chromatography (Biosuite 450 8µm HR SEC, Waters, at a flow of 0.8 ml/min in buffer B). Bound [^{14}C]Pro and [^{3}H]Gly eluting in the ribosome peak were quantified by double-label scintillation counting. Additionally, ribosome bound peptidyl-tRNA was hydrolyzed in 0.5 M KOH for 30 min at 37 °C and subsequently neutralized with acetic acid. Translation products and amino acids were separated by reversed phase HPLC (Nucleosil 300-5 C4, Macherey Nagel) applying a gradient from 0 to 65% ACN /0.1% TFA in 20 min. Free and peptide incorporated [^{14}C]Pro and [^{3}H]Gly were quantified by scintillation counting.

4.11.8 Filter binding experiments

To quantify the amount of ribosome-bound tRNA (e.g. to determine initiation efficiency), the translation mixture was filtered through a nitrocellulose filter (0.2 µM pore size, Sartorius) which allows single tRNA to pass through the pores while ribosome bound tRNAs are retained on the filter. To reduce unspecific binding, filters were washed with ice cold buffer A. The ribosome-bound aa- or peptidyl-tRNA retained on the nitrocellulose filter was quantified by scintillation counting of the specific radioactive labels.

To quantify aminoacylation (e.g. in aminoacylation or hydrolysis reactions) tRNAs were precipitated in ice cold 10% TCA, 50% EtOH and filtered through a nitrocellulose filter (0.2 µM pore size, Sartorius). To minimize unspecific binding the filter was washed with 3 ml cold 5% TCA solution. Precipitated aa-tRNA sticks to the filter and free amino acids are washed through the filter. The extent of aminoacylation was quantified by scintillation counting of the filter.

4.12 Mass spectrometry

The identification and quantification of EF-P modifications was carried out by LC-MSMS and performed by Ingo Wohlgemuth, MPI-BPC, Göttingen (Doerfel et al, 2013). Protein samples (100 µg) were precipitated with acetone. Denaturation with Rapigest (Waters), reduction, alkylation, and trypsination were performed as described (Schmidt et al, 2010). Peptides were separated by reversed-phase Nanoflow chromatography on a Thermo Easy nLcII using chromatographic conditions as described (Schmidt et al, 2010). Eluting peptides were ionized by electrospray ionization (ESI) on a Q Exactive mass spectrometer (Thermo Fisher Scientific) and analyzed in the data-dependent mode. MS scans were acquired in the range *m/z* 350-1600 with a resolution of 70,000 and twelve peaks of the highest intensity were selected for HCD MS/MS fragmentation. The dynamic exclusion was 20 s. Singly-charged ions and ions with unrecognized charge state were excluded. Peptides were quantified by integrating over the corresponding extracted ion chromatograms (XIC). XICs were generated with a mass tolerance of 10 ppm using the Thermo Excalibur software (version 2.2 SPI48). The overall signal intensity in different runs was corrected by normalization, using as internal reference two razor peptides (VPLFVQIGEVIK and GDTAGTGGKPATLSTGAVVK) that were well observable and chemically stable. The charge state of highest intensity (*z*=3 for unmodified EF-P peptide and *z*=5 for lysylated and lysylated/hydroxylated EF-P peptide) and the most prominent peak in the isotope distribution of the respective peptides was selected for quantification by integration. Quantification based on the monoisotopic mass led to similar results, albeit at poor signal-to-noise ratios for low-abundance peptides. Spectra in Fig. S1 show the corresponding peptides with *z*=4 that were less populated but yielded better spectra then those with *z*=5. Because the degree of Met oxidation was reproducibly small, only the unoxidized peptides were quantified.

4.13 Calculation of Activation Energies

Activation parameters were determined on basis of Arrhenius and Eyring equations for 25 °C. The Arrhenius equation describes the temperature dependence of reaction rates,

$$\ln(k) = \ln(A) - \frac{E_a}{R \times T} \quad (3)$$

where A is the pre-exponential factor, E_a the activation energy, R the gas constant (8.314 J/mol*K) and T the absolute temperature. The enthalpy of activation ($\Delta H^{\neq}$) of a reaction can be extracted from a linear Arrhenius plot (ln(k) vs. 1/T) with the slope $E_a = -slope \times R$ according to

$$\Delta H^{\neq} = E_a - RT \quad (4)$$

The free energy of activation ($\Delta G^{\neq}$) was calculated according to

$$\Delta G^{\neq} = -RT \times \ln(\frac{k_{pep} \times h}{k_B \times T}) \quad (5)$$

where h and k_B are the Planck´s and Boltzmann´s constant (6.63 x 10^{-34} J x s and 1.38 x 10^{-23} J/K), respectively. The free energy of activation can be dissected into an enthalpic and an entropic term according to:

$$\Delta G^{\neq} = \Delta H^{\neq} - T\Delta S^{\neq}. \quad (6)$$

When ($\Delta G^{\neq}$) and ($\Delta H^{\neq}$) are known the entropy of activation ($T\Delta S^{\neq}$) can be determined by rearranging equation 6.

4.14 Determination of the pK_a

In section 2.2.2.1 the pK_a of the titrated groups were determined from the pH dependence of the rate under investigation under the assumption that deprotonation is the rate-limiting step for the reaction to occur.

A reaction which depends on the deprotonation of a single group (e.g. the α-amino group in case of peptide bond formation) follows the scheme $HA \overset{K}{\Leftrightarrow} H^+ + A^-$ and the rate of the reaction can be described by (Fersht, 1999):

$$k_{(H)} = \frac{k_{HA} \times [H^+] + k_{A^-} \times K_a}{K_a + [H^+]} \quad (7)$$

Where the dissociation constant K_a for the acid is defined by

$$K_a = \frac{[A^-] \times [H^+]}{[HA]} \tag{8}$$

When the attacking nucleophile is protonated the propensity for the reaction to occur is zero, while it should be maximal when the nucleophile is deprotonated i.e. $k_{HA} = 0$ and $k_{A-} = k_{max}$. Under these assumptions equation 8 becomes:

$$k_{pep\,(H)} = \frac{k^{max} \times K_a}{K_a + [H^+]} \tag{9}$$

With $pK_a = -log(K_a)$ and $pH = -\log(H^+)$ equation 9 results in

$$k_{pep\,(pH)} = \frac{k_{pep}^{max}}{1 + 10^{(pK_a - pH)}} \tag{10}$$

When the pH reaches the pK_a of the titrated group the equation is simplified and the pK_a corresponds to the inflection point of the pH dependence of the reaction.

When two ionizable groups influence the rate of the monitored reaction (as in case of peptidyl transfer to Pmn (Beringer et al, 2003; Katunin et al, 2002; Okuda et al, 2005)) the system can be described by the scheme in Fig. M3.

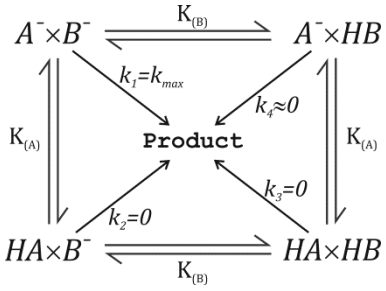

Fig. M3: Reaction scheme involving two ionizing groups

The rate of fMet-Pmn formation depends on two ionizing groups. One group can be assigned to Pmn (A) and the second (B) was assigned to a ribosomal group or a conformational change of the peptidyl transferase center. Both groups have to be deprotonated (A^-B^-) to obtain the maximal rate of product formation.

Hereby A is the α-amino group of the attacking nucleophile and B is a second ionizing group/a conformational change of the peptidyl transferase center (Bieling et al, 2006; Muth et al, 2001). While the deprotonation of the nucleophile (A^-) is a prerequisite for the reaction (→ $k_2 = 0$; $k_3 = 0$), the influence of B is, due to its elusive character, difficult to estimate. In the easiest model, both groups have to be deprotonated for the reaction to occur ($k_1 = k_{max}$ and $k_{2\text{-}4} = 0$). However, the literature suggest that deprotonation of one group is sufficient for the reaction to proceed at low rate ($k_4 \neq 0$) (Katunin et al, 2002).

A simplified description of this situation is a doubly ionizing system ($H_2A \overset{K1}{\Leftrightarrow} HA^- + H^+ \overset{K2}{\Leftrightarrow} A^{2-} + 2H^+$) the rate of which can be described by (Fersht, 1999):

$$k_{(H)} = \frac{k_{H_2A} \times [H^+]^2 + [H^+] \times K_1 \times k_{HA^-} + K_1 \times K_2 \times k_{A^{2-}}}{K_1 \times K_2 + [H^+] \times K_1 + [H^+]^2} \tag{11}$$

Using the conclusions described for the reaction scheme ($k_{H_2A} = k_3 = 0$, $k_{HA^-} = k_2 + k_4 = 0 + X$ and $k_{A^{2-}} = k_1 = k_{max}$) and with the definition $pK_{a1/2} = -log(K_{1/2})$, the following equation is derived to fit a reaction that depends on two ionizing groups:

$$k_{(pH)} = \frac{10^{-pK_{a1}-pK_{a2}} \times k_{max}}{10^{-pK_{a1}-pK_{a2}} + 10^{-pH-pK_{a1}} + 10^{-2pH}} \quad (12)$$

In this case, the pH at which the rate is half maximal is smaller than the pK_a of the residue which deprotonates later.

5 SUPPLEMENTARY INFORMATION

5.1 Determination of the modification status of EF-P

The differently modified EF-P proteins used in this study were purified from *E. coli* cells either in their native state or after expression of EF-P (and its modifying enzymes) from a plasmid in trans. Overexpression of EF-P necessitated to confirm the modification status, which was performed by liquid chromatography-tandem mass spectrometry (LC-MSMS, see Materials & Methods). The data were acquired by Ingo Wohlgemuth, MPI-BPC, Göttingen (Fig. S1).

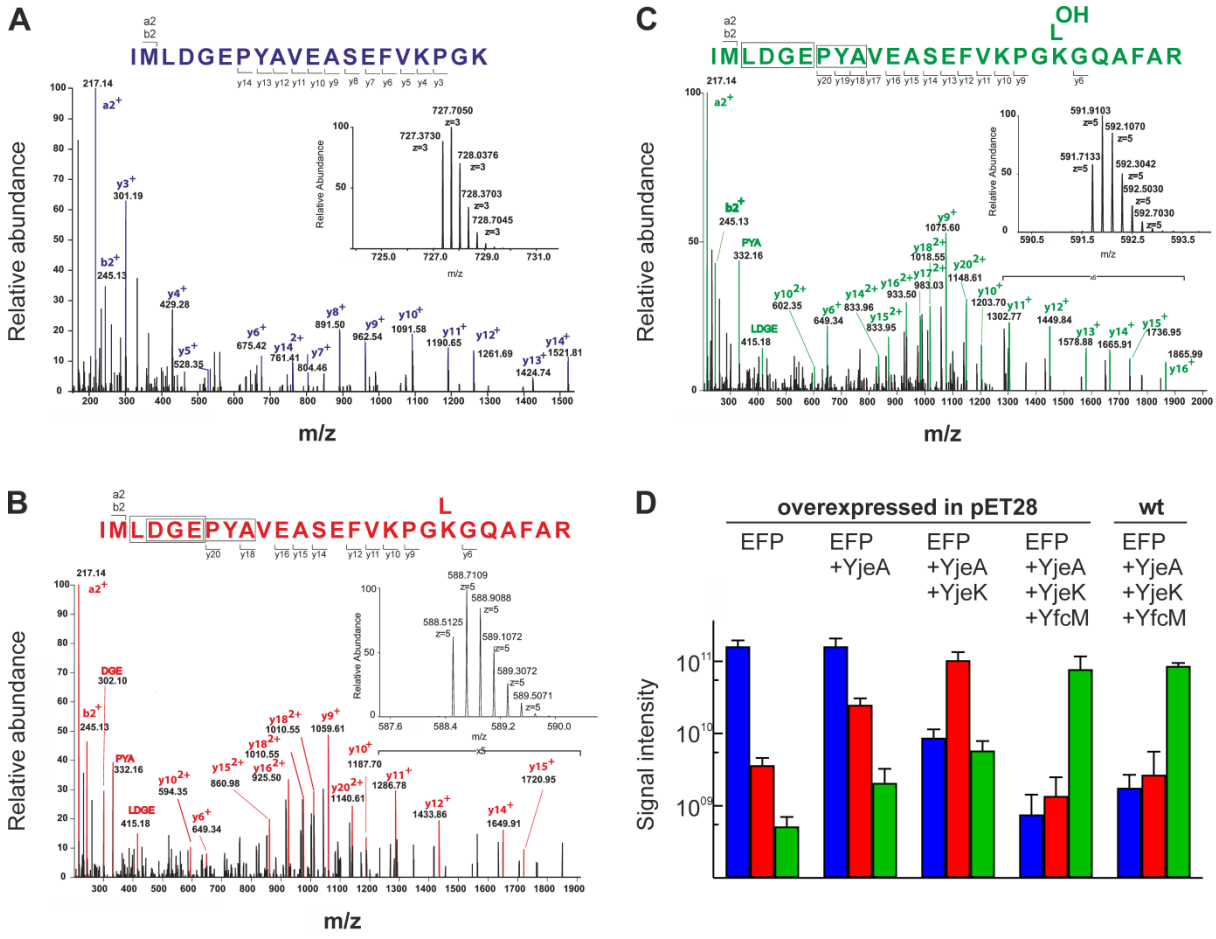

Fig. S1: Analysis of the EF-P modification status by mass spectrometry

A) MS/MS spectrum of the unmodified peptide (amino acids 15-34). The y-type product ion series clearly identify the sequence of the peptide lacking the modification. Inset: MS spectrum (*m/z*= 727.3696) of the intact and unmodified peptide (*z*=3). B) MS/MS spectrum of the lysylated peptide (amino acids 15-40). Inset: MS spectrum (*m/z*= 735.3837) of the intact and lysylated quadruply charged peptide (*z*=4). C) MS/MS spectrum of the lysylated and hydroxylated peptide (amino acids 15-40). Inset: MS spectrum (*m/z*= 739.3825) of the intact, lysylated and hydroxylated quadruply charged peptide (*z*=4). D) Relative quantification of the modifications in different EF-P preparations. The unmodified (blue), the lysylated (red) and the lysylated/hydroxylated (green) peptides were quantified by integration of their respective extracted ion chromatograms (XIC). Error bars represent SD of three technical replicates. For the quantification, the charge states with the maximum signal intensity were used, *z*=3 for the unmodified EF-P and *z*=5 for the lysylated and lysylated/hydroxylated EF-P. Data were acquired by Ingo Wohlgemuth, MPI-BPC, Göttingen.

In agreement with the literature (Ambrogelly et al, 2010; Bailly & de Crecy-Lagard, 2010; Park et al, 2012; Peil et al, 2012; Roy et al, 2011; Yanagisawa et al, 2010), EF-P expressed alone, in parallel to EpmA and EpmB or in parallel to EpmA, EpmB and EpmC resulted in unmodified, lysylated or lysylated/hydroxylated EF-P, respectively. Native EF-P was lysylated and hydroxylated.

5.2 Confirming the functionality of the tRNA transcript

To investigate whether the lack of modifications on the $tRNA^{Pro}$ transcript impairs translation, the kinetics of aminoacylation and tetrapeptide formation were studied (Fig. S2). In both assays the kinetics were virtually identical for the tRNA transcript and native $tRNA^{Pro}$, demonstrating that the lack of modifications in the transcript did not influence the reactions considerably. These results were further supported by previous data, showing that the tRNA body has only minor effects on the kinetics of fMP dipeptide formation (Wang et al, 2014).

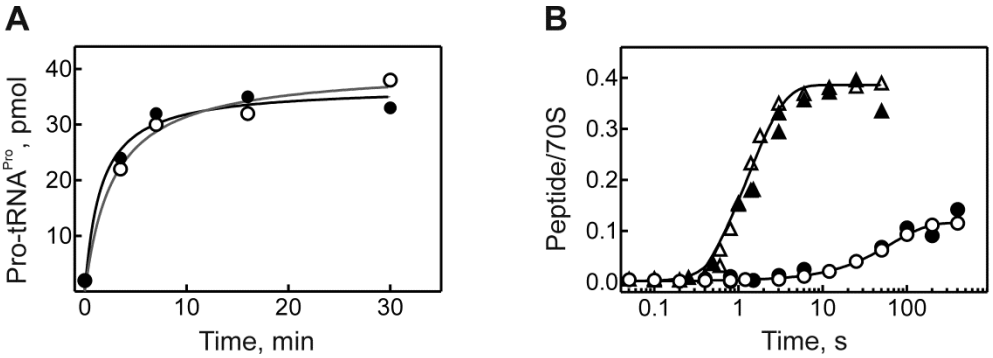

Fig. S2: Comparison of native $tRNA^{Pro}$ and $tRNA^{Pro}$ transcript

A) Aminoacylation of $tRNA^{Pro}$ obtained from cells (closed circles) and by T7 RNA-polymerase transcription (open circles) with [^{14}C]Pro by purified Pro-RS. B) Time course of fMPPG formation with native $tRNA^{Pro}$ (open symbols) and $tRNA^{Pro}$ transcript (closed symbols) in the absence (circles) and presence of EF-P (triangles).

5.3 Purification of the ternary complex Pro*-$tRNA^{Pro}$·EF-Tu·GTP

A problem in incorporating unnatural amino acids into protein can be a reduced affinity of EF-Tu for the respective aa-tRNA (Ieong et al, 2012). For the interpretation of the translation assays it was inevitable to exclude site reactions which could interfere with or limit the rate of the reaction of interest. Because the Pro analogs were not labeled and thus were difficult to detect, an indirect approach was chosen to circumvent problems which arise from inefficiently aminoacylated tRNA or reduced affinities for EF-Tu: Subsequent to aminoacylation of $tRNA^{Pro}$ with the respective Pro analog a TC (Pro*-$tRNA^{Pro}$·EF-Tu·GTP) was formed and purified by size-exclusion chromatography (SEC) (Fig. S3). The sample eluted from the column in three peaks, where the first corresponded to Pro-RS, the second to TC and the third to uncharged tRNA and EF-Tu (the first peak was absent when the TC was formed with purified aa-tRNA and the second peak contained radioactivity when radioactively

labeled aa-tRNAs were used). Because a stable ratio of tRNA to EF-Tu was used for all Pro analogs and Pro, the efficiency of TC formation could be estimated from the ratio of peak2/peak3. Variable efficiencies of TC-formation with different Pro analogs may be traced back to different misacylation efficiencies of $tRNA^{Pro}$ with the respective Pro analogs by Pro-RS. All TCs were stable enough to be isolated under non-equilibrium conditions, indicating that EF-Tu binds the misacylated tRNAs with sufficient affinity. For all experiments the TC obtained from peak 2 was used and thus inefficient delivery of Pro*-$tRNA^{Pro}$ to the A site or underestimated tRNA concentrations are unlikely to influence reaction kinetics.

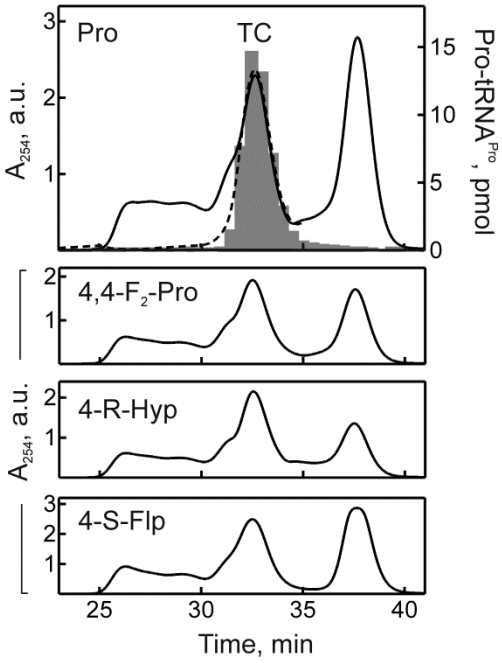

Fig. S3: Purification of TC(P*)

Isolation of the TC by size-exclusion chromatography (SEC). The upper panel shows the purification of [^{14}C]Pro-$tRNA^{Pro}$ in complex with EF-Tu and GTP. The middle peak corresponds to the ternary complex (TC), identified by radioactively labeled aa-tRNA. The first peak corresponds to Pro-RS (the dashed profile was obtained with purified aa-tRNA) and the third peak contains uncharged tRNA and EF-Tu. The lower panels show the profile for TCs with Xaa-$tRNA^{Pro}$ with Xaa= 4,4-F_2-Pro, 4-R-Hyp and 4-S-Flp as representatives for Pro analogs.

5.4 Determination of the optimal nucleophile concentration to monitor aminolysis

To establish the optimal conditions for the aminolysis reaction the decomposition of fMet-$tRNA^{fMet}$ in the presence of increasing glycinamide concentrations was monitored (Fig. S4A). Only the unprotonated molecule participates in the reaction and the titration was limited by the amount of glycinamide dissolvable in the reaction mixture. The titration of glycinamide revealed a linear correlation of the rate of fMet-$tRNA^{fMet}$ decomposition (k_{decay}) and the amount of unprotonated glycinamide present (Fig. S4B).

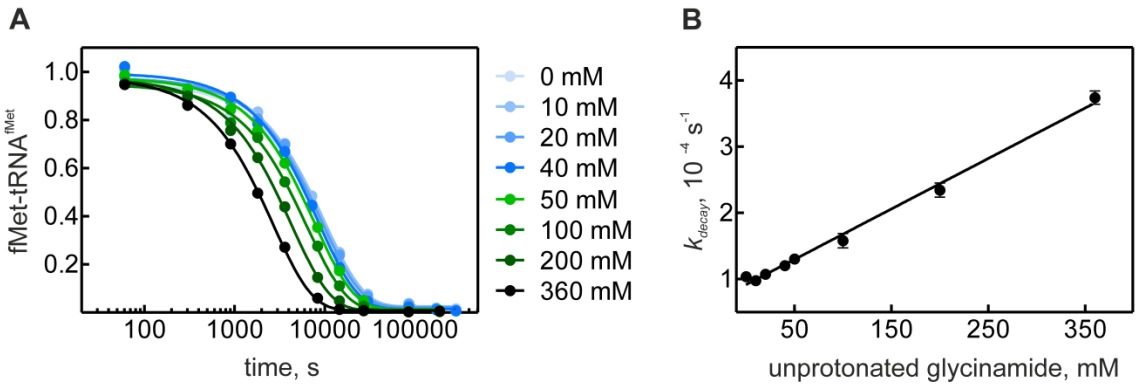

Fig. S4: Dependence of the deaclyation rate on the nucleophile concentration

A) Time courses of fMet-tRNA^{fMet} decomposition at increasing concentrations of glycinamide. Concentrations reflect the amount of unprotonated glycinamide B) The rate of fMet-tRNA^{fMet} decomposition increases linearly with the concentration of unprotonated glycinamide. Average rate and SD of three replicates are plotted.

The Y-intercept in Fig. S4B corresponds to the rate of hydrolysis (k_{hydrol}), which competes with aminolysis. Thus, the rate of aminolysis (k_{aminol}) at a certain glycinamide concentration can be determined according to $k_{aminol} = k_{decay} - k_{hydrol}$. For the aminolysis of fMet-Pro*-tRNA^{Pro} in solution 0.2 M unprotonated amine at pH 7.5 was used as nucleophile concentration (Fig. 34).

5.5 Influence of the $MgCl_2$ concentration on fM-P*P*G formation

As in the case of fM-PPG formation with proline (section 2.2.1.3), addition of $MgCl_2$ could increase the yield of final product by stabilization of the peptidyl-tRNA: At low $MgCl_2$ concentrations fM-P*P*G synthesis, where P* is 4-S-Mep, was inefficient but increased linearly with higher concentrations (Fig. S5, Table S6). For the, compared to proline, poorer substrate 4-S-Mep the $MgCl_2$ optimum was shifted to higher concentrations compared to the reaction with Pro (from ~9 mM to > 14 mM), suggesting that either the substituent on the prolyl ring further destabilizes the peptidyl-tRNA or the decreased rate increased the time window for drop-off. As for Pro (Fig. 24, section 2.2.1.3) with EF-P the amount of final product seems to be independent of the $MgCl_2$ concentration in the range of 4-14 mM. It should be noted that all but the point at 3.5 mM were obtained with unpurified ternary complex. The increase of fM-PPG synthesis with unpurified ternary complex might be due to multiple sampling of TC because EF-Tu/tRNA can be recharged with GTP/amino acids.

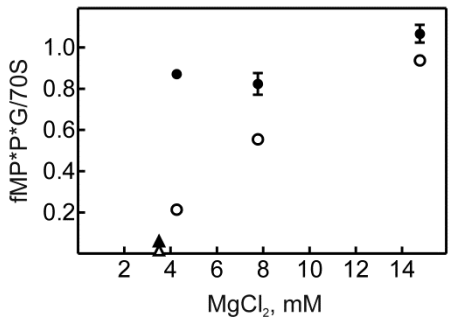

Fig. S5: $MgCl_2$ dependence of tetrapeptide formation

Yield of fMP*P*G tetrapeptide formation as a function of the $MgCl_2$ concentration in the absence (open symbols) and presence (closed symbols) of EF-P; P* is 4-S-Mep using purified (triangles) and unpurified (circles) ternary complex. Error bars from two replicates.

5.6 Supplementary tables

Table S1: Rate constants of di- /tripeptide formation from fMet-(Xaa)-tRNA^{Xaa} and subsaturating Pmn

Xaa	k_{obs}, s^{-1}		acceleration
	no EF-P	EF-P	by EF-P
-	0.16 ± 0.01	0.91 ± 0.05	6
G	0.42 ± 0.05	2.7 ± 0.3	6
P	0.012 ± 0.001	1.1 ± 0.1	85
F	4.1 ± 0.3	5.7 ± 0.7	1
V	3.4 ± 0.4	10 ± 2	3
W	2.2 ± 0.2	4.1 ± 0.4	2
K	5.5 ± 0.9	6.6 ± 0.5	1
R	22 ± 3	18 ± 4	1
Q	22 ± 4	35 ± 4	2
E	7.2 ± 0.7	13 ± 2	2
D	0.78 ± 0.04	4.0 ± 0.8	5

IC, PTC (0.15 µM) vs. Pmn (1 mM for all but fMet, 0.1 mM for fMet). Reaction preformed at 37 °C in 50 mM Tris-HCl pH 7.5, 70 mM NH_4Cl, 30 mM KCl and 7 mM $MgCl_2$ (buffer A) ± EF-P (3 µM).

Table S2: Rate constants of di- and tripeptide formation with a native A-site substrate

	k_{obs}, s^{-1}		acceleration
	no EF-P	EF-P	by EF-P
fM vs. G	28 ± 3	44 ± 5	1.6
fMP vs. G	4.2 ± 0.3	33 ± 3	8
fM vs. F	90 ± 9	104 ± 14	1.2
fMP vs. F	55 ± 5	61 ± 5	1.1
fM vs. P	22 ± 2	32 ± 3	1.4
fMP vs. P	0.33 ± 0.03	5 ± 1	16

IC or PTC (0.2 µM) vs. TC (10 µM) ± EF-P (3 µM). Reactions were performed at 37 °C in 50 mM Tris-HCl pH 7.5, 70 mM NH_4Cl, 30 mM KCl, 3.5 mM $MgCl_2$, 0.5 mM spermidine, 8 mM putrescine and 2 mM DTT (buffer B).

Table S3: Titration of modified and unmodified EF-P on fM-PPG synthesis

EF-P	Unmodified EF-P		Modified EF-P	
µM	k_{obs}, s^{-1}	plateau	k_{obs}, s^{-1}	plateau
0	0.038 ± 0.006	0.041 ± 0.002	0.038 ± 0.006	0.041 ± 0.002
0.05			0.13 ± 0.01	0.182 ± 0.006
0.1			0.16 ± 0.02	0.28 ± 0.01
0.2	0.05 ± 0.01	0.086 ± 0.007	0.33 ± 0.04	0.31 ± 0.01
0.5			0.45 ± 0.04	0.35 ± 0.01
1	0.086 ± 0.007	0.15 ± 0.003	0.52 ± 0.07	0.41 ± 0.01
2	0.12 ± 0.02	0.22 ± 0.01	0.6 ± 0.1	0.42 ± 0.01
3			0.6 ± 0.1	0.41 ± 0.02
4	0.11 ± 0.01	0.29 ± 0.01		
6	0.13 ± 0.01	0.31 ± 0.01		

IC (0.2 µM) vs. TC (2 µM, each) in the presence of EF-G (1 µM). The reaction was performed in buffer B at 37 °C. A and B show single traces, C and D are average and SD.

Table S4: fM-PPG synthesis as a function of EF-G

EF-G	no EF-P		EF-P	
µM	k_{obs}, s^{-1}	plateau	k_{obs}, s^{-1}	plateau
0.0625		0.30 ± 0.01		
0.125		0.31 ± 0.01	0.21 ± 0.04	0.42 ± 0.02
0.25	0.025 ± 0.003	0.21 ± 0.01	0.45 ± 0.06	0.42 ± 0.01
0.5	0.024 ± 0.003	0.17 ± 0.01	0.50 ± 0.08	0.39 ± 0.01
1	0.023 ± 0.007	0.12 ± 0.02	0.58 ± 0.08	0.35 ± 0.01
2			0.48 ± 0.09	0.29 ± 0.01
4			0.49 ± 0.07	0.22 ± 0.01

fM-PPG formation: IC (0.2 µM) vs. TC (2 µM, each) ± EF-P (3 µM); EF-G as indicated. Reaction performed in buffer B at 37 °C.

Table S5: fM-PPG synthesis as a function of $MgCl_2$

$MgCl_2$, mM	Yield of fM-PPG formation	
	no EF-P	EF-P
3.5	0.10 ± 0.03	0.50 ± 0.05
4	0.19 ± 0.01	
5	0.28 ± 0.01	
6	0.36 ± 0.01	
7	0.44 ± 0.02	0.59 ± 0.03
10	0.59 ± 0.02	
14	0.58 ± 0.04	0.57 ± 0.05

IC (0.2 μM) vs. TC (2 μM, each), EF-G (1 μM) ± EF-P (3 μM); $MgCl_2$ as indicated. Reaction was performed in buffer B at 37 °C.

Table S6: fM-P*P*G synthesis as a function of $MgCl_2$

$MgCl_2$, mM	Yield of fM-P*P*G formation	
	no EF-P	EF-P
3.5	0.016 ± 0.004	0.06 ± 0.003
4.3	0.21 ± 0.03	0.87 ± 0.04
7.8	0.55 ± 0.04	0.82 ± 0.09
14.8	0.94 ± 0.03	1.09 ± 0.06

IC (0.2 μM) vs. TC(P*, G) (2 μM, each) with P*= 4-S-Mep, EF-G (1 μM) ± EF-P (3 μM); $MgCl_2$ as indicated. Reaction was performed in buffer B at 37 °C. Except for 3.4 mM $MgCl_2$, unpurified complexes were used.

Table S7: pH dependence of fM-G synthesis

pH	k_{obs}, s^{-1}		x-fold
	no EF-P	EF-P	acceleration
6.66	8.4 ± 1.1	31 ± 2	3.6 ± 0.8
7.12	25 ±3	50 ± 6	2.0 ± 0.5
7.5	48 ± 12	58 ± 5	1.2 ± 0.4
7.9	75 ± 14	64 ± 2	0.9 ± 0.2
8.22	65 ± 13	70 ± 12	1.1 ± 0.4
8.52	70 ± 4	72 ± 5	1 ± 0.1

IC (0.2 μM) vs. TC(G) (10 μM) ± EF-P (3 μM). Reaction performed at 37 °C in buffer B at indicated pH. The standard error for pH was 0.05.

Table S8: pH dependence of fMP-G synthesis

pH	k_{obs}, s^{-1}		x-fold
	no EF-P	EF-P	acceleration
6.67	0.4 ± 0.1	17 ± 2	46 ± 12
7.1	1.6 ± 0.2	35 ± 6	22 ± 4
7.54	5 ± 2	42 ± 4	8 ± 3
7.9	8.5 ± 0.8	35 ± 4	4.1 ± 0.5
8.0		43 ± 3	
8.22	17 ± 3	36 ± 10	2.1 ± 0.3
8.52	28 ± 8	35 ± 13	1.2 ± 0.4
8.7	35 ± 5	40 ± 6	1.2 ± 0.2
8.8	31 ± 10	40 ± 7	1.3 ± 0.2

PTC-fMP (0.2 μM) vs. TC (10 μM) ± EF-P (3 μM). The reactions were performed at 37 °C in buffer B at indicated pH. The standard error for pH was 0.05.

Table S9: Temperature dependence of fMP-G formation at pH 7.5

Temp, °C	k_{obs}, s^{-1}	
	no EF-P	EF-P
10	0.12 ± 0.01	1.9 ± 0.3
15	0.32 ± 0.01	4.9 ± 0.5
20	0.70 ± 0.04	9 ± 1
25	1.66 ± 0.06	16 ± 1
30	2.8 ± 0.3	35 ± 4
37	5 ± 2	36 ± 8

PTC-fMP (0.2 μM) vs. TC(G) (10 μM) ± EF-P (3 μM). The reaction was performed at pH 7.5 in buffer B at indicated temperature.

Table S10: Temperature dependence of fMP-G formation at pH 6.5

Temp, °C	k_{obs}, s^{-1}	
	no EF-P	EF-P
10	0.0022 ± 0.0006 (49%) 0.17 ± 0.03 (51%)	0.42 ± 0.04
15	0.009 ± 0.001 (78%) 0.8 ± 0.2 (22%)	1.45 ± 0.07
20	0.027 ± 0.002	4.7 ± 0.4
25	0.045 ± 0.009	9.1 ± 0.8
30	0.108 ± 0.006	19 ± 3
37	0.31 ± 0.06	28 ± 5

PTC-fMP (0.2 μM) vs. TC(G) (10 μM) ± EF-P (3 μM). The reaction was performed at pH 6.5 in buffer B at indicated temperature.

Table S11: pK_a values for proline and Pro analogues

amino acid	pK_a, amino group	pK_a, carboxyl group		
		s-*trans*	s-*cis*	Weighted average
Pro	10.7	3.55	2.85	3.42
4-S-Flp	9.1	3.41	2.88	3.26
4-R-Flp	9.1	3.19	2.37	3.08
4,4-F_2-Pro	6.5	2.93	2.34	2.80
4-S-Hyp	10	3.62	3.19	3.49
4-R-Hyp	9.7	3.15	2.39	3.04
cis-MePro	9.6	3.5	2.91	3.41
trans-MePro	9.6	3.38	2.78	3.33
4-S-Mep	10.7	3.46	2.77	3.38
4-R-Mep	10.7	3.53	2.81	3.38
3,4-Dhp	9.8	3.03	2.37	2.93
Aze	10.5	3.24	2.73	3.14
Pip	10.8	3.63	3.37	3.60

The values were determined in aqueous buffer at 25 °C (298 K). The pK_a of the carboxyl-group was determined in Ac-Pro*; that of the amino group in the free amino acid. The weight average pK_a was calculated from the *cis* and *trans* pK_as taken the *cis*-*trans* equilibrium into account. If not stated otherwise, data were acquired by Dr. Vladimir Kubyshkin, Institut für Chemie, Technische Universität Berlin, Germany. For comparison, previously determined amino-pK_a values of Pro, 4-R-Flp, 4,4-F_2-Pro and 4-R-Hyp are 10.8, 9.2, 7.2 and 9.7, respectively (Eberhardt et al, 1996; Renner et al, 2001).

Table S12: Parameters of amide rotation for proline and analogues

amino acid	$K_{trans/cis}$ [a]	$-\Delta G_{trans/cis}$ [b] kcal/mol	Reference
Pro	4.60	0.90 ± 0.03	(Shoulders & Raines, 2009)
4-S-Flp	2.50	0.54 ± 0.02	(Shoulders & Raines, 2009)
4-R-Flp	6.69	1.13 ± 0.04	(Shoulders & Raines, 2009)
4,4-F_2-Pro	3.59	0.76 ± 0.03	(Shoulders et al, 2009)
4-S-Hyp	2.30	0.49 ± 0.02	
4-R-Hyp	6.10	1.07 ± 0.04	(Shoulders & Raines, 2009)
cis-MePro	5.81	1.04 ± 0.04	
trans-MePro	10.6	1.40 ± 0.05	
4-S-Mep	7.40	1.19 ± 0.04	(Shoulders & Raines, 2009)
4-R-Mep	3.70	0.77 ± 0.03	(Shoulders & Raines, 2009)
3,4-Dhp	5.40	1.00 ± 0.03	
Aze	4	0.82 ± 0.04	(Kern et al, 1997)
Pip	6.75	1.13 ± 0.05	(Kern et al, 1997)

[a] calculated as $\Delta G = -RT\ln(K_{trans/cis})$ for 298 K; [b] determined at 298 K for Ac-Pro*-OCH_3 peptides, except for Aze and Pip which have been determined in Ac-Pro*-4-nitroanilide. If not stated otherwise, data were acquired by Dr. Vladimir Kubyshkin, Institut für Chemie, Technische Universität Berlin, Germany.

Table S13: pK_a values, parameters of amide rotation and rate constants of peptide bond formation

amino acid	pK_a, amino group [a]	pK_a, carboxyl group [b]			$K_{trans/cis}$ [c]	$-\Delta G_{trans/cis}$ [d]	k_{pep} [e] s^{-1}
		s-*trans*	s-*cis*	Average			
Ala	9.87	3.56	3.11	3.56	170	3.04 ± 0.05	57 ± 4
Phe	9.31	3.42	2.98	3.42	167	3.03 ± 0.01	16 ± 1
Val	9.74	3.55	3.1	3.55	238	3.24 ± 0.11	16 ± 1

Values were determined in aqueous buffer at 298 K; [a] determined for the free amino acid ; [b] determined for Ac-Xaa; [c] calculated as $\Delta G = -RT\ln K$; [d] determined for Ac-Xaa-OH; with Xaa being Ala, Phe or Val; all data were acquired by Dr. Vladimir Kubyshkin (Institut für Chemie, Technische Universität Berlin). [e] determined by fMet-Xaa-Pmn formation (Wohlgemuth et al, 2008).

Table S14: Rate of reactions for Pro and Pro-derivatives

Pro*	fMP*-Pmn, k_{obs}, s^{-1}		fMP*-G, k_{obs}, s^{-1}		fM-P*P*G, k_{obs}, s^{-1}	
	no	EF-P	no	EF-P	no	EF-P
Pro	0.14 ± 0.1	8.2 ± 0.8	4.2 ± 0.3	33 ± 2	0.018 ± 0.02	0.6 ± 0.02
Aze	0.55 ± 0.26 (40%)	45 ± 13 (34%)				
	0.12 ± 0.04 (60%)	2.4 ± 0.3 (66%)				
Pip	0.5 ± 0.06 (68%)	27 ± 3 (81%)				
	0.03 ± 0.01(32%)	0.7 ±0. 3 (19%)				
4-S-Flp	0.003 ± 0.0002	0.23 ± 0.02	0.15 ± 0.02	5 ± 0.5	no product	0.013 ± 0.001
4-R-Flp	21 ± 2	121 ± 33	73 ± 10	63 ± 9	0.22 ± 0.02	0.53 ± 0.06
4,4-F_2-Pro	2.3 ± 0.2	67 ± 5	42 ± 4 (73%)	65 ± 14 (83%)	0.077 ± 0.005	0.7 ± 0.1
			0.07 ± 0.02 (27%)	0.3 ± 0.3 (17%)		
4-S-Hyp	0.007 ± 0.0003	0.64 ± 0.06	0.3 ± 0.03	11 ± 1	0.004 ± 0.001	0.077 ± 0.008
4-R-Hyp	0.2 ± 0.02	9.4 ± 0.5	4 ± 0.3	49 ± 7	0.039 ± 0.004	0.3 ± 0.04
***Cis*-MePro**	$6 \pm 1 \times 10^{-5}$	0.001 ± 0.0004	0.001 ± 0.0001	0.037 ± 0.003	no product	0.013 ± 0.002
***Trans*-MePro**	0.32 ± 0.03	14 ± 2	28 ± 4 (68%)	69 ± 11 (86%)	0.065 ± 0.008	0.64 ± 0.09
			1.7 ± 0.5 (32%)	0.6 ± 0.5 (14%)		
4-S-Mep	0.09 ± 0.002 (21%)	6 ± 1(38%)	9 ± 4 (32%)	26 ± 9 (72%)	0.009 ± 0.004	0.085 ± 0.008
	0.003 ± 0.0002 (79%)	0.18 ± 0.03 (62%)	0.16 ± 0.03 (68%)	1 ± 1 (28%)		
4-R-Mep	0.17 ± 0.03	12 ± 1	19 ± 3 (69%)	73 ± 9 (75%)	0.072 ± 0.006	0.51 ± 0.05
			0.6 ± 0.2 (31%)	1.9 ± 0.6 (25%)		
3,4-Dhp	0.01 ± 0.001	0.62 ± 0.07	2.8 ± 0.4 (67%)	21 ± 4 (82%)	0.005 ± 0.001	0.12 ± 0.01
			0.23 ± 0.07 (33%)	0.2 ± 0.1 (18%)		

fMP*-Pmn, fMP*-G and fM-P*P*G formation performed in buffer B at pH 7.5. Rates of biphasic time-courses were shown with the respective contribution in %.

Table S15: Rate of peptidyl transfer from fMet-(R/S)-Flp-tRNA^{Pro} to Pmn as a function of temperature

Temp., °C	k_{obs}, s^{-1}			
	4-R-Flp		4-S-Flp	
	no EF-P	EF-P	no EF-P	EF-P
15	1.2 ± 0.1	10 ± 1	0.0002 ± 0.00003	0.011 ± 0.001
20	2.4 ± 0.3	23 ± 2		
25	6.1 ± 0.4	45 ± 3	0.0008 ± 0.00004	0.055 ± 0.003
30	9 ± 1	82 ± 11	0.0018 ± 0.0001	0.104 ± 0.006
37	21 ± 2	121 ± 33	0.0028 ± 0.0002	0.23 ± 0.05

PTC-fMP* (0.15 μM) vs. Pmn (10 mM) ± EF-P (3 μM). The reactions were performed at pH 7.5 in buffer B at indicated temperature.

6 REFERENCES

Abratt VR, Mbewe M, Woods DR (1998) Cloning of an EF-P homologue from Bacteroides fragilis that increases B. fragilis glutamine synthetase activity in Escherichia coli. *Mol Gen Genet* **258:** 363-372

Adio S, Senyushkina T, Peske F, Fischer N, Wintermeyer W, Rodnina MV (2015) Fluctuations between multiple EF-G-induced chimeric tRNA states during translocation on the ribosome. *Nature communications* **6:** 7442

Ambrogelly A, O'Donoghue P, Soll D, Moses S (2010) A bacterial ortholog of class II lysyl-tRNA synthetase activates lysine. *FEBS Lett* **584:** 3055-3060

An G, Glick BR, Friesen JD, Ganoza MC (1980) Identification and quantitation of elongation factor EF-P in Escherichia coli cell-free extracts. *Can J Biochem* **58:** 1312-1314

Aoki H, Adams SL, Turner MA, Ganoza MC (1997) Molecular characterization of the prokaryotic efp gene product involved in a peptidyltransferase reaction. *Biochimie* **79:** 7-11

Aoki H, Xu J, Emili A, Chosay JG, Golshani A, Ganoza MC (2008) Interactions of elongation factor EF-P with the Escherichia coli ribosome. *Febs j* **275:** 671-681

Arkov AL, Korolev SV, Kisselev LL (1993) Termination of translation in bacteria may be modulated via specific interaction between peptide chain release factor 2 and the last peptidyl-tRNA(Ser/Phe). *Nucleic acids research* **21:** 2891-2897

Baba T, Ara T, Hasegawa M, Takai Y, Okumura Y, Baba M, Datsenko KA, Tomita M, Wanner BL, Mori H (2006) Construction of Escherichia coli K-12 in-frame, single-gene knockout mutants: the Keio collection. *Mol Syst Biol* **2:** 2006.0008

Bailly M, de Crecy-Lagard V (2010) Predicting the pathway involved in post-translational modification of elongation factor P in a subset of bacterial species. *Biol Direct* **5:** 3

Balibar CJ, Iwanowicz D, Dean CR (2013) Elongation factor P is dispensable in Escherichia coli and Pseudomonas aeruginosa. *Curr Microbiol* **67:** 293-299

Ban N, Nissen P, Hansen J, Moore PB, Steitz TA (2000) The complete atomic structure of the large ribosomal subunit at 2.4 A resolution. *Science (New York, NY)* **289:** 905-920

Barlow DJ, Thornton JM (1988) Helix geometry in proteins. *Journal of molecular biology* **201:** 601-619

Bearson SM, Bearson BL, Brunelle BW, Sharma VK, Lee IS (2011) A mutation in the poxA gene of Salmonella enterica serovar Typhimurium alters protein production, elevates susceptibility to environmental challenges, and decreases swine colonization. *Foodborne Pathog Dis* **8:** 725-732

Bedford GR, Sadler PJ (1974) 13C magnetic resonance study of the ionization of N-acetyl-DL-proline in aqueous solution. *Biochimica et biophysica acta* **343:** 656-662

Behshad E, Ruzicka FJ, Mansoorabadi SO, Chen D, Reed GH, Frey PA (2006) Enantiomeric free radicals and enzymatic control of stereochemistry in a radical mechanism: the case of lysine 2,3-aminomutases. *Biochemistry* **45:** 12639-12646

Berg RA, Prockop DJ (1973) The thermal transition of a non-hydroxylated form of collagen. Evidence for a role for hydroxyproline in stabilizing the triple-helix of collagen. *Biochemical and biophysical research communications* **52:** 115-120

Beringer M (2008) Modulating the activity of the peptidyl transferase center of the ribosome. *RNA (New York, NY)* **14:** 795-801

Beringer M, Adio S, Wintermeyer W, Rodnina M (2003) The G2447A mutation does not affect ionization of a ribosomal group taking part in peptide bond formation. *RNA (New York, NY)* **9:** 919-922

Beringer M, Bruell C, Xiong L, Pfister P, Bieling P, Katunin VI, Mankin AS, Bottger EC, Rodnina MV (2005) Essential mechanisms in the catalysis of peptide bond formation on the ribosome. *The Journal of biological chemistry* **280:** 36065-36072

Beringer M, Rodnina MV (2007a) Importance of tRNA interactions with 23S rRNA for peptide bond formation on the ribosome: studies with substrate analogs. *Biological chemistry* **388:** 687-691

Beringer M, Rodnina MV (2007b) The ribosomal peptidyl transferase. *Molecular cell* **26:** 311-321

Berry J, Rajaure M, Pang T, Young R (2012) The spanin complex is essential for lambda lysis. *Journal of bacteriology* **194:** 5667-5674

Berry J, Summer EJ, Struck DK, Young R (2008) The final step in the phage infection cycle: the Rz and Rz1 lysis proteins link the inner and outer membranes. *Mol Microbiol* **70:** 341-351

Bhattacharyya R, Chakrabarti P (2003) Stereospecific interactions of proline residues in protein structures and complexes. *Journal of molecular biology* **331:** 925-940

Bieling P, Beringer M, Adio S, Rodnina MV (2006) Peptide bond formation does not involve acid-base catalysis by ribosomal residues. *Nature structural & molecular biology* **13:** 423-428

Björnsson A, Mottagui-Tabar S, Isaksson LA (1996) Structure of the C-terminal end of the nascent peptide influences translation termination. *EMBO* **15:** 1696-1704

Blaha G, Stanley RE, Steitz TA (2009) Formation of the first peptide bond: the structure of EF-P bound to the 70S ribosome. *Science (New York, NY)* **325:** 966-970

Brandts JF, Halvorson HR, Brennan M (1975) Consideration of the Possibility that the slow step in protein denaturation reactions is due to cis-trans isomerism of proline residues. *Biochemistry* **14:** 4953-4963

Bretscher LE, Jenkins CL, Taylor KM, DeRider ML, Raines RT (2001) Conformational stability of collagen relies on a stereoelectronic effect. *Journal of the American Chemical Society* **123:** 777-778

Brochier C, Lopez-Garcia P, Moreira D (2004) Horizontal gene transfer and archaeal origin of deoxyhypusine synthase homologous genes in bacteria. *Gene* **330:** 169-176

Brown EL, Belagaje R, Ryan MJ, Khorana HG (1979) Chemical synthesis and cloning of a tyrosine tRNA gene. *Methods Enzymol* **68:** 109-151

Bruice TC, Hegarty AF, Felton SF, Donzel A, Kundu NG (1970) Aminolysis of Esters. IX. The Nature of the Transition States in the Aminolysis of Phenyl Acetates. *Journal of the American Chemical Society* **92:** 1370-1378

Brunelle JL, Youngman EM, Sharma D, Green R (2006) The interaction between C75 of tRNA and the A loop of the ribosome stimulates peptidyl transferase activity. *RNA (New York, NY)* **12:** 33-39

Bullwinkle TJ, Zou SB, Rajkovic A, Hersch SJ, Elgamal S, Robinson N, Smil D, Bolshan Y, Navarre WW, Ibba M (2013) (R)-beta-lysine-modified elongation factor P functions in translation elongation. *The Journal of biological chemistry* **288:** 4416-4423

Calogero RA, Pon CL, Canonaco MA, Gualerzi CO (1988) Selection of the mRNA translation initiation region by Escherichia coli ribosomes. *Proceedings of the National Academy of Sciences of the United States of America* **85:** 6427-6431

Campellone KG, Robbins D, Leong JM (2004) EspFU is a translocated EHEC effector that interacts with Tir and N-WASP and promotes Nck-independent actin assembly. *Dev Cell* **7:** 217-228

Caron MP, Bastet L, Lussier A, Simoneau-Roy M, Masse E, Lafontaine DA (2012) Dual-acting riboswitch control of translation initiation and mRNA decay. *Proceedings of the National Academy of Sciences of the United States of America* **109:** E3444-3453

Chakrabarti P, Pal D (2001) The interrelationships of side-chain and main-chain conformations in proteins. *Progress in biophysics and molecular biology* **76:** 1-102

Charles TC, Nester EW (1993) A chromosomally encoded two-component sensory transduction system is required for virulence of Agrobacterium tumefaciens. *Journal of bacteriology* **175:** 6614-6625

Chattopadhyay MK, Park MH, Tabor H (2008) Hypusine modification for growth is the major function of spermidine in Saccharomyces cerevisiae polyamine auxotrophs grown in limiting spermidine. *Proceedings of the National Academy of Sciences of the United States of America* **105:** 6554-6559

Chattopadhyay MK, Tabor CW, Tabor H (2003) Spermidine but not spermine is essential for hypusine biosynthesis and growth in Saccharomyces cerevisiae: Spermine is converted to spermidine in vivo by the FMS1-amine oxidase. *Proceedings of the National Academy of Sciences* **100:** 13869-13874

Choi S, Choe J (2011) Crystal structure of elongation factor P from Pseudomonas aeruginosa at 1.75 A resolution. *Proteins* **79:** 1688-1693

Cornish PV, Ermolenko DN, Noller HF, Ha T (2008) Spontaneous intersubunit rotation in single ribosomes. *Molecular cell* **30:** 578-588

Craveur P, Joseph AP, Poulain P, de Brevern AG, Rebehmed J (2013) Cis-trans isomerization of omega dihedrals in proteins. *Amino acids* **45:** 279-289

Cruz-Vera LR, Gong M, Yanofsky C (2006) Changes produced by bound tryptophan in the ribosome peptidyl transferase center in response to TnaC, a nascent leader peptide. *Proceedings of the National Academy of Sciences of the United States of America* **103:** 3598-3603

DeRider ML, Wilkens SJ, Waddell MJ, Bretscher LE, Weinhold F, Raines RT, Markley JL (2002) Collagen stability: Insights from NMR spectroscopic and hybrid density functional computational investigations of the effect of electronegative substituents on prolyl ring conformations. *JACS*

Dever TE, Gutierrez E, Shin BS (2014) The hypusine-containing translation factor eIF5A. *Critical reviews in biochemistry and molecular biology* **17:** 1-13

Dincbas-Renqvist V, Engstrom A, Mora L, Heurgue-Hamard V, Buckingham R, Ehrenberg M (2000) A post-translational modification in the GGQ motif of RF2 from Escherichia coli stimulates termination of translation. *The EMBO journal* **19:** 6900-6907

Doerfel LK, Rodnina MV (2013) Elongation factor P: Function and effects on bacterial fitness. *Biopolymers* **99:** 837-845

Doerfel LK, Wohlgemuth I, Kothe C, Peske F, Urlaub H, Rodnina MV (2013) EF-P is essential for rapid synthesis of proteins containing consecutive proline residues. *Science (New York, NY)* **339:** 85-88

Doerfel LK, Wohlgemuth I, Kubyshkin V, Starosta AL, Wilson DN, Budisa N, Rodnina MV (2015) Entropic Contribution of Elongation Factor P to Proline Positioning at the Catalytic Center of the Ribosome. *Journal of the American Chemical Society* **137:** 12997-13006

Dong H, Nilsson L, Kurland CG (1996) Co-variation of tRNA abundance and codon usage in Escherichia coli at different growth rates. *Journal of molecular biology* **260:** 649-663

Dorner S, Panuschka C, Schmid W, Barta A (2003) Mononucleotide derivatives as ribosomal P-site substrates reveal an important contribution of the 2'-OH to activity. *Nucleic acids research* **31:** 6536-6542

Eberhardt ES, Panisik N, Jr., Raines RT (1996) Inductive Effects on the Energetics of Prolyl Peptide Bond Isomerization: Implications for Collagen Folding and Stability. *Journal of the American Chemical Society* **118:** 12261-12266

Elgamal S, Katz A, Hersch SJ, Newsom D, White P, Navarre WW, Ibba M (2014) EF-P dependent pauses integrate proximal and distal signals during translation. *PLoS Genet* **10**

Evans TC, Jr., Nelsestuen GL (1996) Importance of cis-proline 22 in the membrane-binding conformation of bovine prothrombin. *Biochemistry* **35:** 8210-8215

Fahnestock S, Neumann H, Shashoua V, Rich A (1970) Ribosome-catalyzed ester formation. *Biochemistry* **9:** 2477-2483

Fei J, Kosuri P, MacDougall DD, Gonzalez RL, Jr. (2008) Coupling of ribosomal L1 stalk and tRNA dynamics during translation elongation. *Molecular cell* **30:** 348-359

Fersht A (ed) (1999) *Structure and mechanism in Protein Science*:

Fischer S, Dunbrack RL, Karplus M (1994) Cis-Trans Imide Isomerization of the Proline Dipeptide. *Journal of the American Chemical Society* **116:** 11931-11937

Flores-Ortega A, Casanovas J, Zanuy D, Nussinov R, Aleman C (2007) Conformations of proline analogues having double bonds in the ring. *The journal of physical chemistry B* **111:** 5475-5482

Frank J, Agrawal RK (2000) A ratchet-like inter-subunit reorganization of the ribosome during translocation. *Nature* **406:** 318-322

Ganguly HK, Majumder B, Chattopadhyay S, Chakrabarti P, Basu G (2012) Direct evidence for CH...pi interaction mediated stabilization of Pro-cisPro bond in peptides with Pro-Pro-aromatic motifs. *Journal of the American Chemical Society* **134:** 4661-4669

Ganoza MC, Aoki H (2000) Peptide bond synthesis: function of the efp gene product. *Biological chemistry* **381:** 553-559

Ganoza MC, Zahid N, Baxter RM (1985) Stimulation of peptidyltransferase reactions by a soluble protein. *European journal of biochemistry / FEBS* **146:** 287-294

Girgis HS, Hottes AK, Tavazoie S (2009) Genetic architecture of intrinsic antibiotic susceptibility. *PloS one* **4:** e5629

Glick BR, Chladek S, Ganoza MC (1979) Peptide bond formation stimulated by protein synthesis factor EF-P depends on the aminoacyl moiety of the acceptor. *European journal of biochemistry / FEBS* **97:** 23-28

Glick BR, Ganoza MC (1975) Identification of a soluble protein that stimulates peptide bond synthesis. *Proceedings of the National Academy of Sciences of the United States of America* **72:** 4257-4260

Glick BR, Ganoza MC (1976) Characterization and site of action of a soluble protein that stimulates peptide-bond synthesis. *European journal of biochemistry / FEBS* **71:** 483-491

Good NE, Winget GD, Winter W, Connolly TN, Izawa S, Singh RM (1966) Hydrogen ion buffers for biological research. *Biochemistry* **5:** 467-477

Grathwohl C, Wuthrich K (1976) The X-Pro peptide bond as an nmr probe for conformational studies of flexible linear peptides. *Biopolymers* **15:** 2025-2041

Green RH, Glick BR, Ganoza MC (1985) Requirements for in vitro reconstruction of protein synthesis. *Biochemical and biophysical research communications* **126:** 792-798

Gregio AP, Cano VP, Avaca JS, Valentini SR, Zanelli CF (2009) eIF5A has a function in the elongation step of translation in yeast. *Biochemical and biophysical research communications* **380:** 785-790

Gromadski KB, Daviter T, Rodnina MV (2006) A uniform response to mismatches in codon-anticodon complexes ensures ribosomal fidelity. *Molecular cell* **21:** 369-377

Gromadski KB, Rodnina MV (2004) Kinetic determinants of high-fidelity tRNA discrimination on the ribosome. *Mol Cell* **13:** 191-200

Gutierrez E, Shin BS, Woolstenhulme CJ, Kim JR, Saini P, Buskirk AR, Dever TE (2013) eIF5A promotes translation of polyproline motifs. *Molecular cell* **51:** 35-45

Hanawa-Suetsugu K, Sekine S, Sakai H, Hori-Takemoto C, Terada T, Unzai S, Tame JR, Kuramitsu S, Shirouzu M, Yokoyama S (2004) Crystal structure of elongation factor P from Thermus thermophilus HB8. *Proceedings of the National Academy of Sciences of the United States of America* **101:** 9595-9600

Hanessian S, Reinhold U, Gentile G (1997) The Synthesis of Enantiopure ω-Methanoprolines and ω-Methanopipecolic Acids by a Novel Cyclopropanation Reaction: The "Flattering" of Proline. *Angewandte Chemie International Edition in English* **36:** 1881-1884

Hayes CS, Bose B, Sauer RT (2002) Proline residues at the C terminus of nascent chains induce SsrA tagging during translation termination. *The Journal of biological chemistry* **277:** 33825-33832

Hentzen D, Mandel P, Garel JP (1972) Relation between aminoacyl-tRNA stability and the fixed amino acid. *Biochimica et biophysica acta* **281:** 228-232

Hersch SJ, Elgamal S, Katz A, Ibba M, Navarre WW (2014) Translation Initiation Rate Determines the Impact of Ribosome Stalling on Bacterial Protein Synthesis. *The Journal of biological chemistry*

Hersch SJ, Wang M, Zou SB, Moon KM, Foster LJ, Ibba M, Navarre WW (2013) Divergent protein motifs direct elongation factor P-mediated translational regulation in Salmonella enterica and Escherichia coli. *mBio* **4:** e00180-00113

Hesslein AE, Katunin VI, Beringer M, Kosek AB, Rodnina MV, Strobel SA (2004) Exploration of the conserved A+C wobble pair within the ribosomal peptidyl transferase center using affinity purified mutant ribosomes. *Nucleic acids research* **32:** 3760-3770

Heurgue-Hamard V, Karimi R, Mora L, MacDougall J, Leboeuf C, Grentzmann G, Ehrenberg M, Buckingham RH (1998) Ribosome release factor RF4 and termination factor RF3 are involved in dissociation of peptidyl-tRNA from the ribosome. *The EMBO journal* **17:** 808-816

Hiller DA, Singh V, Zhong M, Strobel SA (2011) A two-step chemical mechanism for ribosome-catalysed peptide bond formation. *Nature* **476:** 236-239

Himeno H, Hasegawa T, Ueda T, Watanabe K, Miura K, Shimizu M (1989) Role of the extra G-C pair at the end of the acceptor stem of tRNA(His) in aminoacylation. *Nucleic acids research* **17:** 7855-7863

Hinderaker MP, Raines RT (2003) An electronic effect on protein structure. *Protein Sci* **12:** 1188-1194

Hirokawa G, Demeshkina N, Iwakura N, Kaji H, Kaji A (2006) The ribosome-recycling step: consensus or controversy? *Trends in biochemical sciences* **31:** 143-149

Holtkamp W, Wintermeyer W, Rodnina MV (2014) Synchronous tRNA movements during translocation on the ribosome are orchestrated by elongation factor G and GTP hydrolysis. *BioEssays : news and reviews in molecular, cellular and developmental biology* **36:** 908-918

Hunston RN, Gerothanassis IP, Lauterwein J (1985) A study of L-proline, sarcosine, and the cis/trans isomers of N-acetyl-L-proline and N-acetylsarcosine in aqueous and organic solution by oxygen-17 NMR. *Journal of the American Chemical Society* **107:** 2654-2661

Iannino F, Ugalde JE, Inon de Iannino N (2012) Brucella abortus efp gene is required for an efficient internalization in HeLa cells. *Microb Pathog* **52:** 31-40

Ieong KW, Pavlov MY, Kwiatkowski M, Forster AC, Ehrenberg M (2012) Inefficient delivery but fast peptide bond formation of unnatural L-aminoacyl-tRNAs in translation. *Journal of the American Chemical Society* **134:** 17955-17962

Igarashi K, Kakegawa T, Hirose S (1982) Stabilization of 30 S ribosomal subunits of Bacillus subtilis W168 by spermidine and magnesium ions. *Biochimica et biophysica acta* **697:** 185-192

Improta R, Benzi C, Barone V (2001) Understanding the role of stereoelectronic effects in determining collagen stability. 1. A quantum mechanical study of proline, hydroxyproline, and fluoroproline dipeptide analogues in aqueous solution. *Journal of the American Chemical Society* **123:** 12568-12577

Ingolia NT, Lareau LF, Weissman JS (2011) Ribosome profiling of mouse embryonic stem cells reveals the complexity and dynamics of mammalian proteomes. *Cell* **147:** 789-802

Isom DG, Castaneda CA, Cannon BR, Garcia-Moreno B (2011) Large shifts in pKa values of lysine residues buried inside a protein. *Proceedings of the National Academy of Sciences of the United States of America* **108:** 5260-5265

Ito K, Uno M, Nakamura Y (2000) A tripeptide 'anticodon' deciphers stop codons in messenger RNA. *Nature* **403:** 680-684

Jenko Kokalj S, Guncar G, Stern I, Morgan G, Rabzelj S, Kenig M, Staniforth RA, Waltho JP, Zerovnik E, Turk D (2007) Essential role of proline isomerization in stefin B tetramer formation. *Journal of molecular biology* **366:** 1569-1579

Johansson M, Bouakaz E, Lovmar M, Ehrenberg M (2008) The kinetics of ribosomal peptidyl transfer revisited. *Molecular cell* **30:** 589-598

Johansson M, Ieong KW, Trobro S, Strazewski P, Aqvist J, Pavlov MY, Ehrenberg M (2011) pH-sensitivity of the ribosomal peptidyl transfer reaction dependent on the identity of the A-site aminoacyl-tRNA. *Proceedings of the National Academy of Sciences of the United States of America* **108:** 79-84

Johansson M, Zhang J, Ehrenberg M (2012) Genetic code translation displays a linear trade-off between efficiency and accuracy of tRNA selection. *Proceedings of the National Academy of Sciences of the United States of America* **109:** 131-136

Jordan IK, Kondrashov FA, Adzhubei IA, Wolf YI, Koonin EV, Kondrashov AS, Sunyaev S (2005) A universal trend of amino acid gain and loss in protein evolution. *Nature* **433:** 633-638

Julian P, Konevega AL, Scheres SH, Lazaro M, Gil D, Wintermeyer W, Rodnina MV, Valle M (2008) Structure of ratcheted ribosomes with tRNAs in hybrid states. *Proceedings of the National Academy of Sciences of the United States of America* **105:** 16924-16927

Kang YK, Park HS (2009) Conformational preferences and cis-trans isomerization of L-3,4-dehydroproline residue. *Biopolymers* **92:** 387-398

Kaniga K, Compton MS, Curtiss R, 3rd, Sundaram P (1998) Molecular and functional characterization of Salmonella enterica serovar typhimurium poxA gene: effect on attenuation of virulence and protection. *Infect Immun* **66:** 5599-5606

Karimi R, Ehrenberg M (1996) Dissociation rates of peptidyl-tRNA from the P-site of E.coli ribosomes. *The EMBO journal* **15:** 1149-1154

Karimi R, Pavlov MY, Heurgue-Hamard V, Buckingham RH, Ehrenberg M (1998) Initiation factors IF1 and IF2 synergistically remove peptidyl-tRNAs with short polypeptides from the P-site of translating Escherichia coli ribosomes. *Journal of molecular biology* **281:** 241-252

Katunin V, Soboleva N, Mahkno V, Sedelnikova E, Zhenodarova S, Kirillov S (1994) Effect of the nucleotide-37 on the interaction of tRNA(Phe) with the P site of Escherichia coli ribosomes. *Biochimie* **76:** 51-57

Katunin VI, Muth GW, Strobel SA, Wintermeyer W, Rodnina MV (2002) Important contribution to catalysis of peptide bond formation by a single ionizing group within the ribosome. *Molecular cell* **10:** 339-346

Kearns DB, Chu F, Rudner R, Losick R (2004) Genes governing swarming in Bacillus subtilis and evidence for a phase variation mechanism controlling surface motility. *Mol Microbiol* **52:** 357-369

Kern D, Schutkowski M, Drakenberg T (1997) Rotational Barriers of cis/trans Isomerization of Proline Analogues and Their Catalysis by Cyclophilin. *Journal of the American Chemical Society* **119:** 8403-8408

Kingery DA, Pfund E, Voorhees RM, Okuda K, Wohlgemuth I, Kitchen DE, Rodnina MV, Strobel SA (2008) An uncharged amine in the transition state of the ribosomal peptidyl transfer reaction. *Chem Biol* **15:** 493-500

Kohanski MA, Dwyer DJ, Wierzbowski J, Cottarel G, Collins JJ (2008) Mistranslation of membrane proteins and two-component system activation trigger antibiotic-mediated cell death. *Cell* **135:** 679-690

Konevega AL, Soboleva NG, Makhno VI, Semenkov YP, Wintermeyer W, Rodnina MV, Katunin VI (2004) Purine bases at position 37 of tRNA stabilize codon-anticodon interaction in the ribosomal A site by stacking and Mg2+-dependent interactions. *RNA (New York, NY)* **10:** 90-101

Kothe U, Paleskava A, Konevega AL, Rodnina MV (2006) Single-step purification of specific tRNAs by hydrophobic tagging. *Anal Biochem* **356:** 148-150

Kuhlenkoetter S, Wintermeyer W, Rodnina MV (2011) Different substrate-dependent transition states in the active site of the ribosome. *Nature* **476:** 351-354

Laemmli UK (1970) Cleavage of structural proteins during the assembly of the head of bacteriophage T4. *Nature* **227:** 680-685

Lancaster L, Noller HF (2005) Involvement of 16S rRNA nucleotides G1338 and A1339 in discrimination of initiator tRNA. *Molecular cell* **20:** 623-632

Lassak J, Keilhauer E, Furst M, Wuichet K, Godeke J, Starosta AL, Chen JM, Sogaard-Andersen L, Rohr J, Wilson DN, Haussler S, Mann M, Jung K (2015) Arginine-rhamnosylation as new strategy to activate translation elongation factor P. *Nat Chem Biol*

Ledoux S, Uhlenbeck OC (2008) Different aa-tRNAs are selected uniformly on the ribosome. *Molecular cell* **31:** 114-123

Lucas-Lenard J, Lipmann F (1967) Initiation of polyphenylalanine synthesis by N-acetylphenylalanyl-SRNA. *Proceedings of the National Academy of Sciences of the United States of America* **57:** 1050-1057

Lummis SC, Beene DL, Lee LW, Lester HA, Broadhurst RW, Dougherty DA (2005) Cis-trans isomerization at a proline opens the pore of a neurotransmitter-gated ion channel. *Nature* **438:** 248-252

MacArthur MW, Thornton JM (1991) Influence of proline residues on protein conformation. *Journal of molecular biology* **218:** 397-412

MacDougall DD, Gonzalez RL, Jr. (2015) Translation initiation factor 3 regulates switching between different modes of ribosomal subunit joining. *Journal of molecular biology* **427:** 1801-1818

Manchester KL, Alford T (1979) Activity of protein synthesis initiation factors in cytosol from rat liver and muscle and ascites cells. *Biochimica et biophysica acta* **563:** 155-162

Marman HE, Mey AR, Payne SM (2014) Elongation factor P and modifying enzyme PoxA are necessary for virulence of Shigella flexneri. *Infect Immun* **82:** 3612-3621

Matheisl S, Berninghausen O, Becker T, Beckmann R (2015) Structure of a human translation termination complex. *Nucleic acids research*

Miller-Fleming L, Olin-Sandoval V, Campbell K, Ralser M (2015) Remaining Mysteries of Molecular Biology: The Role of Polyamines in the Cell. *Journal of molecular biology*

Milner-White EJ, Bell LH, Maccallum PH (1992) Pyrrolidine ring puckering in cis and trans-proline residues in proteins and polypeptides. Different puckers are favoured in certain situations. *Journal of molecular biology* **228:** 725-734

Milon P, Carotti M, Konevega AL, Wintermeyer W, Rodnina MV, Gualerzi CO (2010) The ribosome-bound initiation factor 2 recruits initiator tRNA to the 30S initiation complex. *EMBO reports* **11:** 312-316

Milon P, Konevega AL, Peske F, Fabbretti A, Gualerzi CO, Rodnina MV (2007) Transient kinetics, fluorescence, and FRET in studies of initiation of translation in bacteria. *Methods Enzymol* **430:** 1-30

Milon P, Rodnina MV (2012) Kinetic control of translation initiation in bacteria. *Critical reviews in biochemistry and molecular biology* **47:** 334-348

Mittelstaet J (2012) Molecular mechanisms of substrate selection and protein folding on the ribosome. *PhD thesis*

Mittelstaet J, Konevega AL, Rodnina MV (2013) A kinetic safety gate controlling the delivery of unnatural amino acids to the ribosome. *Journal of the American Chemical Society* **135:** 17031-17038

Moazed D, Noller HF (1989) Intermediate states in the movement of transfer RNA in the ribosome. *Nature* **342:** 142-148

Moll I, Grill S, Gualerzi CO, Blasi U (2002) Leaderless mRNAs in bacteria: surprises in ribosomal recruitment and translational control. *Mol Microbiol* **43:** 239-246

Mottagui-Tabar S, Björnsson A, Isaksson LA (1994) The second to last amino acid in the nascent peptide as a codon context determinant. *EMBO* **13:** 249-257

Munro JB, Altman RB, Tung CS, Cate JH, Sanbonmatsu KY, Blanchard SC (2010) Spontaneous formation of the unlocked state of the ribosome is a multistep process. *Proceedings of the National Academy of Sciences of the United States of America* **107:** 709-714

Murakami H, Ohta A, Ashigai H, Suga H (2006) A highly flexible tRNA acylation method for non-natural polypeptide synthesis. *Nat Methods* **3:** 357-359

Muth GW, Chen L, Kosek AB, Strobel SA (2001) pH-dependent conformational flexibility within the ribosomal peptidyl transferase center. *RNA (New York, NY)* **7:** 1403-1415

Muto H, Ito K (2008) Peptidyl-prolyl-tRNA at the ribosomal P-site reacts poorly with puromycin. *Biochemical and biophysical research communications* **366:** 1043-1047

Muto H, Nakatogawa H, Ito K (2006) Genetically encoded but nonpolypeptide prolyl-tRNA functions in the A site for SecM-mediated ribosomal stall. *Molecular cell* **22:** 545-552

Nakahigashi K, Kubo N, Narita S, Shimaoka T, Goto S, Oshima T, Mori H, Maeda M, Wada C, Inokuchi H (2002) HemK, a class of protein methyl transferase with similarity to DNA methyl transferases, methylates polypeptide chain release factors, and hemK knockout induces defects in translational termination. *Proceedings of the National Academy of Sciences of the United States of America* **99:** 1473-1478

Navarre WW, Zou SB, Roy H, Xie JL, Savchenko A, Singer A, Edvokimova E, Prost LR, Kumar R, Ibba M, Fang FC (2010) PoxA, yjeK, and elongation factor P coordinately modulate virulence and drug resistance in Salmonella enterica. *Molecular cell* **39:** 209-221

Nilsson OB, Hedman R, Marino J, Wickles S, Bischoff L, Johansson M, Muller-Lucks A, Trovato F, Puglisi JD, O'Brien EP, Beckmann R, von Heijne G (2015) Cotranslational Protein Folding inside the Ribosome Exit Tunnel. *Cell Rep* **12:** 1533-1540

Nissen P, Hansen J, Ban N, Moore PB, Steitz TA (2000) The structural basis of ribosome activity in peptide bond synthesis. *Science (New York, NY)* **289:** 920-930

Noinaj N, Guillier M, Barnard TJ, Buchanan SK (2010) TonB-dependent transporters: regulation, structure, and function. *Annu Rev Microbiol* **64:** 43-60

Noller HF, Hoffarth V, Zimniak L (1992) Unusual resistance of peptidyl transferase to protein extraction procedures. *Science (New York, NY)* **256:** 1416-1419

Nurenberg E, Tampe R (2013) Tying up loose ends: ribosome recycling in eukaryotes and archaea. *Trends in biochemical sciences* **38:** 64-74

Ohtsuki T, Yamamoto H, Doi Y, Sisido M (2010) Use of EF-Tu mutants for determining and improving aminoacylation efficiency and for purifying aminoacyl tRNAs with non-natural amino acids. *J Biochem* **148:** 239-246

Okuda K, Seila AC, Strobel SA (2005) Uncovering the enzymatic pKa of the ribosomal peptidyl transferase reaction utilizing a fluorinated puromycin derivative. *Biochemistry* **44:** 6675-6684

Owens NW, Braun C, O'Neil JD, Marat K, Schweizer F (2007) Effects of glycosylation of (2S,4R)-4-hydroxyproline on the conformation, kinetics, and thermodynamics of prolyl amide isomerization. *Journal of the American Chemical Society* **129:** 11670-11671

Pal D, Chakrabarti P (1999) Cis peptide bonds in proteins: residues involved, their conformations, interactions and locations. *Journal of molecular biology* **294:** 271-288

Panasik N, Jr., Eberhardt ES, Edison AS, Powell DR, Raines RT (1994) Inductive effects on the structure of proline residues. *Int J Pept Protein Res* **44:** 262-269

Pape T, Wintermeyer W, Rodnina MV (1998) Complete kinetic mechanism of elongation factor Tu-dependent binding of aminoacyl-tRNA to the A site of the E. coli ribosome. *The EMBO journal* **17:** 7490-7497

Park JH, Johansson HE, Aoki H, Huang BX, Kim HY, Ganoza MC, Park MH (2012) Post-translational modification by beta-lysylation is required for activity of Escherichia coli elongation factor P (EF-P). *The Journal of biological chemistry* **287:** 2579-2590

Park MH (2006) The post-translational synthesis of a polyamine-derived amino acid, hypusine, in the eukaryotic translation initiation factor 5A (eIF5A). *J Biochem* **139:** 161-169

Park MH, Nishimura K, Zanelli CF, Valentini SR (2010) Functional significance of eIF5A and its hypusine modification in eukaryotes. *Amino acids* **38:** 491-500

Pavlov MY, Watts RE, Tan Z, Cornish VW, Ehrenberg M, Forster AC (2009) Slow peptide bond formation by proline and other N-alkylamino acids in translation. *Proceedings of the National Academy of Sciences of the United States of America* **106:** 50-54

Peil L, Starosta AL, Lassak J, Atkinson GC, Virumae K, Spitzer M, Tenson T, Jung K, Remme J, Wilson DN (2013) Distinct XPPX sequence motifs induce ribosome stalling, which is rescued by the translation elongation factor EF-P. *Proceedings of the National Academy of Sciences of the United States of America* **110:** 15265-15270

Peil L, Starosta AL, Virumae K, Atkinson GC, Tenson T, Remme J, Wilson DN (2012) Lys34 of translation elongation factor EF-P is hydroxylated by YfcM. *Nat Chem Biol* **8:** 695-697

Peng WT, Banta LM, Charles TC, Nester EW (2001) The chvH locus of Agrobacterium encodes a homologue of an elongation factor involved in protein synthesis. *Journal of bacteriology* **183:** 36-45

Peske F, Kuhlenkoetter S, Rodnina MV, Wintermeyer W (2014) Timing of GTP binding and hydrolysis by translation termination factor RF3. *Nucleic acids research* **42:** 1812-1820

Polikanov YS, Steitz TA, Innis CA (2014) A proton wire to couple aminoacyl-tRNA accommodation and peptide-bond formation on the ribosome. *Nature structural & molecular biology* **21:** 787-793

Rajkovic A, Erickson S, Witzky A, Branson OE, Seo J, Gafken PR, Frietas MA, Whitelegge JP, Faull KF, Navarre W, Darwin AJ, Ibba M (2015) Cyclic Rhamnosylated Elongation Factor P Establishes Antibiotic Resistance in Pseudomonas aeruginosa. *mBio* **6:** e00823

Raleigh DP, Evans PA, Pitkeathly M, Dobson CM (1992) A peptide model for proline isomerism in the unfolded state of staphylococcal nuclease. *Journal of molecular biology* **228:** 338-342

Ramachandran GN, Lakshminarayanan AV, Balasubramanian R, Tegoni G (1970) Studies on the conformation of amino acids. XII. Energy calculations on prolyl residue. *Biochimica et biophysica acta* **221:** 165-181

Reimer U, Scherer G, Drewello M, Kruber S, Schutkowski M, Fischer G (1998) Side-chain Effects on Peptidyl-prolyl cis/trans isomerization. *J Mol Biol* **279:** 449-460

Renner C, Alefelder S, Bae JH, Budisa N, Huber R, Moroder L (2001) Fluoroprolines as Tools for Protein Design and Engineering *Angewandte Chemie (International ed in English)* **40:** 923-925

Rodnina MV (2013) The ribosome as a versatile catalyst: reactions at the peptidyl transferase center. *Current opinion in structural biology* **23:** 595-602

Rodnina MV, Fricke R, Kuhn L, Wintermeyer W (1995) Codon-dependent conformational change of elongation factor Tu preceding GTP hydrolysis on the ribosome. *The EMBO journal* **14:** 2613-2619

Rodnina MV, Fricke R, Wintermeyer W (1994) Transient conformational states of aminoacyl-tRNA during ribosome binding catalyzed by elongation factor Tu. *Biochemistry* **33:** 12267-12275

Rodnina MV, Savelsbergh A, Katunin VI, Wintermeyer W (1997) Hydrolysis of GTP by elongation factor G drives tRNA movement on the ribosome. *Nature* **385:** 37-41

Rodnina MV, Savelsbergh A, Matassova NB, Katunin VI, Semenkov YP, Wintermeyer W (1999) Thiostrepton inhibits the turnover but not the GTPase of elongation factor G on the ribosome. *Proceedings of the National Academy of Sciences of the United States of America* **96:** 9586-9590

Rodnina MV, Wintermeyer W (1995) GTP consumption of elongation factor Tu during translation of heteropolymeric mRNAs. *Proceedings of the National Academy of Sciences of the United States of America* **92:** 1945-1949

Roy H, Zou SB, Bullwinkle TJ, Wolfe BS, Gilreath MS, Forsyth CJ, Navarre WW, Ibba M (2011) The tRNA synthetase paralog PoxA modifies elongation factor-P with (R)-beta-lysine. *Nature chemical biology* **7:** 667-669

Rychlik I, Cerna J, Chladek S, Pulkrabek P, Zemlicka J (1970) Substrate specificity of ribosomal peptidyl transferase. The effect of the nature of the amino acid side chain on the acceptor activity of 2'(3')-O-aminoacyladenosines. *European journal of biochemistry / FEBS* **16:** 136-142

Saini P, Eyler DE, Green R, Dever TE (2009) Hypusine-containing protein eIF5A promotes translation elongation. *Nature* **459:** 118-121

Sallee NA, Rivera GM, Dueber JE, Vasilescu D, Mullins RD, Mayer BJ, Lim WA (2008) The pathogen protein EspF(U) hijacks actin polymerization using mimicry and multivalency. *Nature* **454:** 1005-1008

Sarkar P, Reichman C, Saleh T, Birge RB, Kalodimos CG (2007) Proline cis-trans isomerization controls autoinhibition of a signaling protein. *Molecular cell* **25:** 413-426

Satterthwait AC, Jencks WP (1974) The mechanism of the aminolysis of acetate esters. *Journal of the American Chemical Society* **96:** 7018-7031

Schagger H, von Jagow G (1987) Tricine-sodium dodecyl sulfate-polyacrylamide gel electrophoresis for the separation of proteins in the range from 1 to 100 kDa. *Anal Biochem* **166:** 368-379

Schmeing TM, Huang KS, Kitchen DE, Strobel SA, Steitz TA (2005a) Structural insights into the roles of water and the 2' hydroxyl of the P site tRNA in the peptidyl transferase reaction. *Molecular cell* **20:** 437-448

Schmeing TM, Huang KS, Strobel SA, Steitz TA (2005b) An induced-fit mechanism to promote peptide bond formation and exclude hydrolysis of peptidyl-tRNA. *Nature* **438:** 520-524

Schmidt C, Lenz C, Grote M, Luhrmann R, Urlaub H (2010) Determination of protein stoichiometry within protein complexes using absolute quantification and multiple reaction monitoring. *Anal Chem* **82:** 2784-2796

Schmidt DE, Jr., Westheimer FH (1971) PK of the lysine amino group at the active site of acetoacetate decarboxylase. *Biochemistry* **10:** 1249-1253

Schnier J, Schwelberger HG, Smit-McBride Z, Kang HA, Hershey JW (1991) Translation initiation factor 5A and its hypusine modification are essential for cell viability in the yeast Saccharomyces cerevisiae. *Molecular and cellular biology* **11:** 3105-3114

Schroeder GK, Wolfenden R (2007) The rate enhancement produced by the ribosome: an improved model. *Biochemistry* **46:** 4037-4044

Selmer M, Dunham CM, Murphy FVt, Weixlbaumer A, Petry S, Kelley AC, Weir JR, Ramakrishnan V (2006) Structure of the 70S ribosome complexed with mRNA and tRNA. *Science (New York, NY)* **313:** 1935-1942

Semenkov YP, Rodnina MV, Wintermeyer W (2000) Energetic contribution of tRNA hybrid state formation to translocation catalysis on the ribosome. *Nature structural biology* **7:** 1027-1031

Sharma PK, Xiang Y, Kato M, Warshel A (2005) What are the roles of substrate-assisted catalysis and proximity effects in peptide bond formation by the ribosome? *Biochemistry* **44:** 11307-11314

Shaw JJ, Green R (2007) Two distinct components of release factor function uncovered by nucleophile partitioning analysis. *Molecular cell* **28:** 458-467

Shine J, Dalgarno L (1974) The 3'-terminal sequence of Escherichia coli 16S ribosomal RNA: complementarity to nonsense triplets and ribosome binding sites. *Proceedings of the National Academy of Sciences of the United States of America* **71:** 1342-1346

Shoulders MD, Kamer KJ, Raines RT (2009) Origin of the stability conferred upon collagen by fluorination. *Bioorg Med Chem Lett* **19:** 3859-3862

Shoulders MD, Raines RT (2009) Collagen structure and stability. *Annu Rev Biochem* **78:** 929-958

Sievers A, Beringer M, Rodnina MV, Wolfenden R (2004) The ribosome as an entropy trap. *Proceedings of the National Academy of Sciences of the United States of America* **101:** 7897-7901

Silver LL (2011) Challenges of antibacterial discovery. *Clinical microbiology reviews* **24:** 71-109

Simonetti A, Marzi S, Myasnikov AG, Fabbretti A, Yusupov M, Gualerzi CO, Klaholz BP (2008) Structure of the 30S translation initiation complex. *Nature* **455:** 416-420

Smith-Peter E, Lamontagne AM, Lafontaine DA (2015) Role of lysine binding residues in the global folding of the lysC riboswitch. *RNA biology***:** 0

Solbak SM, Reksten TR, Wray V, Bruns K, Horvli O, Raae AJ, Henklein P, Henklein P, Roder R, Mitzner D, Schubert U, Fossen T (2010) The intriguing cyclophilin A-HIV-1 Vpr interaction: prolyl cis/trans isomerisation catalysis and specific binding. *BMC structural biology* **10:** 31

Starosta AL, Lassak J, Peil L, Atkinson GC, Virumae K, Tenson T, Remme J, Jung K, Wilson DN (2014) Translational stalling at polyproline stretches is modulated by the sequence context upstream of the stall site. *Nucleic acids research* **42:** 10711-10719

Studer SM, Joseph S (2006) Unfolding of mRNA secondary structure by the bacterial translation initiation complex. *Molecular cell* **22:** 105-115

Sunohara T, Abo T, Aiba H (2002) The C-terminal amino acid sequence of nascent peptide is a major determinant of SsrA tagging at all three stop codons. *RNA (New York, NY)* **8:** 1416-1427

Tamae C, Liu A, Kim K, Sitz D, Hong J, Becket E, Bui A, Solaimani P, Tran KP, Yang H, Miller JH (2008) Determination of antibiotic hypersensitivity among 4,000 single-gene-knockout mutants of Escherichia coli. *Journal of bacteriology* **190:** 5981-5988

Tanner DR, Cariello DA, Woolstenhulme CJ, Broadbent MA, Buskirk AR (2009) Genetic identification of nascent peptides that induce ribosome stalling. *The Journal of biological chemistry* **284:** 34809-34818

Thomas LK, Dix DB, Thompson RC (1988) Codon choice and gene expression: synonymous codons differ in their ability to direct aminoacylated-transfer RNA binding to ribosomes in vitro. *Proceedings of the National Academy of Sciences of the United States of America* **85:** 4242-4246

Thompson RC, Dix DB, Gerson RB, Karim AM (1981) Effect of Mg2+ concentration, polyamines, streptomycin, and mutations in ribosomal proteins on the accuracy of the two-step selection of aminoacyl-tRNAs in protein biosynthesis. *The Journal of biological chemistry* **256:** 6676-6681

Trobro S, Aqvist J (2005) Mechanism of peptide bond synthesis on the ribosome. *Proceedings of the National Academy of Sciences of the United States of America* **102:** 12395-12400

Trobro S, Aqvist J (2006) Analysis of predictions for the catalytic mechanism of ribosomal peptidyl transfer. *Biochemistry* **45:** 7049-7056

Ude S, Lassak J, Starosta AL, Kraxenberger T, Wilson DN, Jung K (2013) Translation elongation factor EF-P alleviates ribosome stalling at polyproline stretches. *Science (New York, NY)* **339:** 82-85

van Stelten J, Silva F, Belin D, Silhavy TJ (2009) Effects of antibiotics and a proto-oncogene homolog on destruction of protein translocator SecY. *Science (New York, NY)* **325:** 753-756

Vitagliano L, Berisio R, Mastrangelo A, Mazzarella L, Zagari A (2001) Preferred proline puckerings in cis and trans peptide groups: implications for collagen stability. *Protein Sci* **10:** 2627-2632

Wallin G, Aqvist J (2010) The transition state for peptide bond formation reveals the ribosome as a water trap. *Proceedings of the National Academy of Sciences of the United States of America* **107:** 1888-1893

Wang J, Kwiatkowski M, Pavlov MY, Ehrenberg M, Forster AC (2014) Peptide formation by N-methyl amino acids in translation is hastened by higher pH and tRNA(Pro). *ACS chemical biology* **9:** 1303-1311

Waudby CA, Launay H, Cabrita LD, Christodoulou J (2013) Protein folding on the ribosome studied using NMR spectroscopy. *Progress in nuclear magnetic resonance spectroscopy* **74:** 57-75

Weber K, Pringle JR, Osborn M (1972) Measurement of molecular weights by electrophoresis on SDS-acrylamide gel. *Methods Enzymol* **26:** 3-27

Weinger JS, Parnell KM, Dorner S, Green R, Strobel SA (2004) Substrate-assisted catalysis of peptide bond formation by the ribosome. *Nature structural & molecular biology* **11:** 1101-1106

Weixlbaumer A, Jin H, Neubauer C, Voorhees RM, Petry S, Kelley AC, Ramakrishnan V (2008) Insights into translational termination from the structure of RF2 bound to the ribosome. *Science (New York, NY)* **322:** 953-956

Wieden HJ, Gromadski K, Rodnin D, Rodnina MV (2002) Mechanism of elongation factor (EF)-Ts-catalyzed nucleotide exchange in EF-Tu. Contribution of contacts at the guanine base. *The Journal of biological chemistry* **277:** 6032-6036

Wilson DN, Beckmann R (2011) The ribosomal tunnel as a functional environment for nascent polypeptide folding and translational stalling. *Current opinion in structural biology* **21:** 274-282

Wohlgemuth I, Beringer M, Rodnina MV (2006) Rapid peptide bond formation on isolated 50S ribosomal subunits. *EMBO reports* **7:** 699-703

Wohlgemuth I, Brenner S, Beringer M, Rodnina MV (2008) Modulation of the rate of peptidyl transfer on the ribosome by the nature of substrates. *The Journal of biological chemistry* **283:** 32229-32235

Wohlgemuth I, Pohl C, Rodnina MV (2010) Optimization of speed and accuracy of decoding in translation. *The EMBO journal* **29:** 3701-3709

Wolfenden R, Snider M, Ridgway C, Miller B (1999) The Temperature Dependence of Enzyme Rate Enhancements. *JACS* **121:** 7419-7420

Woolstenhulme CJ, Guydosh NR, Green R, Buskirk AR (2015) High-precision analysis of translational pausing by ribosome profiling in bacteria lacking EFP. *Cell reports* **11:** 13-21

Woolstenhulme CJ, Parajuli S, Healey DW, Valverde DP, Petersen EN, Starosta AL, Guydosh NR, Johnson WE, Wilson DN, Buskirk AR (2013) Nascent peptides that block protein synthesis in bacteria. *Proceedings of the National Academy of Sciences of the United States of America* **110:** 19

Xia J, Levy RM (2014) Molecular dynamics of the proline switch and its role in Crk signaling. *The journal of physical chemistry B* **118:** 4535-4545

Xiong L, Polacek N, Sander P, Bottger EC, Mankin A (2001) pKa of adenine 2451 in the ribosomal peptidyl transferase center remains elusive. *RNA (New York, NY)* **7:** 1365-1369

Yanagisawa T, Sumida T, Ishii R, Takemoto C, Yokoyama S (2010) A paralog of lysyl-tRNA synthetase aminoacylates a conserved lysine residue in translation elongation factor P. *Nature structural & molecular biology* **17:** 1136-1143

Yaron A, Naider F (1993) Proline-dependent structural and biological properties of peptides and proteins. *Critical reviews in biochemistry and molecular biology* **28:** 31-81

Youngman EM, Brunelle JL, Kochaniak AB, Green R (2004) The active site of the ribosome is composed of two layers of conserved nucleotides with distinct roles in peptide bond formation and peptide release. *Cell* **117:** 589-599

Zanelli CF, Maragno AL, Gregio AP, Komili S, Pandolfi JR, Mestriner CA, Lustri WR, Valentini SR (2006) eIF5A binds to translational machinery components and affects translation in yeast. *Biochemical and biophysical research communications* **348:** 1358-1366

Ziv G, Haran G, Thirumalai D (2005) Ribosome exit tunnel can entropically stabilize alpha-helices. *Proceedings of the National Academy of Sciences of the United States of America* **102:** 18956-18961

Zou SB, Hersch SJ, Roy H, Wiggers JB, Leung AS, Buranyi S, Xie JL, Dare K, Ibba M, Navarre WW (2012) Loss of elongation factor P disrupts bacterial outer membrane integrity. *Journal of bacteriology* **194:** 413-425

Zou SB, Roy H, Ibba M, Navarre WW (2011) Elongation factor P mediates a novel post-transcriptional regulatory pathway critical for bacterial virulence. *Virulence* **2:** 147-151

7 Appendix

7.1 List of abbreviations

Abbreviation	Description
A site	acceptor site
A. tumefaciens	Agrobacterium tumefaciens
aa	amino acid
aa-tRNA	aminoacyl-transfer RNA
AmiB	N-acetylmuramoyl-L-alanine amidase
Aze	Azetidine-2-carboxylic acid
B. subtilis	*Bacillus subtilis*
B. abortus	*Brucella abortus*
(cis/trans)-MePro	4,5-(cis/trans)-Methanoproline
DOHH	deoxyhypusine hydroxylase
DHS	deoxyhypusine synthase
E site	exit site
E. coli	*Escherichia coli*
EF	elongation factor
EpmA	EF-P modifying enzyme
FlhC	flagellar transcriptional regulator
Flk	flagellar regulator
IC	initiation complex
IF	initiation factor
Lys-RS2	class II Lys-tRNA synthetase
mRNA	messenger RNA
nt	nucleotide
P site	peptidyl-tRNA binding site
Pip	pipecolic acid
Pmn	puromycin
PrmC	release factor glutamine methyltransferase
PTC	posttranslocation complex
P. aeruginosa	*Pseudomonas aeruginosa*
RF	release factor
RRF	ribosome recycling factor
Rz1	outer membrane subunit Rz1
s	second
S. cerevisiae	*Saccharomyces cerevisiae*
S. typhimurium	*Salmonella enterica serovar typhimurium*
S. oneidensis	*Shewanella oneidensis*
S. flexneri	*Shigella flexneri*
T. thermophilus	*Thermus thermophilus*
3,4-Dhp	3,4-Dehydroproline
4,4-F2-Pro	4,4-Difluoroproline
4-(R/S)-Flp	4-(R/S)-Fluoroproline
4-(R/S)-Hyp	4-(R/S)-Hydroxyproline
4-(R/S)-Mep	4-(R/S)-Methylproline

7.2 List of Figures

Fig. 1: Overview of the prokaryotic translation cycle 2
Fig. 2: Reaction scheme of aminolysis in solution and on the ribosome 5
Fig. 3: Structures of EF-P/eIF5A, tRNA and the ribosome 7
Fig. 4: Modification of EF-P, e/aIF5A 8
Fig. 5: Steric properties of the prolyl ring 10
Fig. 6: EF-P does not influence initiation 13
Fig. 7: Influence of EF-P on di- and tripeptide formation with Pmn 14
Fig. 8: Influence of EF-P on di- and tripeptide formation with native A-site substrates 15
Fig. 9: Oligopeptide formation in the presence and absence of EF-P 16
Fig. 10: Drop-off of peptidyl-tRNA from the ribosome 18
Fig. 11: EF-P prevents ribosome stalling on PPG and PPP sequences engineered into PrmC. 19
Fig. 12: Identification of the stalling site in PrmC 20
Fig. 13: Rescue of stalled ribosomes by EF-P 21
Fig. 14: EF-P alleviates PPP/PPG-induced stalling during synthesis of native *E. coli* proteins 22
Fig. 15: *In-vitro* translation of proteins containing polyproline stretches 23
Fig. 16: *In-vitro* translation of PrmC containing a PPP motif encoded by different Pro-codons 24
Fig. 17: Influence of the tRNA identity on peptide bond formation 25
Fig. 18: EF-P in termination 26
Fig. 19: Effect of the EF-P modification on the translation of the PPG motif 28
Fig. 20: Impact of the EF-P modification state on its catalytic proficiency 29
Fig. 21: Model for fMPPG formation 30
Fig. 22: A site-bound tRNA speeds up the dissociation of fMet-Pro-Pro-tRNA^{Pro} from ribosomes 30
Fig. 23: Impact of the interplay of EF-P and EF-G on peptide synthesis 31
Fig. 24: $MgCl_2$ increases the yield of fMPPG tetrapeptide formation 33
Fig. 25: Impact of the sequence context on peptide bond formation 34
Fig. 26: Impact of EF-Ps modification on fMet-Pmn formation 35
Fig. 27: pH dependence of fM-G formation 36
Fig. 28: Peptidyl transfer from fMet-Pro-tRNA^{Pro} to Gly-tRNA^{Gly} at different pH 38
Fig. 29: Temperature dependence of fMP-G formation at pH 7.5 39
Fig. 30: Temperature dependence of fMP-G formation at pH 6.5 40
Fig. 31: Structure of proline and proline analogs 42
Fig. 32: Impact of prolyl ring substitutions on translation 43
Fig. 33: Similar contribution of EF-P to catalysis 44
Fig. 34: Decay of peptidyl-tRNA fMet-Pro*-tRNA^{Pro} 46
Fig. 35: Correlation between substituent effects on the ribosomal and in-solution reactions. 47
Fig. 36: The electrophilicity of the P-site substrate does not correlate with the reaction rate. 48
Fig. 37: Peptide bond formation is faster with R analogs 48
Fig. 38: Impact of ring size on peptide bond formation 49
Fig. 39: Temperature dependences of Pmn reaction 50
Fig. 40: Model of lysylated EF-P with aminoacyl-tRNA 59
Fig. 41: pH dependent fM-G and fMP-G formation. 60

Fig. S1: Analysis of the EF-P modification status by mass spectrometry 85
Fig. S2: Comparison of native tRNA^{Pro} and tRNA^{Pro} transcript 86

Fig. S3: Purification of TC(P*) 87
Fig. S4: Dependence of the deaclyation rate on the nucleophile concentration 88
Fig. S5: $MgCl_2$ dependence of tetrapeptide formation 88

7.3 List of Tables

Table 1: Oligopeptide formation 17
Table 2: Influence of tRNA identity on the rate of peptide bond formation 25
Table 3: EF-P dependence of fMPPG synthesis 29
Table 4: Peptidyl transfer to glycine as a function of the P-site substrate 34
Table 5: Activation parameter of fMP-G formation at pH 7.5 39
Table 6: Activation parameter of fMP-G formation at pH 6.5 41
Table 7: Rates of fMet-Pro*-$tRNA^{Pro}$ decay 46
Table 8: Influence of the ring size on the rate of peptidyl-transfer 49
Table 9: Activation parameter for fMP*-Pmn formation with P* = 4-(R/S)-Flp 51

Table S1: Rate constants of di- /tripeptide formation from fMet-(Xaa)-$tRNA^{Xaa}$ and subsaturating Pmn 89
Table S2: Rate constants of di- and tripeptide formation with a native A-site substrate 89
Table S3: Titration of modified and unmodified EF-P on fM-PPG synthesis 89
Table S4: fM-PPG synthesis as a function of EF-G 89
Table S5: fM-PPG synthesis as a function of $MgCl_2$ 90
Table S6: fM-P*P*G synthesis as a function of $MgCl_2$ 90
Table S7: pH dependence of fM-G synthesis 90
Table S8: pH dependence of fMP-G synthesis 90
Table S9: Temperature dependence of fMP-G formation at pH 7.5 90
Table S10: Temperature dependence of fMP-G formation at pH 6.5 90
Table S11: pK_a values for proline and Pro analogues 91
Table S12: Parameters of amide rotation for proline and analogues 91
Table S13: pK_a values, parameters of amide rotation and rate constants of peptide bond formation 91
Table S14: Rate of reactions for Pro and Pro-derivatives 92
Table S15: Rate of peptidyl transfer from fMet-(R/S)-Flp-$tRNA^{Pro}$ to Pmn as a function of temperature 93

8 Acknowledgements

I am very grateful to Marina V. Rodnina for accepting me as PhD student in her department, for the interesting and challenging project, for providing excellent working conditions and support during the last 4 years. I would like to thank Heinz Neumann, Holger Stark and Marina V. Rodnina for their support and advice during the thesis committee meetings and the members of the examination board Ralf Ficner, Manfred Konrad and Markus T. Bohnsack.

I am grateful to Ingo Wohlgemuth for his supervision, enthusiasm, total commitment and discussions during these fruitful years. I would like to thank Frank Peske for the supervision during my first year of PhD studies and for the EF-P constructs. I would like to thank Dirk Görlich for the EF-P antibody and Pohl Milon and Riccardo Belardinelli for discussions. I would like to thank Daniel N. Wilson, Agata L. Starosta, Nedilkjo Budisa and Vladimir Kubyshkin for a great collaboration. Furthermore, I would like to thank Albena Draycheva for her help on countless occasions at every time of the day. I thank Akanksha Goyal and Michael Thommen for creating a very pleasant environment in our lab corner and all other colleagues who contributed to a pleasant time. I thank all technical assistants of the department for organizing and maintaining excellent working conditions; with special thanks to Olaf Geintzer who solved all my computer problems and Christina Kothe for fast, efficient or simply excellent technical support.

I thank my family for their support. I am exceptionally grateful to Bernhard Kuhle for invaluable discussions and suggestions, his encouragement as well as most critical comments on drafts of this thesis.

9 Contribution

If not stated otherwise, experiments were performed, analyzed and interpreted by Lili K. Dörfel. The thesis was supervised by Ingo Wohlgemuth, who conceived the project, identified proline as putative EF-P target and performed and analyzed presented mass spectrometry experiments.